

JPRS-CST-89-002

27 JANUARY 1989



**FOREIGN  
BROADCAST  
INFORMATION  
SERVICE**

# ***JPRS Report***

## **Science & Technology**

---

***China***

16TH INTERNATIONAL CONGRESS OF THE INTERNATIONAL  
SOCIETY FOR PHOTOGRAVIMETRY AND  
REMOTE SENSING--VOL II

JPRS-CST-89-002

27 JANUARY 1989

SCIENCE & TECHNOLOGY

CHINA

16TH INTERNATIONAL CONGRESS OF THE INTERNATIONAL  
SOCIETY FOR PHOTOGRAMMETRY AND  
REMOTE SENSING--VOL II

Kyoto Selections from INTERNATIONAL ARCHIVES OF PHOTOGRAMMETRY  
AND REMOTE SENSING in English Vol 27, 1988 Parts B8, B9, B10, B11

[For Volume I of this report see JPRS-CST-89-001 dated  
26 January 1989.]

CONTENTS

AEROSPACE

Performance Evaluation of ERS-1 Synthetic Aperture Radar Fast Delivery Processor [J.P. Guignard, P. Hasan] .....	1
The Brazilian Experience in Handling 15 Years of Remote Sensing Satellite Data [Marcio Nogueira Barbosa, Sergio de Paula Pereira] .....	8
ESA's Activities and Plans for Remote Sensing Data Systems [Livio Marelli] .....	24
The Possibilities of Application of Satellite Data for Monitoring Ice Condition in the Antarctic Region [N.N. Shvyrkov] .....	35
Sea Spectra as Determined From Low-Altitude SLAR Images [Konstantin Voliak] .....	41
Lidar Measurements of Sea Surface Waves [K.I. Voliak, M.V. Solntsev] .....	55
National Program for Handling Large Volumes of Satellite Data [B.L. Deekshatulu] .....	66
Real Time SAR Processing Techniques [Roland Schotter] .....	75

Simulation of ERS-1/OPS by the Use of Airborne Spectroradiometer [H. Watanabe, T. Osanai] .....	83
Noise Reduction From Synthetic Aperture Radar Imagery [Olli Sirkia] .....	96
The New Generation SPOT Satellites SPOT 4 and 5 [Michel Arnaud, Marc Leroy] .....	102
Design Aspects of a System for Geocoding Satellite SAR Images [G. Schreier, et al.] .....	115
A Survey of Aerial Image Quality Assessment Methods [Anders Boberg] .....	129
The Processing of SPOT Imagery in Brazil [Machado e Silva, et al.] .....	142
Data Processing and Calibration of SAR Data in Japan [Korehiro Maeda, Hideo Sato] .....	151
Studies on Object Reconstruction From Space Using Three Line Scanner Imagery [Heinrich Ebner, et al.] .....	164
Earth Observation Programs in Japan [Tomifumi Godai] .....	175
Estimation of the Simulated JERS-1 Data [T. Takemura, et al.] .....	186

AEROSPACE

Performance Evaluation of ERS-1 Synthetic Aperture Radar Fast Delivery Processor

43070007a Kyoto Selection from INTERNATIONAL ARCHIVES OF PHOTOGRAHAMETRY AND REMOTE SENSING in English Vol 27 1988 Part B8 pp 1-7

[Article by J.P. Guignard, European Space Research and Technology Centre (ESTEC), Keplerlaan 1, 2201 AZ Noordwijk, The Netherlands; P. Hasan, MacDonald Dettwiler, 3751 Shell Road, Richmond B.C., Canada V6X 2Z9, Commission No. II]

[Text] Abstract

The Factory Acceptance Test (FAT) of ESA's ERS-1 Synthetic Aperture Radar Fast Delivery Processor (SAR FDP) took place recently at MacDonald Dettwiler in Vancouver, Canada. The process will eventually be installed in the principal ERS-1 ground station in Kiruna, Sweden.

This paper describes the comprehensive set of tests performed during the FAT. It focusses on the tests and measurements of:

--image quality parameters (3-dB resolution, side lobe level, etc.);

--throughput for both image and wave mode product generation;

--operational aspects of the processor demonstrating its ability to run in an operational environment.

The SAR FDP shows a significant improvement in throughput compared to previous SEASAT processors, while preserving the integrity of the image quality.

## 1.0 Introduction

The development of the ESA ERS-1 satellite offers an opportunity to develop a fast processor for Synthetic Aperture Radar (SAR) data.

The key requirement is to minimize the delay between data acquisition and delivery of processed images to users. A maximum delay of three hours is allowed for both the image and wave modes. In the image mode the satellite acquires SAR data for 100 x 100 km earth surface images. In the wave mode SAR data is acquired for 5 x 5 km images of the ocean surface at along-track intervals of 200 or 300 km. The SAR FDP processes wave mode data to an intermediate image, and then to a final image spectrum product. Sea state information (wave spectrum product) will be derived from the image spectrum product. The image mode operates only while the satellite is visible from a ground station, while the wave mode can operate around the orbit, since data can be recorded on-board and later downlinked to the ground station (see [1]).

The features of a SAR processor capable of meeting such a requirement while preserving the quality of the product have been defined and an ESA contract placed with MacDonald Dettwiler for the processor's development. Development based on the design presented in [2] is now complete, and this paper describes the processor's actual performance.

## 2.0 Methodology

The SAR FDP was tested against all detailed requirements stated in the SAR FDP requirements specifications. A verification cross reference matrix was used to map each requirement to the test number in the acceptance test procedures document.

A total of 16 main tests, each of them consisting of various subtests, were developed. These tests were designed to demonstrate that the SAR FDP meets its image quality requirements as well as its operational requirements.

The image quality tests were done by processing simulated point targets as well as pre-processed SEASAT data and then analysing the processed images. The operational aspects of the processor were tested by scheduling the processor to generate all possible products from image mode and wave mode data. The processor was also tested against possible errors in commands from the control computer, or in the input raw data.

## 3.0 Test Data Specifications

### 3.1 Simulated Point Targets

Point target data is generated using a specially developed simulator running on the ST-100 array processor (developed and manufactured by STAR Technologies Inc.). Both image mode and wave mode data are simulated using ERS-1 parameters and copied to High Density Digital Tape (HDDT), which conforms to the ERS-1 downlink format.

Parameters are chosen to simulate extreme conditions such as maximum squint angle and maximum and minimum pulse repetition frequencies.

Point target positions are chosen to allow image quality measurements across the whole image. In particular, point targets are placed at the boundaries of the processor range invariance regions to demonstrate that image quality parameters are not degraded by any implementation specific restrictions.

### 3.2 Simulated Wave Data

The simulated wave data is used to test generation of the image spectrum product, which is the final SAR FDP wave mode product.

The wave data is approximated as a sinusoidal function characterized by its wavelength and direction.

Several data sets are generated using different wavelengths and directions so the averaging process and the rectangular to polar coordinates transformation during spectrum product generation can be tested extensively.

### 3.3 Pre-processed SEASAT Data

Pre-processed SEASAT data is used to demonstrate that the SAR FDP can process real SAR data with image quality parameters comparable to those produced by MacDonald Dettwiler's SEASAT processor.

The pre-processing includes shifting the SEASAT data to baseband frequency so that the raw data is represented as complex numbers (real and imaginary parts) rather than as real numbers. Furthermore, the data is converted to 5-bit to resemble ERS-1 data and then copied to HDDT to conform with the ERS-1 downlink format.

## 4.0 Performance Test Results

The performance tests include image quality parameter measurements such as spatial resolution, side lobe level, Integrated Side Lobe Ratio (ISLR), and also throughput measurements. Typical results of the measurements are shown below. These results are compared with the values stated in the processor's requirements specification.

### 4.1 Spatial Resolution and Side Lobe Level

The spatial resolution is the 3-dB width of the point target response measured in both range and azimuth directions. The side lobe level is the highest side lobe level in the point target response relative to the main peak level. Results from the simulated point target data are as follows:

	Requirement	Measured
3-db width in slant range:	< 1.44 pixels	1.29 pixels
3-db width in azimuth:	< 1.66 pixels	1.35 pixels
side lobe level in range:	< -20.0 dB	-24.5 dB
side lobe level in azimuth:	< -20.0 dB	-24.1 dB

Spatial resolution of the SEASAT image is also measured and compared with the image processed by the original SEASAT processor. Two SEASAT scenes, Goldstone and Vancouver, are used for the test. The result is as follows:

	SEASAT	SAR FDP
3-db width in ground range:	24.8 metres	25.2 metres
3-db width in azimuth:	22.0 metres	22.3 metres

#### 4.2. Integrated Side Lobe Ratio (ISLR)

The integrated side lobe ratio is the ratio expressed in dB between the side lobe power and the main lobe power of the response from a point target. The main lobe power is the total power inside an area centered about the main peak and extending three resolution lengths in the range and azimuth directions. The side lobe power is the total power outside the main lobe but within an area bounded by ten resolution lengths in the range and azimuth directions.

The result of this ISLR measurement is -20.0 dB while the stated ISLR requirement is that the value be less than -12.0 dB.

#### 4.3. Point Target Misregistration

The point target misregistration is the misregistration of a point target's energy from its expected zero doppler location caused by approximations in the SAR processor. Misregistration due to orbit data and terrain height error is not included.

The results of the misregistration measurements are as follows:

	Requirement	Measured
Range misregistration	+ 2.88 pixels	0.47 pixel
Azimuth misregistration	+ 3.32 pixels	1.56 pixels

#### 4.4. Radiometric Linearity

Radiometric linearity is measured by the correlation coefficient between output point target peak power regression and input point target power.

The simulated point target area is generated with varying power so that the data cover the dynamic range of the ERS-1 input data. The radiometric linearity value is required to be greater than 0.95, and the measured value is 0.98.

#### 4.5. Product Localisation

The SAR FDP is required to compute the geographical position of the four corner points and the centre point of a 100 x 100 km image. The geographical positions are expressed in terms of geodetic latitude and longitude.

The computation is checked by comparing results with those obtained from an independent software program developed by ESA. Typical results are as follows:

	Latitude	Longitude
ESA program result	36.369 degrees	239.338 degrees
	36.369 degrees	239.337 degrees

#### 4.6 Throughput

The SAR FDP is required to generate the following image mode products within one orbit:

- three fast delivery image mode products (100 x 100 km scene);
- two image mode noise statistic and drift calibration pulse products;
- three image mode chirp replica products.

If the SAR FDP is configured to process wave mode data it is required to generate the following products within one orbit:

- 150 wave mode intermediate products (5 x 5 km scene);
- 150 fast delivery wave mode products (image spectrum);
- ten wave mode noise statistic and drift calibration pulse products;
- 150 wave mode chirp replica products.

The throughput has to be sustained from orbit to orbit for up to ten consecutive orbits. Considering all ground station operational

restrictions such as data acquisition and HDDT positioning, the SAR FDP is required to generate one fast delivery image mode product in less than 28 minutes. The tests show that one 100 x 100 km image mode scene can be generated in 27.3 minutes.

Similar consideration of the ground station operational restrictions during low rate data processing shows that one chirp replica, one intermediate and one image spectrum wave mode product must be generated in less than 28 seconds. The throughput measurement during the test shows these products can be generated in 26 seconds.

## 5.0 Operational Aspects

The operational aspects of the SAR FDP are tested by scheduling the processor to generate all possible combinations of products. These include all the products listed for the throughput tests plus extraction products such as raw data products, general header products, and instrument header products. All products are checked against the output product specifications in terms of their formats and expected values in the product headers.

In addition, several tests are designed to test the error handling strategy of the SAR FDP. The simulated errors include the following:

- errors in the command parameters (inconsistent parameters)
- invalid commands
- errors in the system software configuration (e.g., a missing parameter table)
- missing lines in the input data
- insufficient input data
- overlapping and obsolete wave mode source packets
- error in spacecraft time code
- range line counter wrap around (caused by the 16-bit representation)

The SAR FDP is verified to handle these possible errors correctly. The verification was done by examining the SAR FDP responses and also the generated products.

## 6.0 Conclusion

The SAR FDP as developed by MacDonald Dettwiler under the ESA contract represents the newest implementation of the well proven SAR range-doppler algorithm.

The development's most significant achievements are its processing speed improvement (27 minutes per image compared to a few hours) and its preservation of image quality in a ground station operational environment.

#### 7.0 Acknowledgement

The authors wish to thank P. George and D. Meier of MacDonald Dettwiler for their contribution to the design and development of the SAR FDP.

#### 8.0 References

- [1] G. Duchossois "Overview and Status of the ERS-1 programme." Proceedings of IGARSS '86 (ESA SP-254 Vol. 1), August 1986.
- [2] P. George & J.P. Guignard "ERS-1 Synthetic Aperture Radar Fast Delivery Processor." IEEE Transactions on Geoscience and Remote Sensing, Vol. GE-25, No. 6, November 1987.

/08309

The Brazilian Experience in Handling 15 Years of Remote Sensing Satellite Data

43070007b Kyoto Selections from INTERNATIONAL ARCHIVES OF PHOTOGRAHMETRY AND REMOTE SENSING in English Vol 27 1988 Part B8 pp 15-29

[Article by Marcio Nogueira Barbosa, Sergio de Paula Pereira, MCT-INPE Instituto de Pesquisas Espaciais; Rod. Presidente Dutra, km 40 12630 -- Cachoeira Paulista, SP Brazil; Commission II; Working Group II/4]

[Text] ABSTRACT

This paper describes the Brazilian experience in acquiring, storing, processing and disseminating Remote Sensing data collected from satellites since the first Landsat in 1973 up to SPOT I in 1987/1988. INPE's roles in operating, upgrading, specifying, designing and integrating the related systems are covered, giving an evolution history which can be useful to other developing countries in the field of Remote Sensing.

1. INTRODUCTION

Fifteen years ago a decisive action taken by the Brazilian Government placed our country in the promising position of becoming one of the leaders in the Remote Sensing field of activities in the Southern Hemisphere. Thus, at that time, presidential authorization was granted to install and operate in Brazil a LANDSAT (ERTS-1) Ground Station, the third in the world to become operational, after only Canada and United States.

The initial availability of data from the LANDSAT series of satellites since 1972 and the operation of its own ground station from 1973 on gave to Brazil the required conditions to develop their Remote Sensing plans in a more effective manner.

Today, fifteen years have passed and the activities and perspectives in Remote Sensing have undergone an unequivocal evolution giving rise to a solid Brazilian experience in the field.

This experience is represented both by the practical know-how and maturity of specialists in the use of orbital remotely sensed data for a wide variety of applications, and by their consolidated experience in the operation of satellite ground stations as well as in developing and establishing new image generating and processing systems for satellite data applications.

## 2. HISTORIC RETROSPECT

It seems proper to review now the results obtained during this long range effort and their main consequences in conjunction with the governmental priorities and the perspectives at internal level.

During this time two different (but complementary) actions were developed in Brazil on the Government Level: the RADAMBRASIL Project and the Satellite Remote Sensing Program.

The RADAMBRASIL Project, initially established to perform the Land Resources Integrated Survey of an area of 1,500,000 km<sup>2</sup> in the Amazonic Region, was gradually increased until, by 1975, to cover about the entire 8,500,000 km<sup>2</sup> of the Brazilian territory, thus becoming the world's largest airborne radar (SAR) data coverage project. 38 reports with excellent thematic maps in the 1:1,000,000 scale were generated and became important assets for Government planners both on the Federal and State levels. This event gave rise to a very important by-product which was the training of large number of technicians on the handling and assessment of non-conventional images. Until then, the Brazilian technical people were used almost exclusively to handle aerophotographs.

Today, both the data generated by RADAMBRASIL project and a fairly large number of specialists can be found in the IBGE Foundation, the Brazilian Institute for Geography and Statistics, in Rio de Janeiro.

A different strategy had to be pursued, however, by the Satellite Remote Sensing Program. First, it was soon recognized the priority need of preparing the people for the then unknown techniques (even at international level) for generating and handling earth resources satellite data. Opportunities were then created to send Brazilian technicians abroad to be submitted to different levels of specialization (i.e., from short on-job-training courses all the way to MSc's and PhD's).

Further, it was enough just to look at the characteristics of Brazil to infer that very shortly the country would turn into a very important user of the data generated by these earth resources satellites. The authorization for purchasing a complete LANDSAT Satellite Ground Station was then issued by the Government in 1972, guided by the urgent need of better knowing the large country's territorial area and its renewable and non-renewable natural resources, the need of checking on the progress of large projects at remote areas, the need to access, in a global basis, the results of an agricultural policy, and the cost involved in obtaining data for these objectives using traditional methods.

Benefiting from the strategic location of Cuiaba Receiving Station in the continent, a huge amount of data of our own territory and also of several other countries in South America became then directly accessible to a growing and potentially active user community.

During these past years a considerable experience was gathered by INPE technicians in the process of developing techniques and methodologies and also in the identification of problems which could be either solved or mitigated with the use of satellite images.

In this period a very large number of specialists from governmental agencies, universities and private companies were trained at INPE, through the offering of specialization courses in several levels and graduate courses, MSc level.

Such an effort was intended primarily to spread the Remote Sensing disciplines and techniques through the user community in order to awake them for this exciting new technology and its potential applications in many areas of earth resources management and monitoring of the environment. A well trained user community would surely promote the country's economic growth using satellite technology.

Using the experience gathered from monitoring, operating, adapting and enhancing sophisticated receiving and processing equipments and associated software to meet satellite specifications of the LANDSAT series and the requirements of a growing user community, INPE gradually became a competent R&D center able to develop fairly complex units mainly in the areas of receiving and data processing stations as well as

image analysis systems. It is worth to mention that this experience enabled INPE to reach, in the early 80's, the status of co-participant in the design and implementation of the new LANDSAT 4/5 Brazilian ground processing system. In the mid 80's INPE, reaching a deeper knowledge and experience among its technical personnel, focused its attention to the French Satellite SPOT getting prepared to answer alone the requirements for the full integration of a ground processing system to handle SPOT data.

Nowadays the industry, strengthened by the government policies, is able to make and sell abroad, competitively, not only items but also systems developed by INPE.

Unfortunately, the economic crisis which hit Brazil in the last years reached very severely the R&D Centers, INPE among them. Suffering from lack of financial support and struggling for survival from lack of financial support and struggling for survival INPE (and some other important government R&D Centers too) was forced to pursue application target areas which naturally should have been transferred to the private companies, for example, bidding for the execution of projects using technologies already established.

However, with the new Government installed in March 1985, opportunities were granted to review every policy in the country, including the Remote Sensing subject.

Meanwhile, a simple inspection of what is happening in the western countries led the observer to conclude that the satellite remote sensing activities are going now through the transition from a well proven technology to a commercial venture, with a very high probability of success. The new policy from the Remote Sensing in Brazil should certainly take these facts in consideration.

Thus, in harmony with the aims and priorities of the new Brazilian Administration and guided also by international trends, INPE, from 1985 on, revised its own policy and structure in the area of Remote Sensing with the firm objective of intimately interact with the user community, universities and private industry in order to attain a highly desirable technological union. This will end up positioning the satellite remotely sensed information as the decisive tool for the investigators, specialists, planners and managers to achieve daily, weekly, monthly, seasonal, annual or long term monitoring of changes in the country's environment and resources. In particular, consolidating its union with the private sector, INPE is in process to promote, as said, the country's economic growth using satellite technology.

### 3. SIGNIFICANT STEPPING STONES

#### 3.1 Ground Stations and Instrumentation

Once acquired its first Receiving and Processing Ground Station in 1972/1973, few months after launching of LANDSAT-1, INPE, in a gradual

way, became capable of modifying and upgrading the station to handle data from new satellites of the initial series (LANDSATs 2 and 3), to fulfill new operational needs and to improve overall efficiency. The knowledge absorbed in this process allowed INPE the effective participation in the system design and analysis as well as software development and system integration of the new ground station, capable of receiving and processing the Thematic Mapper data from the LANDSAT-D series of satellites, to come, sharing these efforts with the supplier.

These efforts were managed within what was called "INPE LANDSAT-D Project" which set up, from late 1980 on, several phased activities aiming the establishment of the new facility which would allow the Brazilian Remote Sensing user community to access the markedly improved capabilities of the new instrument. Not only that but it would also fulfill the increasing requirements of this fast growing community in terms of timely, accurate and reliable data on earth resources. The new ground station for TM then came to reality, starting in early 1984 the generation of Thematic Mapper products.

This joint development program was fundamental in giving INPE the ability to modify, improve and expand its station as needed. New products have been placed available to the user community these last years and several extensions were made in the overall processing software to allow easier management, higher throughput and accuracy, and better quality of products.

This ability is being also put to test, in the last two years, through the efforts for upgrading the receiving and processing systems to handle the data from the French satellite SPOT. The development, implementation and tests of SPOT software as well as full system integration activities are being totally carried out by INPE specialists.

At this point it is most appropriate to mention the full support INPE has received from the Government in the procurement of the hardware subsystems necessary to upgrade their station for receiving and processing SPOT's data. This financial support was provided despite the severe economic crisis the country is lately suffering, in clear recognition from the governmental planners of the priorities and importance of INPE's role in fulfilling the country's needs.

INPE has also been developing equipments for meteorological satellite stations and for Data Collection Platforms (DCP's). In order to stimulate the use and fabrication of PCDs in Brazil long range efforts were engaged by INPE, reaching finally the successful development and testing of an ARGOS PCD prototype. This prototype was certified by ARGOS Service in France, end of 1983. Once certified the ARGOS PCD, INPE transferred to the Brazilian industry the associated technology endowing the country with this very effective tool for collecting data under remote conditions.

Efforts are also being conducted to test, certify and transfer to the industry PCDs compatible with GOES satellites, and a mini-station for directly receiving and processing ARGOS PCD data. The developments of both GOES PCD prototype and the ARGOS mini-stations have been concluded and the test and certification phases are in progress now. Worth to mention is also the development of the GOES-AAA format synchronizer capable of processing the new data format pertinent to the GOES-6 and 7 satellites. A prototype has been already developed and transferred to the industry which is now delivering the units to the national agencies which operate similar meteorological GOES stations.

Concerning the TIROS/NOAA Satellites, a software package has been developed to correct, in the digital domain, radiometrically and geometrically, the high resolution image data provided by the AVHRR instrument.

### 3.2 - Image Generation and Distribution

Table 1 and figures 1.1 and 1.2 summarize the volume of data (in photographic media and digital tapes) distributed to the users during these fifteen years.

The data above indicates an unprecedented utilization of photographic images by the user community during the years of '77, '78 and '79. However, during these years a big percentage (over 40 percent) of delivered products were processed in the smaller scales 1:3,704,000 and 1:1,000,000 (black and white). Only about 15 percent of the products were requested in the 1:250,000 scales. The profile of the requests indicated a user community mainly oriented to the use of LANDSAT products in global studies or analysis in smaller scales.

A very significant reduction in the user demand occurred particularly in the years of '83 and '84 as a result of the very restraining financial actions taken by the Brazilian private companies and governmental agencies in general great difficulties in reaching their desired annual budget.

TABLE 1 - IMAGES DISTRIBUTED TO USERS

YEAR	IMAGES (PHOTO)	CCTS	TOTALS
73	323	0	323
74	1,230	10	1,240
75	2,094	55	2,149
76	10,255	141	10,396
77	15,409	132	15,541
78	18,049	141	18,190
79	19,051	146	19,197
80	11,400	176	11,576
81	8,291	184	8,475
82	6,098	125	6,223
83	4,061	188	4,249
84	3,700	239	3,939
85	3,859	419	4,278
86	6,347	287	6,634
87	8,216	430	8,646

The situation changed and in the last three years a clear recovery is being observed. Not only that but the user tendency is now markedly towards the larger scales 1:250,000 and 1:100,000 which account for more than 50 percent of the total volume of photo products distributed in the year. The interest for color products has significantly increased being now around 20 percent of the total. These reflect the growing maturity and knowledge of the user community which is accessing more deeply the greater potential of the remote sensing products and is using more sophisticated ways for monitoring the environment and managing of earth resources, taking advantage of the finer resolution and accuracy of the new sensors.

Another aspect which deserves notice is the increase of the number of CCTs distributed to the users. This is a clear answer from the community to the efforts INPE is conducting to make more known and accessible to the users the image analysis systems called SITIMs, manufactured by the Brazilian industry.

Brazil has an outstanding position among the countries operating the LANDSAT system. The data base includes nowadays nearly 200,000 LANDSAT images. The number of users (mostly institutions) is steadily growing and today exceeds 1,500, many of them being from outside the country.

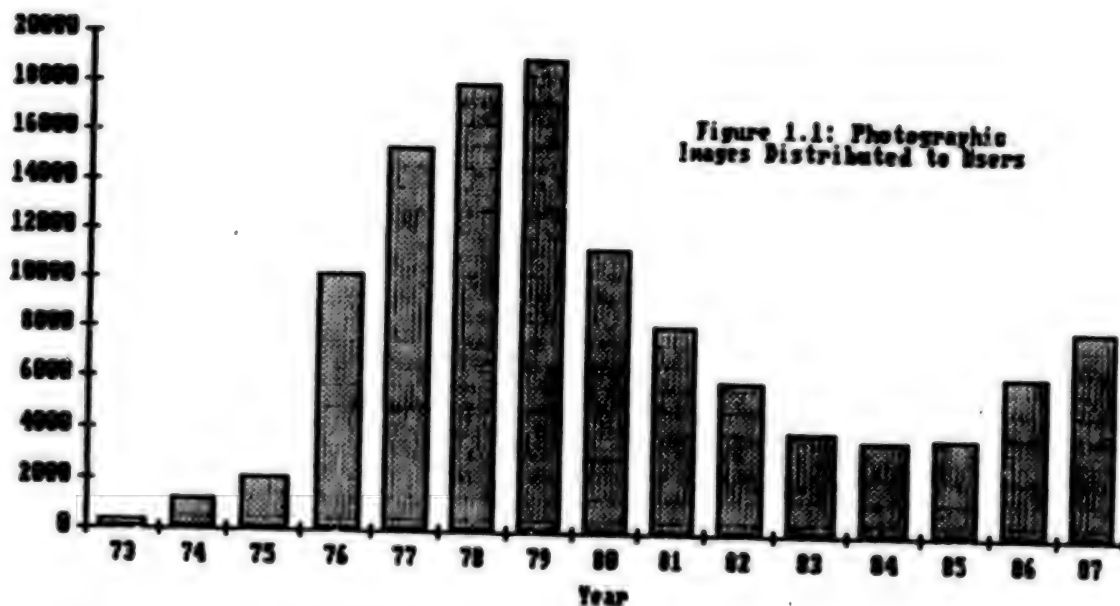


Figure 1.1: Photographic Images Distributed to Users

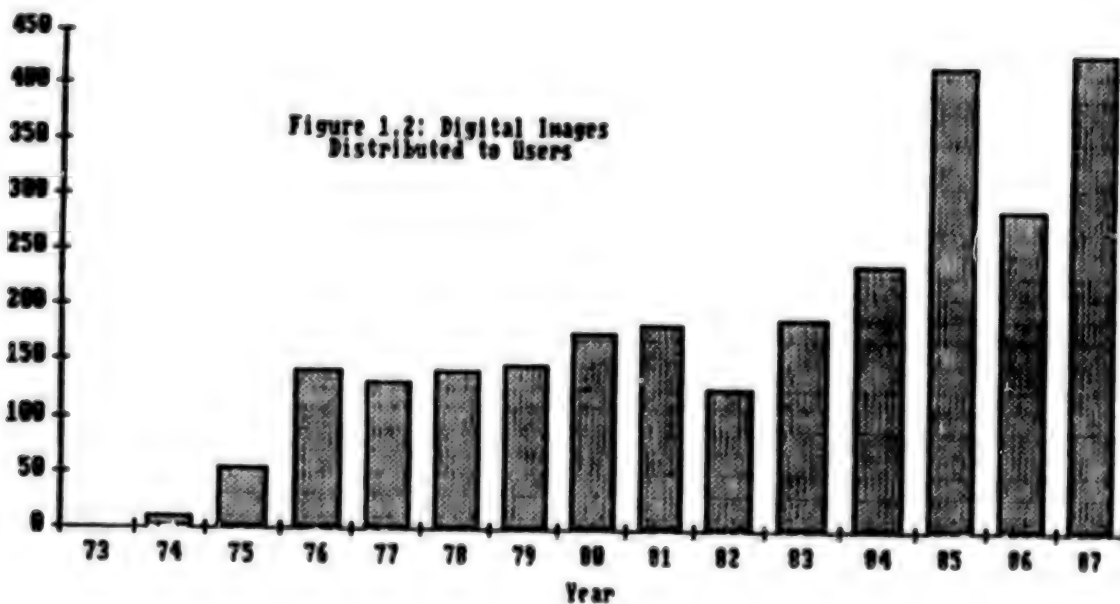


Figure 1.2: Digital Images Distributed to Users

During these fifteen years INPE has taken under its own responsibility the activities of marketing, selling and distributing the remote sensing images. In the last two years, a preparation is in progress to

gradually transfer to the private sector, particularly the Aerosurvey Companies, the activities of marketing and commercialization of the data. This surely can improve the overall efficiency besides yielding better service to the user community. This is indeed most opportune, once SPOT data, which are being already handled in a commercial basis, are being acquired directly at the INPE Ground Station, and are in process to be placed available to the user community.

### 3.3 - Cartography

It is significant to mention the efforts developed by INPE since 1980 towards the implementation of techniques for geometric correction of orbital imagery, mainly LANDSAT-MSS data, in order to transform the images into means more efficiently usable by the cartographic community.

After TM data became available it was soon recognized their enormous potential for cartographic applications. The advanced characteristics of the orbital platform, the new geometry of the instrument and the precise knowledge of its behaviour and associated modelling, made TM data of unprecedented value for cartography from space. Taking advantage of all these benefits, INPE specialists developed and implemented a processing station software capable of generating TM fully system-corrected products of very encouraging performance: internal geometric errors of the order of one pixel "rms," with no use of ground control points.

Benefitting, therefore, from special image treatments and from the existence of more advanced sensors, INPE has been directing its cartographic activities towards: a) production of planimetric satellite image-maps for future inclusion of altimetric information, b) production of thematic maps in different scales, and c) updating of conventional topographic maps in 1:250,000 and 1:100,000 scales. An achievement which also deserves notice is the successful experiment of digital mosaicking of two adjacent TM fully system-corrected scenes (Barbacena image-map), in preparation for the creation of a 1:250,000 satellite image-map. This product is particularly important in poorly mapped areas of the country.

Presently, INPE specialists are refining the operational procedures for the production of such image maps at 1:1,000,000 and larger scales.

### 3.4 - Image Analysis Systems

Intensive efforts have been made by INPE to develop, in the last few years, a family of image analysis systems called SITIMs. These systems, based on Brazilian-made microcomputers, are used mainly in the analysis of natural resources, although their frames allow the use in other areas such as Metallurgy, Meteorology and Medicine.

Four of these systems are presently installed at Image Processing Labs of INPE, supporting directly research and application projects in Remote Sensing and Meteorology. Twelve units are installed in other agencies.

Engineers and system analysts specialized in digital processing, modelling and simulation techniques have, since 1975, been doing research in enhancing, filtering, classification, registration, geometric correction and image analysis techniques.

INPE is also working in the field of Geographic Information Systems, conducting a project where satellite imagery is being incorporated and associated to other related information plans (maps, digital terrain models, etc.) with a wide variety of image analysis techniques, everything manipulated through a user-friendly software package. The hardware concept is based on Brazilian-made microcomputers and the first version is finished and being submitted to an evaluation from the user standpoint. Finished this phase it will be also transferred to the private industry.

### 3.5 - Environmental Analysis

Qualified people of INPE in the field of Environmental Analysis have been conducting projects on techniques and methods for gathering remote sensing environmental data through the use of orbital and airborne imagery. These projects have been oriented to the following areas:

- a) Environmental Geomorphology with studies of erosion and equilibrium of inland water systems,
- b) Hydric Systems with studies on water basin managing and water quality and availability analysis,
- c) Land use with studies on the soil occupation, and
- d) Urban Areas with studies of their growth and use.

### 3.6 - Geology

In Geology, studies have been conducted for mining and energy (i.e., oil, gas) surveys through the analysis of the land surface from not only satellite imagery but also airborne data and field conditions. It is known that to extract geological information from remote sensing data is necessary a careful work by experienced geological interpreters knowledgeable of both remote sensing system characteristics and field conditions. The reason is that most of the observed surface phenomena are often related to geologic parameters in only a tenuous manner. Despite these difficulties success has been verified on various cases being worth to mention projects on: a) Mineral and Energetic Resources with mineral and oil deposit studies through remote sensing for the establishment of prospection models, b) Geological Mapping with structural analysis and identification of lithostratigraphic units in different scales seeking the definition of evolutionary models, c) Engineering and Hydrological Geology with remote sensing applications on geotechnical and hydrogeological problems.

### 3.7 - Forestry

In the field of forestry INPE efforts have had the objectives of research and development of methodologies for utilization of remote sensing data in the effective monitoring and management of the forest resources. The main project lines in this area have been: vegetation mapping, forest management and inventory, estimates of timber volumes, detection and assessment of damages due to burns, diseases or droughts. A number of forestry agencies are also becoming increasingly involved in the development of techniques for applying remote sensing methods to environmental monitoring problems.

### 3.8 - Agriculture

The use of remote sensing techniques to carry out projects on crop survey and potential yield of areas is of utmost importance for the national economy. In this framework INPE has conducted research and studies on wheat, soybean, corn, rice and sugar-cane. Estimates of planted and/or tilled areas are done through visual and/or automatic interpretation of satellite or airborne imagery, thus performing the integral or sampled mapping of regions of interest. These techniques can also be used to estimate the losses caused by plagues, diseases and periodic events such as frost or drought.

Yield estimates are obtained through modelling with data from orbital remote sensing, eventually supported from airborne data and conventional meteorological studies.

### 3.9 - Basic Research in Remote Sensing

The efforts in this area have been conducted primarily to increase the knowledge about the remote sensing data and its possible correlations with terrain features. Research activities encompass the study and analysis of the parameters which affect data acquisition and registration, such as characteristics and conditions of terrain features, spectral and radiometric properties, atmospheric effects, sensor specifications and image geometry, among others.

The efforts also deal with evaluation studies of the capability of certain sensors to well characterize certain target areas of the country. Under this point of view efforts are also being conducted to access the potential of SPOT data over the Brazilian territory.

### 3.10 - Technology Transfer and Technical Orientation

As said, the Brazilian remote sensing user community is steadily growing and INPE is vitally interested in promoting the establishment of a large team of specialists throughout the country in order to maximize the use of the advanced remote sensing tools and to join efforts with the universities and private companies in such way that a strategic bridge will be established between the space technology and the social and economical development of our country.

The efforts developed towards these objectives in the last years, particularly from 1985 on, can be summarized below:

- a) Graduate courses in remote sensing and image analysis, with regular courses beginning in February each year and leading to a MSc Degree.
- b) On-the-job training for professionals needing a familiarization with the remote sensing techniques.
- c) User assistance and orientation service with a specialized team, when applicable, INPE's user-aid services units spread throughout the country are used to facilitate user access to the data or to the technique (presently there are centers in the following Brazilian cities: Natal, Manaus, Brasilia, Rio de Janeiro, Sao Jose dos Campos, Cachoeira Paulista and Campina Grande).
- d) International cooperation in remote sensing with other countries and international agencies. To the present INPE develops cooperation programs with Argentina, Bolivia, Chile, Colombia, Ecuador, Canada, GDR, France, FRG, Great Britain, Iraq, Japan, Panama, Paraguay, People's Rep. of China, Peru, Uruguay, USA, FAO, UN, World Bank and the Interamerican Development Bank.
- e) International training courses, for Latin American Specialists (1985-1986) and for African Specialists (1987-1988), being offered in cooperation with the U.N. Outer Space Affairs Division and supported by other agencies such as SELPER (Latin American Society of Remote Sensing Specialists), ESA (European Space Agency) and CNPq (National Council of Scientific and Technological Development of Brazil).
- f) Dissemination and establishment of regional remote sensing laboratories, organization of symposia, seminars, lectures, workshops, demonstrations, etc., on remote sensing have been very active in INPE in the last years. The goal is to familiarize the different professionals with the most recent developments in the field.

INPE is also working on another powerful way of transferring to the user community the remote sensing knowledge absorbed during this long range experience, which is the planning and installation of regional remote sensing laboratories. They are oriented, in general, to work guided by the characteristics and needs of each region. Regional Remote Sensing Laboratories are already in operation in Campina Grande, at Northeast of the country, and Belem, at the North. Eight new laboratories are already approved for the period '88-'89.

#### 4. EXAMPLES OF RECENT APPLICATIONS AND ACTIVITIES ON REMOTE SENSING IN BRAZIL

##### 4.1 - Land Reform Program

The Brazilian Land Reform Program which is being conducted by the

Ministry of Land Reform and Agrarian Development includes among its activities the identification and selection of nonproductive land parcels for redistribution among small farmers. These activities include the identification of land suitable to establish new settlements. This process tackles with technical, social, political and legal issues. The way it has been conducted in the past has been subject of criticism and laid on political grounds. INPE developed a methodology using satellite remote sensing techniques and is helping the government in the process of land identification and selection of land areas for allocation.

To date remote sensing techniques have been used to examine 1,000,000 km<sup>2</sup> in Brazil for the Land Reform Program. The following major conclusions may be mentioned regarding the application of remote sensing techniques in land reform issues:

R.S. techniques have allowed to establish a technical approach to lessen the political aspects related with land redistribution.

--R.S. techniques have provided for lowering the cost of land selection and inspection and have expedited the process of land identification and selection.

--Satellite data have allowed multitemporal analyses which permitted the study of the historical evolution of the land use practice or degree during a time interval. This has provided a strong argument concerning the history of the occupation of the land.

--R.S. techniques have permitted to unveil "make up" practices. Some farmers, knowing that their lands were subject to land act decrees, would fastly plow their lands and question in judge government land misqualifications or errors. Through the historical archive of satellite images it has been possible to show the status of the land use before and at the time of the land reform acts.

--Government lawyers have been briefed upon remote sensing techniques, study areas, and provided with a kit of satellite images and reports on the historical land use. These space data have been present to the judges. Thus, remote sensing has been used now also as a legal tool.

#### 4.2 - National Irrigation Program

Brazil has devoted considerable efforts in the development of its agriculture. In 1986 the federal government decided to promote an increase in grain production of the order of 20 percent, based on a National Irrigation Program. In order to reach that goal government has to apply the resources of the irrigation program in areas which have an agriculture vocation or a return potential. This required to know in a short period of time the actual distribution of the agriculture activities, a task that by conventional methods could take years. Based on this, INPE has developed a six-month remote sensing project which has covered an area of 3,500,000 km<sup>2</sup>. The resulting maps provide updated

information on the distribution of crops. Based on this information, government may now establish priority project areas and apply the resources more effectively.

#### 4.3 - Water Resources

The Government of the Pernambuco State has been concerned with the drought in the semiarid Northeast of Brazil and has asked INPE to present alternative plans in 45 days. First it was identified by the governor himself that the first priority should be the man, that is, water for drinking. Drought periods in Northeastern Brazil causes migration of population from rural to urban areas or to more developed cities in Southern Brazil. During drought periods the government has to hire water trucks to distribute water to the population. INPE has developed a forty-five-days remote sensing project for the whole State of Pernambuco (91,000 km<sup>2</sup>) which has included 1:100,000-scale maps containing information on the distribution of alluvial-sediment areas, updating of surface water resources (dams, ponds, drainage, etc.), human activity concentrations, actual drainage (including intermittent drainage) and road networks, and existing water wells.

Based on the maps provided to the government, a strategic and more efficient plan for water distribution might be made. Planning of the distribution of the water trucks and schedules (e.g., population versus pond distribution), planning for the establishment of public fountains and other actions may be taken.

### 5. FUTURE PERSPECTIVES

A challenging step has been taken by the Brazilian Government with the official approval of the so-called Brazilian Complete Space Mission, MECB. MECB has the objective of designing, building, integrating, testing, launching and operating four national application satellites: two for Data Collection and two for Remote Sensing. The launcher is being developed in Brazil by the IAE--Institute of Space Activities (Ministry of Aeronautics). The expected date for the first satellite launching is mid 1989. The first two satellites, i.e., the data collection ones, will use the Brazilian made DCP's (Data Collecting Platforms) which are an economically viable option for national applications. The greatest advantage of the telemetry via satellite is that costs are not too high and are not related to the distances involved.

The remote sensing satellites, whose launching is foreseen to occur early 1993 will relay information on natural resources evaluation, through moderate resolution and a highly repetitive global coverage, using an onboard Multispectral Earth Observation Camera. This will enable the country to achieve its own data bank at low cost and on nearly real time.

The INPE's opportunity to work as the designer and system integrator in the SPOT ground station turned out to be a necessary and very important

step towards the preparation for the Remote Sensing Mission of the MECB where both ground and space segments will be designed and built in Brazil by INPE with the help of the Brazilian industry. There are similarities on both missions. For example, the experience gathered in the calibration, correction and processing of the charge-coupled-detector (CCDs) arrays featured by the SPOT imaging process will be shared by the MECB-Remote Sensing which is using the same process in its multispectral camera.

Nowadays, as it has been already mentioned, the policy among the western countries is the transference to the private sector of the space technologies, which have been fully tested and approved after years of operation. This has happened to the telecommunication satellites, and is happening now with the French Satellite SPOT which the French Government operates under commercial basis through the SPOT Image Co. LANDSATS 6 and 7, to be launched in the early '90s, will also be operated in a commercial basis by the EOSAT Co. in USA.

Drawn this picture, it becomes imperative the need for Brazil to possess its own satellites.

A satellite configuration is chosen to attend the aims of its owners. In a domestic satellite, the spectral bands and the channels of the observation camera are established as a function of parameters the country wants to observe, measure or collect. These actions will allow the establishment of long range economical and social programs, without incurring in the heavy satellite fees often imposed by the satellite operators abroad as well as gaps in the data availability due to political or economical reasons.

The definition of the Remote Sensing Mission of the MECB was then conducted in accordance with the above aspects. Aware of the present constraints of the satellite and taking them into account the remote sensing specialists of INPE have come to a proposal of certain mission characteristics in order to better fit it, as much as possible, to known needs in the areas of research and application of the Remote Sensing in Brazil.

A technically oriented inquiry was also conducted by these specialists to evaluate closely the needs of Brazilian user community in terms of remote sensing data.

As a result of this joint analysis it came up a mission with the following main characteristics: moderate spatial resolution, high temporal resolution with larger distance swath and a sensitivity in both the red and near-infrared regions of spectrum, most oriented to studies where the target phenomena are characterized by a high dynamics especially in the areas of Agriculture, Environmental Control and Oceanography.

Still in the international scenario, an ever growing number of new satellites and data acquisition systems will be placed in orbit, so that

satellites and data acquisition systems will be placed in orbit, so that natural resources surveying processes and environmental monitoring techniques will become more and more simple, precise and less expensive.

So it is time to plan ahead, thinking in terms of the future.

Brazil has today thousands of Landsat images of its territory and a complete radar coverage (SAR) is available. Besides, it has data gathering and processing facilities which may be upgraded at reduced costs to handle future satellite data. More important, it has quite a reasonable number of skilled technicians who can make adequate use of the available technologies.

However, it is high time to bring in the private industry. Our electronics and informatics industries are capable of producing the items required by the remote sensing specialist. Besides, the aerosurvey companies can also be present in the data commercialization, thus improving the overall efficiency and yielding better service to the users community. The Government would stay in the area of the research of new technologies, improving the existing facilities (e.g., installing Regional Remote Sensing Laboratories), training personnel and warranting the data access to new satellites and systems of interest.

This way the base which will allow the Brazilian society to have an effective participation in defining future Space Missions, either national or international, will be established.

## 6. REFERENCES

Barbosa, M.N., Bastos Netto, D., Cunha, R.P.: Overview of the Brazilian Satellite Remote Sensing Program and Selected Examples of Recent Applications. 38th International Astronautical Congress of the IAF, Brighton, United Kingdom, Oct. 11-17, 1987.

Barbosa, M.N., Bastos Netto, D.: Brazilian Satellite Remote Sensing Program. International Conference Remote Sensing for Development, Berlin, East Germany, Sept. 1-7, 1986.

Parada, N.J.: Brazilian Remote Sensing Receiving, Recording and Processing Ground Systems in the 1980's. 18th International Symposium of the Environment, Paris, France, Oct. 1-5, 1984.

/08309

7/2

## AEROSPACE

### ESA's Activities and Plans for Remote Sensing Data Systems

43070007c Kyoto Selections from INTERNATIONAL ARCHIVES OF PHOTOGRAHAMTRY AND REMOTE SENSING in English Vol 27 1988 Part B8 pp 84-94

[Article by Dr. Livio Marelli, ESA/ESRIN, Frascati, Italy]

#### [Text] 1. INTRODUCTION

The European Space Agency (ESA) is involved in Earth Observation from space since the mid 1970s. This has been through the Meteosat programme, operated now on behalf of Eumetsat, and through the Earthnet programme, which up until now have acquired, archived, processed and disseminated data from non ESA remote sensing satellites like Landsat, SPOT, MOS-1, TIROS-AVHRR (Advanced Very High Resolution Radiometer) plus, in the past, Seasat, HCMM (Heat Capacity Mapping Mission) and Nimbus-7.

At present ESA is building ERS-1 which is an ocean and ice monitoring satellite due for launch in 1990. The Earthnet programme is upgrading its facilities to meet this new challenging mission. It will guarantee service not only to the science and research community, but also to global and regional weather and sea state forecasting organisations, offering near real time sea state information.

Recently, the Long Term Plan of ESA has been approved (up to the year 2000) and within the plan, a comprehensive Earth Observation programme is included. The plan involves, in particular, a second flight unit of the ERS series and the participation of Europe to the Polar Platform complex developed in the framework of the International Space Station (ISS) programme.

Within each one of the phases of ESA's activities in remote sensing mentioned above, the problem of data systems have, and will be, central and will involve major technical and operational challenges.

This paper outlines the programmatic approach followed so far, and describes the evolution planned for the coming generation of ERS satellites as well as the preliminary end-to-end system concept envisaged for the Polar Platforms later in the 1980s.

## 2. THE PAST EXPERIENCE

Up until very recently remote sensing has been mostly an area of research and proof of concept: missions like Seasat, HCMM, Nimbus-7, and to some extent Landsat Multi Spectral Scanner (MSS) and Return Beam Vidicon (RBV), were aimed at demonstrating the feasibility of specific sensing techniques for a number of research/application domains.

The satellites mentioned above were not developed by ESA and had no assurance of continuity: in fact, Landsat is the only service which has maintained practical data continuity over the years.

Another aspect of the series of satellites launched towards the end of the 70s was the fact that they relied mostly on regional ground stations to collect data since only some had on-board recorders, the vast majority of which proved rather unreliable.

ESA's philosophy for the data systems associated with the above missions can be summarised as follows:

--Decentralised network of ground stations covering the major areas of interest for the European users (e.g., Europe, Scandinavia/Greenland and the Arctic region, North Africa and the Sahel).

--Each regional station charged with data acquisition, archiving and pre-processing (bulk correction) on request.

--Centralised network management and users interface service including catalogue, quick-looks, order handling and quality control.

--Dissemination system, exclusively off-line delivering digital and photographic products through mail and/or special delivery to nominated centres in participating countries or to individual users.

The archiving task is restricted in preserving the original raw data recorded digitally on High Density Digital Tape (HDDT) (one should bear in mind that Seasat Synthetic Aperture Radar (SAR) and Landsat RBV were transmitting in analog form) or on Computer Compatible Tape (CCT) for HCMM/Nimbus-7.

Data received was screened systematically to generate quick-looks and catalogue entries primarily to obtain reliable cloud cover information, although the cloud cover assessment was assigned by operators with computer support.

The catalogue of such missions as Landsat was assessable on-line from low speed land lines or packet switching networks.

A full set of quick look prints of data available was set up at the centralised user services facility (ESRIN, Frascati) as well as at most of the national centres which act as points of contact for their national user community.

Products were generated exclusively upon user request in view of the large difference between data collected and data actually exploited: it should be mentioned that, in the case of Europe, up to 70 percent of acquired data are cloud covered for a good part of the year. As regards acquisition strategy, two approaches were adopted:

- a) Landsat data was acquired systematically over the coverage of member states and to a lesser extent over the Arctic due to swath overlap.
- b) The experimental satellites were handled instead according to an agreed science plan defined between Principal Investigators (PIs), NASA and Earthnet.

So far the system has provided an acceptable service and the large archives have proved accessible longer than expected though the old Landsat data ('75-'78) cannot be guaranteed any longer as the rest.

All attempts of purging the data sets of cloud covered passes have demonstrated that the exercise doesn't pay off because, transcriptions are labor intensive and strain the old HDDTs which are difficult to maintain after so many years.

On the other hand, user demand for very old data is so modest that it doesn't justify major investments.

For several years, quick-looks for Landsat MSS were compacted on microfiches but also this exercise proved costly and of limited value to users due to long delays between sensing and the availability of the microfiches.

In the specific case of Meteosat, the handling of the archive on HDDT proved infeasible and it was decided to transfer data on 6250 bpi CCTs: the volume of data involved and the importance of the data set for such projects as FGGE made the exercise worthwhile. Figure 1 gives some general indication on volume of data handled so far by Earthnet.

### 3. THE PRESENT GENERATION OF REMOTE SENSING MISSIONS

Starting with the launch of Landsat 4/5 in the early '80s and later with the launch of Spot 1, a new generation of pre-operational/commercial missions have become available.

Furthermore, the remote sensing user community became more fully aware of the value of the AVHRR of the TIROS-N series which though designed originally for polar meteorology, proves very valuable for a number of other applications (vegetation index, etc.).

Lastly NASDA, in Japan, launched their first remote sensing satellite MOS-1 which Earthnet is acquiring with its network of ground stations.

The peculiarities of the mission mentioned dictated some evolution in the system used with ESA which will be briefly reviewed here after.

The overall philosophy adopted for Landsat Thematic Mapper (TM) and MOS is not significantly different from the one quoted in the previous chapter with few exceptions:

--The quick-look system is undergoing modifications to allow generating of colour masters which are expected to improve users ability to determine suitability of images for their applications.

--The network of ground stations is permanently linked via leased lines to the Central User Service (CUS) facilities which allows daily updates of the catalogue and reception of stations logs including information about data acquired, quality assessment reports on products generated, etc.

--Experiments were successfully carried out disseminating within 6 to 8 hours from acquisition MSS full resolution scenes over areas of interest to a number of pilot/demonstration projects using high speed satellite link.

Spot operations in Maspalomas (Canary Islands) are carried out with the same basic philosophy, however, since the access fee is linked to the number of scenes requested acquisitions are not systematic but scheduled to match resources and user demands.

At present, Maspalomas can only acquire and record data while processing, when requested by users, is carried out by Spotimage in Toulouse. Later on this year a standard Spot processing chain will be installed at the station which will then serve users directly.

The TIROS-N/AVHRR and TOVS (Tiros Operational Vertical Sounder) data are part of a newly started activity of Earthnet aimed at preserving those data which are widely used in Europe for meteorological purposes but are thereafter not usually kept for long term exploitation.

The approach adopted here is somewhat different: having recognised that many stations are already in existence, Earthnet has negotiated agreements with national High Resolution Picture Transmission (HRPT) operators to host at their premises a data archiving subsystem which extracts the data to be preserved, derives catalogue parameters including cloud cover, sunglint, etc., generates a more advanced quick-look and evaluates, based on specific criteria, whether or not data should be preserved in a long term archive. In view of the more manageable volume of data involved, archiving is carried out on optical disks (12", 2Gbytes disks). The optical disk generated at the various HRPT stations will eventually converge onto a centralized archives where historical products requested by users will be generated when required.

A central computerized catalogue connected with the archival stations is available on-line from ESRIN. Another feature of interest in the TIROS system is that the archival strategy is decided centrally and the system, based upon the planned HRPT operations and on actual cloud cover evaluation, results will automatically direct station to or not to archive data so that specific cloud free data sets over area of interest be secured.

The option of generating automatically at the stage of data archiving, level 2 products like vegetation index over land, sea surface temperature over sea, etc., is being evaluated in cooperation with major user groups.

#### 4. THE ERS-1 PAYLOAD DATA SYSTEM

ERS-1 is the first major remote sensing mission developed by the European Space Agency.

ERS-1 has scientific and application objectives: for this reason ESA is committed to provide, within three hours from sensing, geophysical parameters associated with global sea state (wind fields, wave high and wave image spectra, etc.) plus high resolution regional data over Europe derived from the SAR.

ERS-1 payload data system has been designed as an end-to-end complex which includes the following main components:

--a number of Real Time Acquisition stations charged with the task of acquiring from the on-board recording system over an orbit and processing it to geophysical level and make it available for dissemination.

--a number of SAR acquisition stations capable of generating few SAR scene in near Real Time. This service is exclusively available for the European coverage.

--a centralized user services centre (based at ESRIN, Frascati) in charge of handling all interfaces with the users, cataloguing, order handling, quality assurance network management and, upon delegation, mission management.

--a number of archive and processing facilities in charge of preserving data generated by ERS and generate products for the users either on request or by retrieving relevant products which had been generated by systematic processing.

--a wide band data dissemination system ensuring the distribution of near real time data products to users in nominated centres of member states.

--a number of national or foreign acquisition/processing centres having signed agreement with ESA to have access to ERS-1 data.

The salient feature of the ERS payload data system are:

--all ERS raw data are going to be preserved for at least 10 years after the lifetime of the satellite. Figure 2 summarizes the anticipated volumes involved.

--global Low Bit Rate (LBR) data will be systematically processed and disseminated in near real time while SAR products will be generated and disseminated exclusively upon user request.

--the archival task will be carried out in a decentralized way separately from the data acquisition facilities. Processing and Archiving Facilities (PAFs) have been selected as centres of expertise in different application domains of ERS. These PAFs shall, in particular, support the Agency in the calibration and validation of the mission, its sensors and products, in the definition of novel or improved or additional products to be extracted from ERS either off-line or in near real time as well as in the definition and validation of quality assessment methods and procedures.

--the central catalogue shall provide information about data already acquired as well as on acquisition plans: likewise the users shall have the capability of placing orders for products from the archive but also for data yet to be sensed and for products to be made available in near real time as well as off-line.

The catalogue shall contain reference to all data collected for ERS-1 including those acquired by foreign stations and users will not be bothered to know where physically data they need is kept or production is carried out.

At present it is not anticipated to generate the equivalent of Landsat or Spot quick looks: it is possible that such a service might be developed for the Along Track Scanning Radiometer (ATSR) which is an experimental sensor provided as an instrument of opportunity but it is not planned for the SAR.

ERS-1 will represent a major challenge as regards the payload data system and will allow development and validation of a number of novel features which will be applied for the Polar Platform complex.

## 5. THE POLAR PLATFORMS

The polar platform complex is a part of the international space station programme which is being finalized between ESA, Japan, Canada and Europe.

The polar platforms will carry on-board a very large number of sensors of scientific and application nature and they are aimed at a long term earth monitoring system lasting well into the next century.

The polar platforms will rely on a complex space infrastructure developed as part of ISS which will greatly enhance the system and will also impose significant changes to the payload data handling design and implementation: typical examples are the Data Relay satellites (TDRSS, European DRS and Japanese DRS) which will allow real time world wide access to data from the platforms.

At present ESA is only studying the Polar Platforms' (PPFs) end-to-end data systems. Therefore, only very preliminary considerations on its final set up can be provided to date. We anticipate that in a number of aspects the PPF payload data system will be similar to the one presently in place, or that foreseen for ERS-1 e.g.:

--the system will be decentralized making use of several regional facilities as well as of specialized centres in charge of specific services along the lines of ERS PAFs. Such facilities however, will not be operated necessarily just off-line but could receive global data through data Relay channels.

--specialized user community like meteorology could and probably shall set up dedicated facilities to handle sensors data of specific interest.

--the centralized user services will offer information about data available for the PPF complex rather than for individual missions.

--near real time as well as off-line services will be ensured with systematic and "on request" operations according to the product type and associated user requirements.

Conversely, a number of new aspects will have to be addressed and solved with novel approaches:

--the central user service for Europe will have to integrate user requests for instrument operated on non-European platforms and liaise with the relevant mission management centres to ensure their feasibility and actual implementations.

--data collected in the United States or in Japan needs to be transferred to Europe when required, either in near real time or in an off-line mode, be processed and delivered to the requesting users. This data traffic may well prove to be complex and expensive and needs therefore to be optimized.

--the data dissemination systems of the major partners covering NORTH AMERICA, EUROPE and Japan might need to be interconnected.

--standardization and intercalibration of products will become an essential requirement to allow users to handle indifferently data generated by different sensors operating on different platforms and received and processed by different partners in the system.

--the different nature of the sensors operated on PPFs being either scientific/application or commercially orientated will imply complex problems of data allocation, protection, accounting, etc.

The challenge is major but this path appears the only viable one to address the complex issues of environmental monitoring or global change studies.

## 6. CONCLUSIONS

Remote sensing systems seems to change generation every 5 to 6 years: Landsat-1 in 1972, Landsat-3, Seasat, Nimbus, HCMM in 1978, Landsat-5/Spot in 1984/86, ERS, JERS, TOPEX 1990-92, PPFs in 1995-97.

Within such a time span two major aspects evolve:

- 1) User requirements
- 2) Technology available

We have attempted to describe how in Europe the transition from experimental to pre-operational space remote sensing system is taking place, and its impact on data systems. The technology evolution is obviously playing an equally important role but unfortunately, each generation of remote sensing systems operates approximately with the technology prevailing during the previous generation and little can be done to modify this pattern.

So far the most glamorous evolution in remote sensing payload data handling is in the area of available computing power and on-line storage.

High speed recording technology has not yet evolved at the same pace.

Archival technology based on optical recording is reaching maturity only in these last years and has a long way to go before adequate standardization is enforced.

High speed data dissemination and networking are becoming increasingly available and are likely to impact on traditional remote sensing services in a significant way.

Remote sensing is on the move to become a major resource management tool in the next decade and beyond.

Future is indeed a big challenge in this area.

	MSS	TM	MOS-1	TIROS	NIMBUS
FUCINO	247366	63447	8600	-	-
KIRUNA	177657	68472	17300	-	-
MASPALOMAS	29089	3896	13600	1998	2134
TROMSOE	-	-	7300	465	-
LANNION	-	-	-	-	1291
<b>T O T A L</b>	<b>454112</b>	<b>135815</b>	<b>46800</b>	<b>2463</b>	<b>3425</b>

-----  
Total Gbytes

One MSS scene	equals	35 Mbytes	MSS	15894
One TM scene	equals	256 Mbytes	TM	34760
One MOS-1 scene	equals	16 Mbytes	MOS-1	748
One TIROS pass	equals	70 Mbytes	TIROS	172
One nimbus pass	equals	90 Mbytes	NIMBUS	308
<b>T O T A L</b>				<b>51882</b>

Fig. 1. Scenes Acquired by the Earthnet Stations up to Spring '88

**EXPECTED GLOBAL VOLUME PER LBR INSTRUMENT PER YEAR**

<b>Instrument</b>	<b>Raw Data</b>	<b>FDP + IP</b>
Wave	870 Gbyte	302 Gbyte
Wind	472 Gbyte	3 Gbyte
RA	72 Gbyte	2 Gbyte
ATSR	600 Gbyte	-
<b>T O T A L   L B R</b>	<b>2014 Gbyte</b>	<b>306 Gbyte</b>

**POSSIBLE TOTAL VOLUME FOR SAR PER YEAR FOR ALL  
REGIONAL STATIONS**

<b>Instrument</b>	<b>I Data</b>	<b>FDP</b>
SAR	28000 Gbyte	990 Gbyte

**Fig. 2 ERS-1 Yearly Data Volumes**

/08309

The Possibilities of Application of Satellite Data for Monitoring Ice Condition in the Antarctic Region

43070007d Kyoto Selections from INTERNATIONAL ARCHIVES OF PHOTOGRAMMETRY AND REMOTE SENSING in English Vol 27 1988 Part 8B pp 1-6

[Article by N.N. Shvyrkov, All Union Research Institute for Marine Fisheries and Oceanography; V. Krasnoselskaya 17a, 107140 Moscow B-140 USSR; Commission IV]

[Text] ABSTRACT

Based on satellite observation in visible and microwave ranges the possibility of investigation of ice formation process and ice melting in high latitude zones of the World Ocean is considered. The modern methods of data acquisition of the borders of drift ice, size of ice fields, age of ice formations are analysed. The methods of construction of weekly ice charts of the Arctic and Antarctic regions resulting from satellites, aircrafts and vessel observations are considered. The analysis of ice distribution in the Antarctic region in light period of 1980-1984 seasons is made. Annual and seasonal dynamics of ice cover is estimated. The results obtained are of practical and theoretical interest for ecological studies and for the investigations of possibilities of exploitation of live resources of the Antarctic region. The data available can be used for the development of some methods for prediction of ice conditions in the South Ocean.

The processes of ice formation and ice destruction are the main elements of oceanographic regime in the high latitudes of the World Ocean and in the seas of temperate latitudes. Ice is the major factor which produces the effect on the security of navigation and performance of various sea operations. The successful fishery in freezing seas is possible only on the basis of good understanding of the ice situation. The knowledge of the peculiarities of ice regime is necessary in planning and performance of the scientific research in different almost inaccessible region.

Sea ice can be used as a tracer in studying large-scale oceanic circulations, streams, rotations and other sea water dynamic features. The quantity of ice in partially freezing seas is the main index of winter type and good predictor of some productive processes in forecoming spring period.

The process of melting ice in the Antarctic region provides the complex of hydrometeorological processes at the edge of drifting ice and icebergs. The production of phytoplankton in these regions can be compared with some highly productive zones of the World Ocean. High abundance of phytoplankton at melting edges of drift ice is responsible for considerable formations of macrozooplankton and various fish species. Therefore, the investigations carried out aboard the R/V "Gizhiga" in the Atlantic sector of Antarctic region revealed a group of icebergs around which at the distance of 50 miles a concentration of macrozooplankton was observed. The total biomass of this concentration was estimated at about several hundreds of thousand tons.

Sea ice serves as a habitat for numerous marine animals such as penguins and crabeater seals. In high latitudes the ice distribution and shift produces a considerable impact on marine animal migrations, promoting the distribution of some species and restricting the distribution of the others.

Due to its physical properties ice is considered to be one of few parameters of marine environment which can be easily detected by remote sensing. Ice formations can be observed in visible, infra-red and radio-range waves of the electromagnetic spectrum. Each method mentioned above has its own advantages and limitations.

At present TV-images, obtained from meteorologic satellites or "Meteor" are used in the Soviet Union for operative deciphering. The application of these images allows for the determination of large ice-floes, icebergs, ice-fields, the locations of channels and polynyas, ice unity and age with a high degree of accuracy. On the basis of this information the Hydrometeorological Service of the USSR regularly constructs 5-day charts of ice situation in Arctic and Antarctic region.

After geographical bridging of some TV-images from satellite the composite photographs in the polar stereographic projection (the scale 1:15,000,000) are made.

By deciphering the borders of drift ice, the location of fast shore ice, the position of ice-fields, borders of various density and age, the location of channels and polynyas are determined. The data obtained from the analysis of satellite information are refined and supplied by

some information from shore stations, vessels and aircrafts. The refined information is transferred to the blank of the charts of Arctic and Antarctic region in the composite photograph scale and projection. Weekly charts serve as the synthesis of satellite information, observation of aircraft, vessels and shore stations. Since 1985 for the construction of charts the radar data obtained from satellite "Kosmos-1500" was used. The satellite equipment allowed for the acquisition of data on motion and ice distribution irrespective of the condition and synoptical situation. On the radar images the ice fields and icebergs, vast extensive zones, shelf and continental glaciers are easily differentiated. The series of several radar images of the same aquatic area allows for the detection of general drift of sea ice, for estimation of the dynamics of large polynyas and for the determination of the tendencies of ice compression and rarity. Figure 2 demonstrates the composite of the Antarctic ice cover. This figure is made on the basis of radar images of satellite "Kosmos-1500." Various ice formations are perfectly distinguished on the images.

Weekly charts are used for the estimation of seasonal dynamics and annual changes of ice conditions and for the determination of the extreme borders of the ice cover development. Ice charts serve as the basis for the estimation of ice drift rate and can be used for various predictions.

Recently the Soviet Union as well as the other countries performs the studies on biological resources of the South Ocean. The investigation of the biological structure of the South Ocean demonstrated that existence of the whole complex of sea organisms functioning on the basis of macrozooplankton abundance occurring in the highly productive pelagic zone combined with the natural zone of drift ice. The viability of the whole complex of these organisms are found to depend on ice conditions, which becomes more intensive in summer.

Based on satellite data the monitoring of ice conditions in high latitude zones was carried out. The charts broadcasted by Hydrometeorological Service of the USSR are received by the vessels and by different scientific institutions. The charts thus obtained are registered by graphical table on the magnetic disks and demand future processing. In particular for the performance of monthly analysis of the ice processes in Antarctic region the charts of the average monthly and extremal borders of ice cover development both in the whole South Ocean and in some region are made.

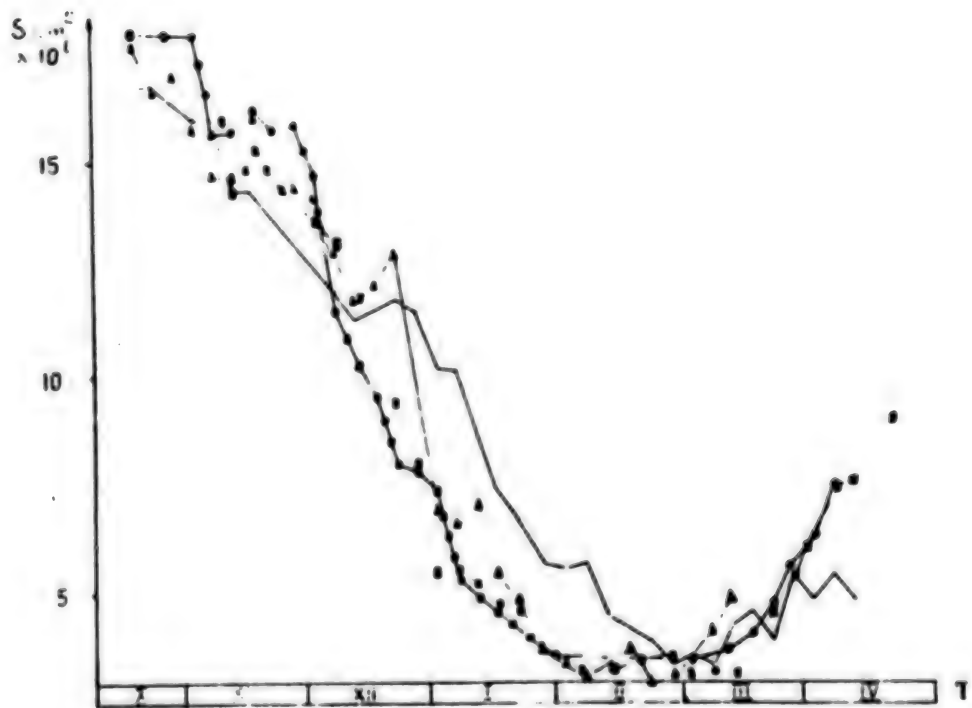


**Fig. 3 Changes of the areas of Antarctic region covered by drift ice in 1980-1984**

—○— 1980-81, —●— 1981-82, —□— 1982-83, —×— 1983-84

The location of the edges of the drift ice is compared with the average year-to-year data. The aquatic areas of waters covered by ice are

calculated. The degree of accessibility of some regions is also evaluated in seasonal and year-to-year aspects. Figure 3 demonstrates the graphical changes of the areas covered by drift ice in 1980-1984. As a rule the maximal development of ice-cover is observed in October. The edge of the drift ice is approximately located at latitude of 60 degrees S. The area covered by ice was 17-18 mln. km<sup>2</sup>. When the Antarctic spring begins the ice area gradually reduces. The most intensive destruction of ice cover is observed in late December-early January. The intermediate maximum observed in late November and December in all years are of interest. By early February the area of the drift-ice reaches its minimal values and composes 2.5-3 mln. km<sup>2</sup>. In the whole the edge of fast shore and drift-ice almost coincides with the slope of slightly mobile ice of the Antarctic regions. By late March a new period of ice formation begins. By the end of observation (in mid-April) the ice area doubles and reaches 6-7 mln. km<sup>2</sup>. In spite of the common tendencies in the process of ice formation in the Antarctic region in some years the several variations in the rate of ice-formation and ice-melting were observed. Thus the presented diagram illustrates the considerable variations in 1983-1984 as compared with previous seasons. It is known, that the first half of the season the ice conditions were more severe. In January and February the area of water was covered by ice by 2-3 mln. km<sup>2</sup> more than usual. In the second part of the season the tendency changed. Figure 4 illustrates the extremal boundaries of drift ice in light period of 1982-1984.

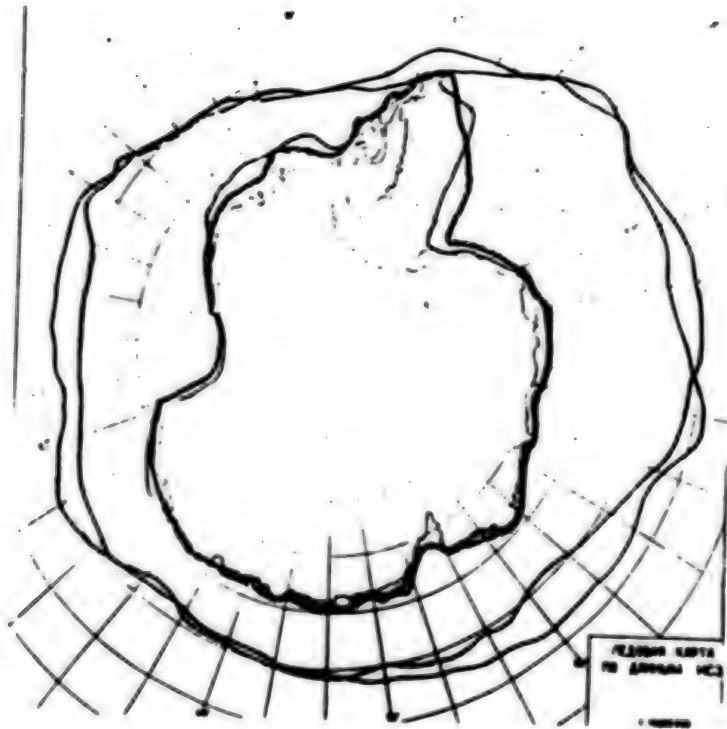


**Fig. 4 Extremal boundaries of drift-ice in season  
~~~~~ 1982-83 and — 1983-84**

In 1983-1984 the maximal development of the ice cover was observed in October-November. From the beginning of October till late November the ice area reduced from 18 to 13 mln. km<sup>2</sup>, which was by 2-3 mln. km<sup>2</sup> less than observed last year. The most significant changes in the location of the borders of maximal development of ice cover were observed in central parts of the Indian and Pacific Ocean sectors. The average monthly edge of October 1983 was located 2-4 degrees southward than that in last year. From the beginning of December 1983 till middle of February 1984 the ice area reduced from 13 to 4 mln. km<sup>2</sup>. During these months more severe ice condition were registered. In December 1983 the ice area was by 2-4 mln. km<sup>2</sup> more than last year. By the end of March-early April 1984 the ice area extended to 5.5 mln. km<sup>2</sup>. In this period in 1983 the process of ice formations was more intensive. By the beginning of April 1983 the area of drifting ice was 7.5 mln. km<sup>2</sup>.

All the above mentioned examples show that the satellites provide the valuable information on distant regions. The results of satellite observations are of great practical value for researches. The material obtained can serve as a basis for improving of the prediction of ice conditions in the Antarctic region.

/08309

Sea Spectra as Determined From Low-Altitude SLAR Images

43070007e Kyoto Selections From INTERNATIONAL ARCHIVES OF PHOTOGRAMMETRY  
AND REMOTE SENSING in English Vol 27 1988 Part 88 pp 58-67

[Article by Konstantin Voliak, General Physics Institute of USSR Ac.  
Sci.38 Vavilov st., 117942 Moscow, USSR, Commission VII]

[Text] ABSTRACT

The analytic composite theory for the surface of Gaussian slope statistics has revealed that backscattering of vertically (V) polarized microwaves from the sea at large angles of incidence might have an azimuthal characteristic, which corresponds to the angular dependence of the small-scale Bragg spectrum, with an accuracy to within the slope variance of long waves. For horizontally (H) polarized radiowaves, the model relates the image speckles to the statistics of spikes in a random surface-wave field. Fourier analysis and photometry of radioimages taken over various seas have allowed us to estimate the spectra of large- and small-scale sea surface waves as well as to study other phenomena imprinted on surface waves.

1. INTRODUCTION

Imaging radars yield principally novel data on the physical state of the sea. The aim of this paper is to develop simple models for image formation by an airborne real-aperture side-looking radar (SLAR) at different polarizations as well as to elaborate experimental methods and data processing techniques to effectively extract sea parameters, particularly wave spectra, from radioimages.

2. THEORY OF MICROWAVE SCATTERING FROM THE SEA SURFACE

Microwave backscatter from highly conducting surfaces, including the sea, depends strictly on polarization. At fairly large angles of incidence,  $\theta$ , the H-polarized backscattered Bragg power is notably weaker than the V-polarized one. Generally the V-polarized power (Fig. 1a) shows up in a scattered field of the first order, which is rather

smoothly modulated by sea surface features. On the other hand, an H-polarized backscatter (Fig. 1b) produces an image formed by randomly spaced bright spots, or by the so-called speckles, whereas the Bragg return is virtually at the noise level. A similar temporal behavior of polarized scattered fields was first established by Long. [1]

The composite theory allows us to decode V-polarized SLAR images of the sea. Assuming that the conventional specular component and the second-order scatter, i.e., depolarization, are negligible at  $\theta > 30$  degrees, we can write a local cross-section of V-backscattering[2]:

$$\sigma_v^*(\theta, \alpha, \beta) = k_0^4 \cot^4 \theta_i |G|^2 W(2k_0 \sin \theta', 2k_0 \cos \theta' \sin \beta), \quad (1)$$

where  $k_0 = 2\pi\lambda^{-1}$ ;  $\cos \theta_i = \cos \theta' \cos \beta$ ,  $\theta' = \theta + \alpha$ ,  $\alpha$  and  $\beta$  are the angles between the smoothed surface and the horizon in the plane of incidence and in the plane normal to the latter,  $\epsilon$  is the dielectric constant,  $W(K, K)$  is the roughness spectrum, the x-axis lies in the plane of incidence.

$$G = [\epsilon(1 + \sin^2 \theta_i) - \sin^2 \theta_i] T_1 \sin^2 \theta' \cos^2 \beta + T_2 \sin^2 \beta, \quad (2)$$

$$T_1 = (\epsilon - 1)(\epsilon \cos \theta_i + \sqrt{\epsilon - \sin^2 \theta_i})^{-2}, T_2 = (\epsilon - 1)(\cos \theta_i + \sqrt{\epsilon - \sin^2 \theta_i})^{-2}.$$

The average cross-section,  $\sigma_v^*$ , is determined by an integral over all the slopes within an irradiated area:

$$\sigma_v^*(\theta) = \iint \sigma(\theta, \alpha, \beta) p(\tan \alpha, \tan \beta) d(\tan \alpha) d(\tan \beta), \quad (3)$$

where, neglecting the shadowing factor,

$$p(\tan \alpha, \tan \beta) = p_0(\tan \alpha; \tan \beta') \cos \theta_i / \cos \theta, \quad (4)$$

$p(\tan \alpha; \tan \beta')$  is the anisotropic probability density of sea slopes along its principal axes, the coefficient  $\cos \theta_i / \cos \theta$  is related to the 'area defect' in the slope distribution, observed at an angle of incidence  $\theta$  [3]. The averaged value of (3) is conventionally computed for an isotropic normal distribution without any areal correction and for a certain (usually isotropic) spectral model. However,  $\sigma_v^*$  can be also evaluated analytically avoiding numerical computations.

## 2.1 Radar Gross-Section Evaluation.

The actual long-wave slopes are small,  $|\alpha|, |\beta| = O(\mu) \ll 1$ , and their distribution is approximately Gaussian [4]. Within a fairly good accuracy  $O(\mu^2)$  for slightly rough seas, i.e., neglecting the slope skewness, we can replace the tangents of small angles in (3), (4) by their arguments. Further assuming  $|\epsilon| \approx 100$  for cm and dm microwaves, the calculation of  $\sigma_v^*$  reduces to a series expansion of  $|G|^2 \cot^4 \theta$  and  $W(2k_0 \sin \theta', 2k_0 \beta' \cos \theta')$  in  $\mu$  and  $|\epsilon|^{1/2}$ , followed by their product averaging over slope distribution (4). Here, we can restrict

ourselves to the terms  $\propto |\epsilon|^{-1/2} \cdot \mu^2$ . The result, accurate to a few per cent, is

$$S(\theta, p) = B k_o^4 (1 + \sin^2 \theta)^2 (2 k_o \sin \theta)^{-2} |1 + (\sqrt{\epsilon} \cos \theta)^2|^4 f(p) M, \quad (5)$$

where  $\theta$  is the azimuthal angle along the principal axes, the typical roughness spectrum is given by the power-law [5]

$$W(k, p) = B k^{-s} f(p), \quad (6)$$

the modulation is expressed by

$$M(\bar{\alpha}_o, \bar{\beta}_o, \bar{\beta}, \beta_o) = 1 + m_1 \bar{\alpha} + m_2 \bar{\beta} + m_{11} \alpha_o^2 + m_{12} \beta_o \alpha_o + m_{22} \beta_o^2 + \propto |\epsilon|^{-1/2} \mu^2, \quad \bar{\alpha} \text{ and } \bar{\beta}$$

are the average slopes, the tilt the variance

( $m_1, m_2$ , and  $m_{11}, m_{12}, m_{22}$ ) modulation transfer functions ( $m.t.f.$ 's) depend evidently on  $\theta$ ,  $|\epsilon|^{-1/2} \mu^2$ ,  $s$ , and  $f(p)$ .

## 2.2 Tilt and Variance Modulation

The m.t.f.'s behave quite differently with respect to  $\theta$ . For instance, at a saturated spectrum (6) of the actual azimuthal factor [3], assuming  $s=4$ ,  $|f'/f| < 0.5$ ,  $|f''/f| < 1$ , the functions  $M(\theta)$  are similar to those in Fig. 2. They are calculated for  $\lambda = 2.5$  cm, i.e. for (cf. [6])  $\epsilon = 50-351$ .

When  $\theta < 70^\circ$  the power scattered from an anisotropic sea is modulated in a complex way by all the slope components. In this case, the backscatter from isotropic waves [2], [7] is slightly sensitive to slopes owing to the small m.t.f.'s, when  $\theta > 71^\circ$ , however,

$|m_1| \gg |m_2|$ ,  $|m_{11}| \gg |m_{22}|$ ,  $|m_{12}|$  . and the modulation arises primarily from the slopes of long waves oriented in the plane of incidence. At grazing angles,  $|m_1|$ ,  $|m_2|$  are proportional to  $\tan \theta$ ,  $\tan^2 \theta$ , respectively. Hence, the modulation by such slopes should predominate over other [7] scatter modulation types, which are somewhat limited. The number of 5 has a very slight bearing on the m.t.f.'s and, as it changes from 3.5 to 4.5, the considered angles are shifted only by 1.5 degrees. These m.t.f.'s occur over a wavelength range up to  $\lambda = 1$  m, while the angles shift slightly towards  $\theta = 90$  degrees.

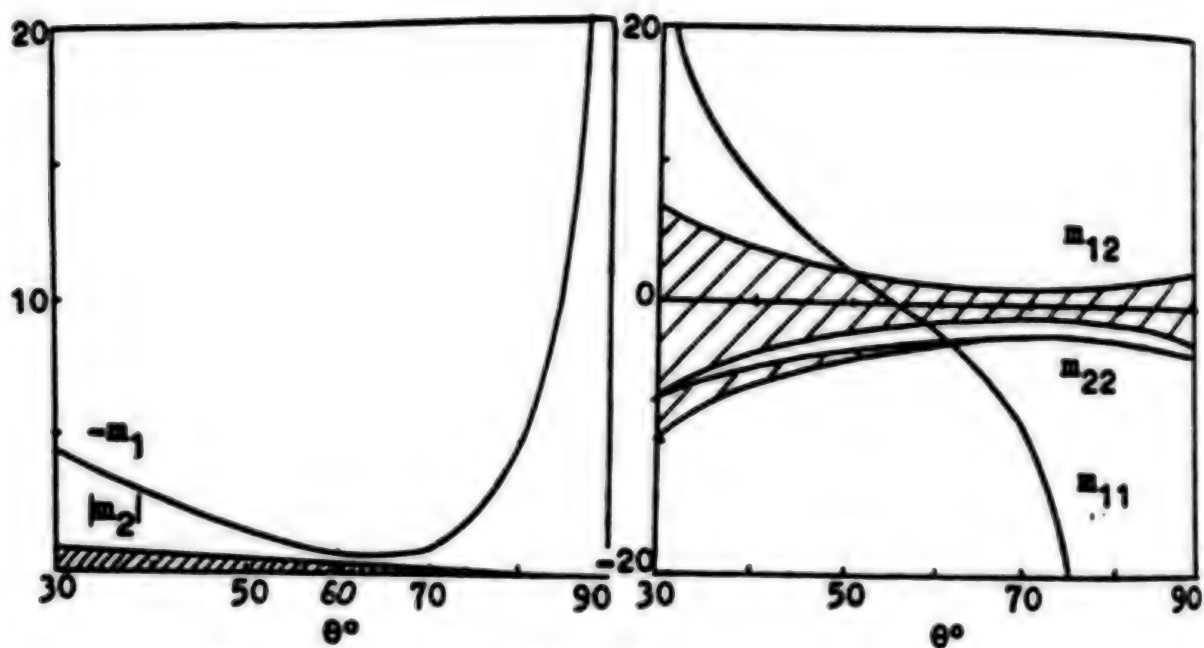


Fig. 2. M.t.f's versus  $\theta$  for  $\lambda = 2.5$  cm.  
 $|f'/\tau| \leq 0.5$ ,  $|f''/\tau| \leq 1$

### 2.3 Radar Measurement of Bragg Resonant Wave Spectra

Another form of (6) yields

$$\sigma^*(\theta, \rho) = (1 + \sin^2 \theta)^{-1} |1 + f(\cos \theta)|^{-1} W(k_a \sin \theta, \rho) [1 + O(\mu, |s|^{-1})]. \quad (7)$$

Thus, by measuring the backscattered power at various azimuths and angles of incidence and by averaging it over the longest sea wavelength, we can define, accurate to an order of long-wave slope variance, i.e., to a few per cent, the directional spectrum  $W(k, \varphi)$  of short resonant waves of  $\lambda = m(k_a \sin \theta)$ . For isotropic long waves, (7) agrees with the numerical findings [2]. It is also clear that (7) implies an accordance between the azimuthal anisotropy of  $\sigma^*(\rho)$  and the angular spreading  $f(\rho)$  (6). For large averaging scales, all the conclusions drawn are also valid, sometimes at the expense of accuracy, for any kind of scatter modulation [7]. For directional spectrum measurements, SLARs and synthetic aperture radars (SARs) are most suitable. If their antenna vertical aperture admits angles  $30^\circ \leq \theta \leq 90^\circ$ , the measured spectral range can be as large as  $\Delta k = 2k(\theta = 30^\circ)$ . The high spatial resolution of SARs and SLARs permits, in principle, a more accurate spectral measurement than is achievable with conventional scatterometers. The azimuth can be varied by changing the aircraft heading.

## 2.4. Long-Wave Spectra From an Image Fourier Analysis

The problem of how an image Fourier-transform can conform to the actual sea is still disputable. It can be resolved, on the basis of the foregoing examination, for angles of 70-80 degrees and moderately developed seas. A SLAR operates as a low-pass filter with a cut-off at

$K_L = 2\pi L^{-1}$ ,  $L$  being resolution. Then, in the first approximation, the images recorded at  $\varphi = \text{const}$  correspond for  $\lambda > L$  to a spatial pattern of the smoothed slope  $a_\varphi = a$  in the azimuthal plane. A Fourier transform of the image yields distribution of  $a_\varphi$  in wave numbers and directions.

Following [8], we examine the transformation of a coherent plane light wave passing through a radioimage modulated in amplitude as

$$I(\vec{R}) = T_0 [1 + m_{so} a_\varphi(\vec{R})], \quad (8)$$

where  $\vec{R} = (X, Y)$  is the coordinate in the image;  $T_0$  is its average transparency;  $m_{so}$  is the mean value of  $m(\cos hY)$ ;  $h$  is the SLAR altitude;  $Y$  stands for the range. The light intensity in an off-axis region in the focal plane of a converging lens is proportional to

$$I(\vec{R}) = I \int \int a_\varphi(\vec{R}) \exp(-i\vec{k}\vec{R}) d\vec{R} |^2, \quad (9)$$

where  $\vec{R}$  is the radius vector in the plane of transform. Measuring intensity (9), we determine the directional spectrum of long-wave slopes  $a_\varphi$ .

## 3. MODEL OF H-RADIOIMAGE FORMATION

At oblique angles of incidence, the Bragg H-scatter may be a few dozens of decibels lower than that of specular reflection and the so-called 'wedge' [10] scatter. The two mechanisms occur only at the surface of breaking or nearbreaking waves. This point is corroborated by numerous experiments, in which a noticeable H-backscattering appears simultaneously with the onset of white capping. A spike of the reflection, even averaged over radar resolution may prove an order of magnitude more intense than the Bragg background and, hence, may produce a saturated density of recording films. Thus, each bright spot should be referred to a site at the sea that has undergone breaking during irradiation. To develop a simple model of the phenomenon, we assume that there exists a certain limiting amplitude of waves. If the amplitude is exceeded, waves are no longer stable and start to break [9]. Then, the speckle statistics in images reduces, in general, to the statistics of overthrows of a two-dimensional random function above a specified height level.

### 3.1. Statistics of a Random Sea Surface

To simplify the solution to the problem, we consider the Gaussian field of sea waves because their actual statistics differs just slightly from the normal case [4]. Most important for us is the mean number of overthrows of the random function  $\zeta(x,y)$  above some appropriate level  $\ell = a$  per unit area. If the level  $a$  is fairly high, the number of overthrows for an anisotropic random Gaussian field is determined by [11].

$$N_a = \left( \frac{\pi}{2} \right)^2 \left( \frac{m_{00}}{m_{11}} \right)^{1/2} (2m_{00})^{-3/2} a \exp(-a^2/m_{00}). \quad (10)$$

where  $m_{ij} = \int \int K K_x^i K_y^j dK_x dK_y$  stands for spectral momenta.

Take simple power-law spectrum (6) in the range  $K_0 \leq K \leq K_1$  as a saturated sea model, where  $K_0$  corresponds to the high-energy component,  $K_1$  is the high-frequency cut-off. This yields the momenta and (10) changes over to

$$N_a = \left( \frac{\pi}{2} \right)^2 B^{-\frac{1}{2}} \left( \frac{f_{00}}{f_{11}} \right)^{\frac{1}{2}} \left( \ln \frac{K_1}{K_0} \right) K_0^3 a \exp\left(-\frac{a^2 K_0^2}{B f_{11}}\right), \quad (11)$$

where  $f_{ij} = \int f(\rho) \cos \rho^i \sin \rho^j d\rho$ .

Hence, we see that the speckle density depends strongly on the typical width  $f_{00}$  of an azimuthal spreading. Another important feature is the exponential dependence of  $N_a$  on the square of breaking wave steepness  $(aK_0)^2$ . It is noteworthy that measurement of speckle density in images is a very special procedure. A more common practice is photometering of an image density. A description of this operation shows that, at Gaussian seas, the mean signal obeys largely the same rules as does the number of spikes.

### 3.2. Current-Induced Variations in the Spike Statistics

If a surface wave runs to an inhomogeneous surface current  $\bar{U} = \bar{U}(x,y)$ , the former and the latter undergo an energy exchange. Waves over an opposite-directed current are supplied by the energy from it, while, in the case of a divergent current, the reverse effect occurs. To analyze the spike statistics of the sea on currents which are due, for example, to internal waves, we use the conservation law of kinematic wave density

$$\nabla(\sigma + \bar{U}\bar{K}) = \sigma_0, \quad (12)$$

where  $\sigma = (gK)^{1/2}$  is the wave frequency at  $\bar{K}\bar{U} = KU \cos \varphi = 0$ . Using (12), we obtain variations in the wave number

$$K' = 4K(1 + (1 + 4U\sqrt{K/g} \cos \varphi)^{-2})^{-1/2} = K(1 - 2U\sqrt{K/g} \cos \varphi) + O(U\sqrt{K/g}). \quad (13)$$

For saturated spectra on the current, the high-energy and the cut-off components shift as  $K_0 \rightarrow K'_0$  and  $K_1 \rightarrow K'_1$ , respectively. Substituting (13) into (10), we derive variations in  $N_e$  on the current  $U$

$$\Delta N_e / N_e \ll -U \cos \phi \left( 1 + \alpha_a k^2 \right). \quad (14)$$

Thus, the speckle density in H-radioimages increases on currents moving against the wind and decreases in the opposite case. In addition, we evaluate the nonlinear effects in the speckle statistics and estimate essential corrections  $\alpha_a k^2$  to the speckle density due to the second-order nonresonant nonlinearity of gravity waves.

#### 4. EXPERIMENTS

##### 4.1. Experimental Procedures

Circular flights, which are conventional in azimuthal measurements [3], have been undertaken. A SLAR operated at  $\lambda = 2.2$  cm was installed aboard the Antonov-24 aircraft of the 'Aeroflot' Co. Due to the high spatial resolution of the instrument we have taken azimuthal scattering characteristics in detail. The flights were performed in the coastal areas of the Pacific near Kamchatka and of the Barents Sea near Kola Peninsula as well as in the Black Sea. The other flights were various 'boxes' and 'stars', similar to that of Fig. 3.

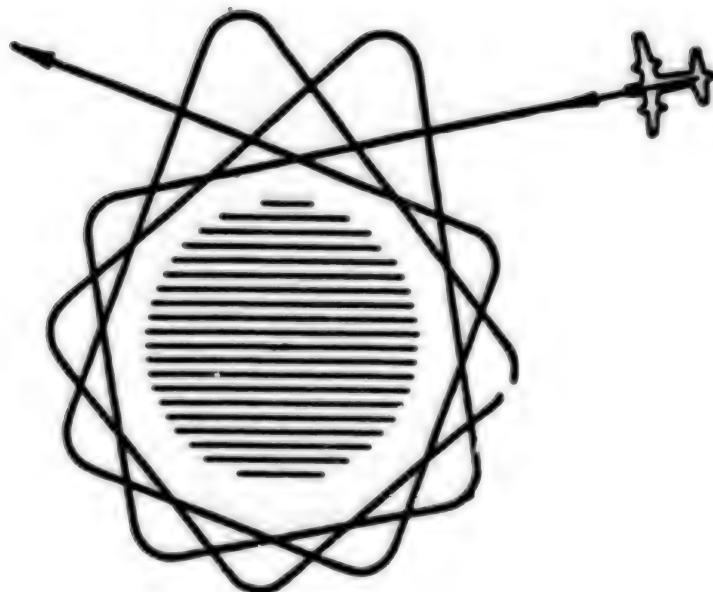


Fig. 3. Aircraft 12-tack flight of the 'rotating box'-type

#### 4.2. Azimuthal Measurements

With stable SLAR parameters, an average image density is proportional to the scattering cross section. Fig. 4 shows  $\sigma_0$  for V-polarized (crosses) and H-polarized (dots) scatter versus azimuth  $\varphi$ . The scattering was averaged over an area of  $500 \times 250 \text{ m}^2$  ( $3 \times 1.5^\circ$ ) at  $\theta = 57^\circ$ , and then normalized to its maximum. The ratios of the circle diameters presented of Figs. 4 a,b to that in Fig. 4 c are 0.1 : 1 and 0.72:1, respectively. The weather conditions shown in the caption were reported by a ship drifting 20 km away from the center of the experiment area.

The azimuthal characteristics have conventionally an axis of symmetry coinciding with the wind direction, so Fig. 4a suggests, for instance, the direction of a calm breeze. Figs. 4b and c differ very strongly in spite of close wind velocities. Thus unlike [3], this velocity is not a single parameter determining the backscatter. Its nature is quite different for different polarizations. Evidently, at V-polarization only Fig. 4c corresponds within a fairly good accuracy to the actual spreading  $f(\varphi)$  for capillary-gravity waves of  $\lambda=1.3\text{cm}$ . According to the theory, this accuracy is provided by a deep azimuthal dependence of and by virtually symmetric scatter related to the wind direction. The other two V-characteristics reproduce  $f(\varphi)$ , involving some distortions due to the skewness of long-wave slopes. While H-scattering is, in practice, isotropic under the calm (Fig. 4a), it is highly anisotropic

even at moderate winds (Figs. 4b, c). Processing the azimuthal characteristics for the H-backscatter in the sector  $\theta = 45\text{--}60$  yields the second spectral momenta and estimates nonlinear skewness and kurtosis of long-wave slopes. It is remarkable that the estimates are in a very good accordance with [12], while those made according to [4] under our experimental conditions, are considerably higher.

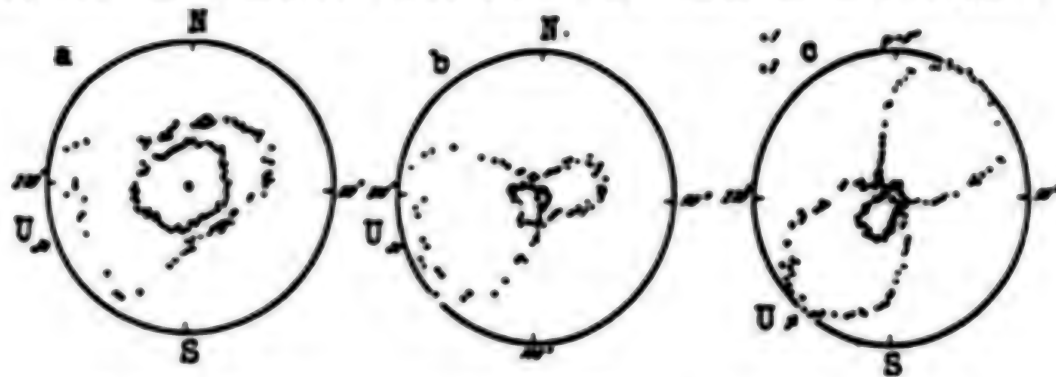


Fig. 4. Azimuthal characteristics  $\sigma(\phi)$  at  $\theta = 57^\circ$ : crosses - V-polarization, dots - H-polarization; (a) calm,  $U = 0$ , (b) steady wind,  $U = 6 \text{ mm}^{-1}$ , (c) gusty wind,  $U = 6 - 8 \text{ mm}^{-1}$

#### 4.3. Fourier Analysis of Sea Radioimages

Two-dimensional Fourier transform of radioimages is observed in the focal plane of a converging lens in a coherent optical system [8]. V-images, taken over each of the 12 tacks of the flight and shown in Fig. 3, were processed in the analyzer. A series of optical spectra is presented in Fig. 5, where each spectrum is placed at the azimuth of an original image. In the center, there is a spectrum of reference grating with  $\lambda = 50\text{m}$ .

A feature of importance to us is the disappearance of waves at azimuths orthogonal to the wind, namely, at  $\varphi = 150^\circ, 180^\circ, 330^\circ$ , and  $0^\circ$  degrees. Conversely, in directions almost collinear to the wind, the waves are clearly pronounced. This confirms the theory asserting the predominant modulation of V-backscatter by long-wave slopes.

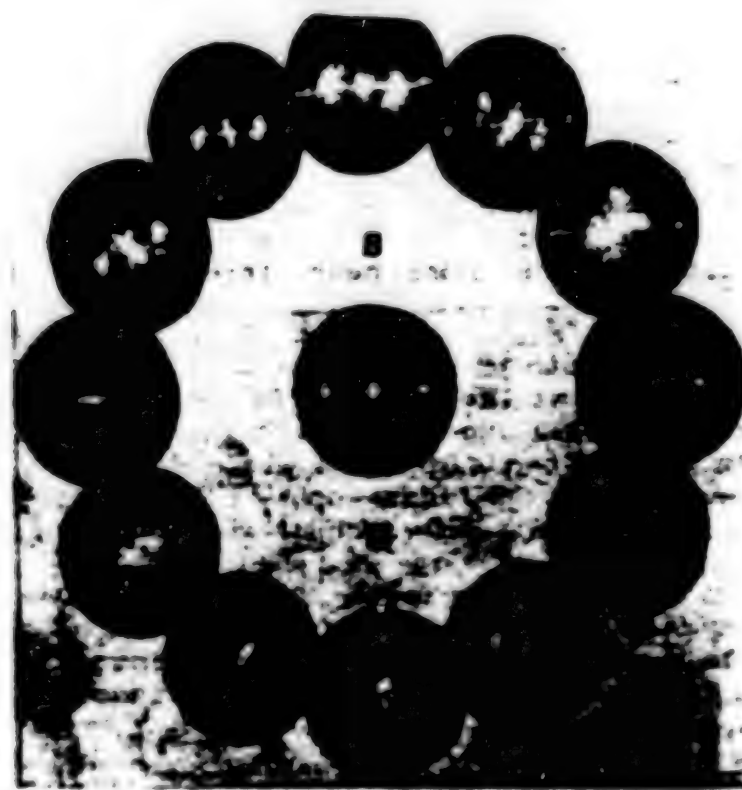


Fig. 5. Optical spectra of the 12 SLAR 'rotating box' tacks

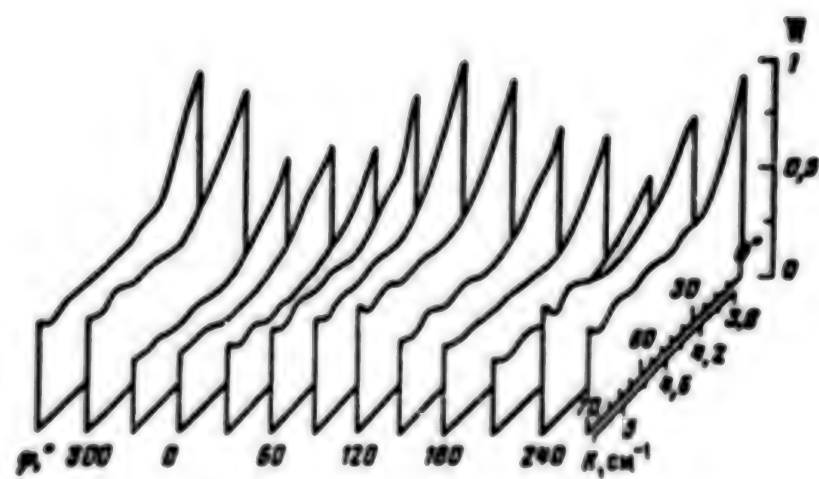


Fig. 6. Resonant-wave spectrum WClO versus azimuth  $\phi$  as determined from the 12 SLAR tacks

#### 4.4 Spectra of Short-Wave Resonant Roughnesses

The radar cross-section for each of the 12 azimuths was determined by measuring the image density versus slant range. Using a transform inverse to (7), the spectral density  $W(k_x \sin\theta)$  was computed. Fig. 6. shows 12 of such spectra cut-off at  $\theta \leq 70^\circ$  to avoid strong modulations and covering the total azimuthal circle. At  $42^\circ \leq \theta \leq 70^\circ$  all the spectra decline with increasing  $\theta$  to obey the universal power-law  $W(k) \propto k^{-0.8 \pm 0.2}$ . Note that these angles cover the wavelengths  $1.2 \leq \lambda \leq 1.7$  cm.

#### 4.5 Nonlinear Wave Interaction as Observed by an Imaging Radar

The typical Pacific radioimages were analyzed in a spectral domain. Part of the obtained spectra displayed several wave systems, some of which originated probably from the nonlinear interaction. Let us consider, for instance, the smoothed spectrum presented in Fig. 8., where one can see three wave systems. Two of them, making angles 55 and -25 degrees with the horizon, are found in other spectra. Hence, they are fundamentals. The third (additional) wave system makes an angle of around 30 degrees with the aircraft heading, and it is just interesting as a probable result of the nonlinear interaction between the fundamentals.



Fig. 7 Smoothed radioimage spectrum and corrected wave vectors near the spatial resonance

To verify the hypothesis, Fig. 8. plots the spatial resonance for the vectors of the additional (central) wave  $k_z$  and of the fundamental

(side) waves  $K_2$ ,  $K_3$ . This plot is superimposed on the equal spectral density lines after corrections, to account for the relative motion of the platform referred to the sea scatterers. It results in the fact that the frequency resonance  $\frac{K_1^{1/2}}{so} + \frac{K_2^{1/2}}{so} = \frac{2K_3^{1/2}}{so}$  is fulfilled within

a very good accuracy, while the considerable phase detuning  $\Delta K = \frac{2\bar{K}_3}{so} - \frac{\bar{K}_2}{so} - \frac{\bar{K}_1}{so}$  is measured from Fig. 10.

It follows from theory that such nonsynchronous waves interact quasistationarily. Thus, the central wave component is expected to have some spatial beats. To check this claim, the spectrum of Fig. 8 was multiplied by a binary filter, which is totally transmitting over a sector 20 degrees oriented along  $K_{40}$  and nontransparent in other directions. The product was Fourier-transformed. The density of the reconstructed image is presented in Fig. 9. Here one can see the spatial beats of a period of 450-700m marked with broken lines. The theoretical spatial period was estimated to be about 500 m, which is close to the beats in the filtered-out image.

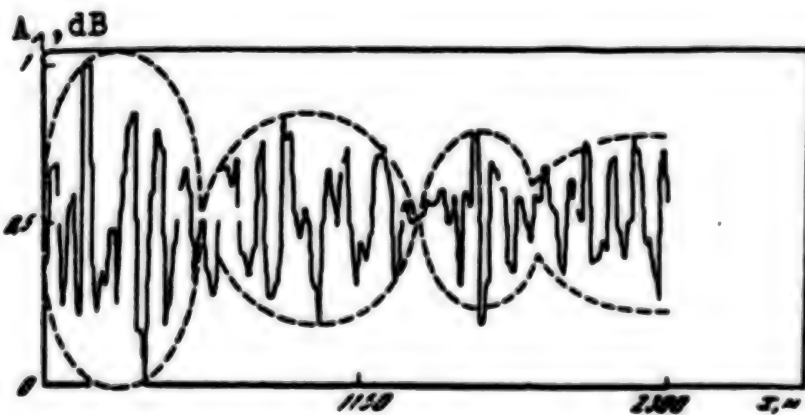


Fig. 8 Spatial Beats of the Central-wave Amplitude as a Result of the Image Processing

## 5. CONCLUSIONS

- (i) The modulation of the sea radioimages of V-polarization, taken at oblique angles, is due to the long-wave slopes in the plane of antenna look.
- (ii) The speckles of H-polarized sea radioimages are explained by the statistics of specular reflections and wedge scatter from steep waves. The speckle structure depends strongly on the directional spectrum and

(ii) The speckles of H-polarized sea radioimages are explained by the statistics of specular reflections and wedge scatter from steep waves. The speckle structure depends strongly on the directional spectrum and nonlinearity of the sea as well as on the inhomogeneous surface currents.

(iii) The developed models provide imaging radar methods to be used for experimental measurement of sea spectra of different scales and for observation of the effects of various atmospheric and oceanic processes.

## 6. REFERENCES

1. Long M.W. On a two-scatterer theory of sea echo. IEEE Trans. Antennas Propagat. AP-22, 667-672, 1974.
2. Valenzuela G.R., Laing M.B. and Daley L.C. Ocean spectra for the high-frequency waves as determined from airborne radar measurements. J. Marine Res. 29, 69-84, 1971.
3. Moore R.K. and Fung A.K. Radar determination of winds at sea. Proc. IEEE 67, 1504-1521, 1979.
4. Cox C. and Munk W. Measurement of roughness of the sea surface from photographs of the sun's glitter. J. Opt. Soc. Amer., 11, 838-850, 1954.
5. Phillips O.M. The Dynamics of the Upper Ocean. Camb. Univ. Press, Lond., 1977.
6. Saxton J.A. and Lane J.A. Electrical properties of sea water. Wireless Eng. 29, 269-275, 1952.
7. Alpers W.R., Ross D.B. and Rufenach C.L. On the detectability of ocean surface waves by real and synthetic aperture radar. J. Geophys. Res. C86, 6481-6498, 1981.
8. Goodman, J.W. Introduction to Fourier Optics. McGraw-Hill, N.Y., 1968.
9. Longuet-Higgins M.S., On wave breaking and the equilibrium spectrum of the wind-generated waves. Proc. Roy. Soc. Lond. A310, 151-159, 1969.
10. Lyzenga D.R., Maffett A.L. and Shuchman R.A. The contribution of wedge scattering to the radar cross section of the ocean surface. IEEE Trans. Geosci. Remote Sens. GE-21, 502-505, 1983.

11. Nosko V.P. Determination of the number of random field overthrows above a fixed level. Teorija Verojatnosti i Jejo Primeneni 24, 592-596, 1979.
12. Longuet-Higgins M.S. The effect of non-linearities one statistical distributions in the theory of sea waves. J. Fluid Mech. 17, 459-480, 1963.

/08309

### Lidar Measurements of Sea Surface Waves

43070007f Kyoto Selections from INTERNATIONAL ARCHIVES OF PHOTOGRAMMETRY AND REMOTE SENSING in English Vol 27 1988 Part 88 pp 68-77

[Article by K.I. Voliak and M.V. Solntsev, General Physics Institute of the USSR Ac. Sci.; 38 Vavilov St., 117942 Moscow, USSR, Commission VII]

#### [Text] ABSTRACT

A lidar method is developed to measure the sea wave spectrum and other sea characteristics by using a narrow amplitude-modulated beam. Some techniques are suggested for determining the slope and curvature variance from a backscattered (reflected) power. The model field experiment was carried out at an oceanographic platform. The experimental data demonstrate that the introduced method is highly effective.

#### 1. INTRODUCTION

To study spatial-time structures of sea waves is urgent for solution of various scientific and applied problems arising in the field of oceanic physics. Remote sensing methods seem to be very appropriate for this purpose. The most highly developed technique of oceanic remote sensing is associated with the use of air-space imaging radars. Now in radiooceanography the so-called synthetic aperture radars [1], recording the coherent backscatter from the sea, or the noncoherent side-looking radars [2] enjoy great favor.

Since the early 1970s laser methods of sea probing have been also developing. They are superior to radiooceanography in several respects. First, lidars can provide higher spatial-time resolution, which is suitable for measuring small-scale waves. For instance, a sharp-focused laser beam permits us to measure waves of a horizontal scale up to 1 mm, while the microwave radar resolution is limited just to several meters.

The duration of a radar pulse is typically from  $10^{-7}$  to  $10^{-9}$  s [3]; accordingly, the spatial resolution is  $15 \div 15$  m. In the optical

range one can produce pulses as short as  $5 \cdot 10^{-13}$  s [4] enabling a resolution of 0.08 mm to be obtained. We observe the principal difference between radar and lidar probings in the reflection of signals by the sea. The radar wave length exceeds often those of the capillary waves, and therefore, various diffraction effects are of importance here. Meanwhile the laser wave length is considerably shorter than any surface one, and the mechanism of laser reflection is reasonably explained in terms of geometric optics. This aspect gives rise to much simpler relations between the statistics of the lidar return and that of the sea surface, compared to radars. One of the important parameters of the lidar return is its average power. As shown theoretically [5], [6], lidar measurement of an average backscattered power at different incidence angles establishes variances  $B_x$  and  $B_y$  of the downwind and crosswind components of the surface slope.

Presently there are two principal ways of oceanic lidar remote sensing, namely, pulse ranging and phase profilometry. The former [7] involves determination of the time delay between sounding and reflected pulses as well as analysis of their shapes and durations. Depending on the experimental facilities and position (for example, on the beam divergence and vertical or slant incidence), we can estimate the significant wave height, the slope probability density, or measure roughly the sea surface profile. Laser measurement of the profile can be also carried out with airborne phase altimeters. Continuous flight altitude measurements permit reconstruction of the surface profile along the flight ground line [8].

An analysis of the state of the art in these methods [9] reveals that the two techniques are effectively applicable to investigation of sea waves as long as 10mm and more. But in many field experiments it is important to study both large-scale and comparatively short waves. A good example of this situation is the interaction between internal and surface waves, where most changes are observed just in the short surface wave spectrum. Further development of laser investigations of cm and dm sea waves requires a finer spatial resolution. In the field of pulse ranging one can decrease the sounding pulse duration. The use of subnanosecond laser techniques calls for faster and, hence, more sophisticated receivers.

## 2. NARROW-BEAM LIDAR RETURN FROM THE SEA SURFACE

Let a laser beam of an intensity  $I(r,0)$ , where  $r$  is the distance from the beam axis and  $0$  is the azimuthal angle, be normally incident upon the sea surface. In the horizontal plane at above-surface elevation  $H$ , there is placed a receiving aperture  $D$  (Fig. 1). The distance between the axes of the beam and the aperture equals  $l$ . The characteristic diameter of a sounding beam is equal to  $d$ . Then introduce the coordinates  $(x,y,z)$  with their origin at the receiver axis. The coordinates  $x,y$  lie in the horizontal plane of an undisturbed surface, and  $z$  is directed upwards. Any point of the surface is defined by its elevation  $\xi(x,y)$  and the slope vector

$$\hat{\rho}(x,y) = (\xi_x = dx/dx, \xi_y = dy/dy) . \quad (1)$$

where  $K = (K_1, K_2)$  is the wavevector of surface random disturbance.

The moments of the directional surface spectrum  $E(k_x, k_y)$  can be written in the form:

$$n_j = \iint E(k_x, k_y) k_x^j k_y^j dk_x dk_y, \quad i, j = 0, 1, 2, \dots \quad (2)$$

where  $\vec{k} = (k_x, k_y)$  is the wavevector of surface random disturbance.

To evaluate the statistics of the return, it is necessary to assume the following: (i) the surface slopes are obviously gentle,  $m_{ad} m_{os} \ll 1$ ; (ii) the altitude is great,  $H D \ll r^2$ ; (iii) the sea return is homogenous within the beam spot,  $nH \ll m_{ad} m_{os}$ ; (iv) the transmitter and the receiver are nearly coaxial  $1/H \ll m_{ad} m_{os}$ ; (v) the beam is narrow,  $nS \ll 1$ , where  $n$  is the density of specular points at surface slopes  $\xi = \theta = 0$ , and  $S$  stands for the spot square; and (vi) the surface is illuminated from the 'far' range,  $D |R| / H \ll n^{-1/2}$ , where  $|R|$  is the average modulus of the radius of surface curvature. Under all these conditions the lidar return from the sea surface is provided by the specular points within the lidar spot. The power returned from a single specular point is

$$P_s = 0.082\pi |\Omega|^{-1} (D/H)^2 \rho_s I(r, \theta). \quad (3)$$

Here  $\rho_s \approx 0.02$  is the sea reflectivity at the normal incidence,  $\Omega$  is the total curvature at the specular point. Let us normalize the point return as

$$P_s^0 = \begin{cases} 1, & \text{if the specular point is placed inside the beam spot,} \\ 0, & \text{if it is outside the spot.} \end{cases}$$

Assuming that the sea surface is a random Gaussian field, one can obtain some statistical quantities: the average power

$$\langle P_s \rangle = \alpha \delta ; \quad (4)$$

the power variance

$$\langle P_s^2 \rangle = \frac{\alpha^2 \langle |\Omega|^{-1} \rangle}{P_s^2 \delta} \iint I^2(r, \theta) r dr d\theta ; \quad (5)$$

and the average normalized return

$$\langle P_s^0 \rangle = \langle |\Omega| \rangle S \delta = nS. \quad (6)$$

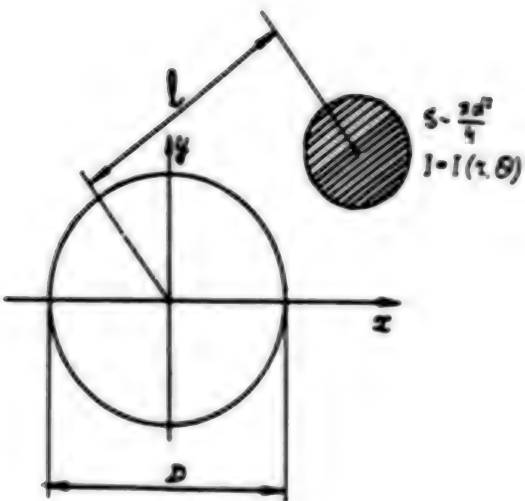


Fig. 1. Horizontal cross-section of the probing geometry.

Here  $\alpha = 0.0825nD^2H^{-2}A_3 P_0$ ,  $P_0$  is the radiated power,  $\delta = 2\pi A_3^{1/2}$ , and  $A_3 = (A_x A_y)^{1/2} = m_{20} m_{02} - m_{11}$  is the surface invariant, which depends on the wave steepness and divergence.

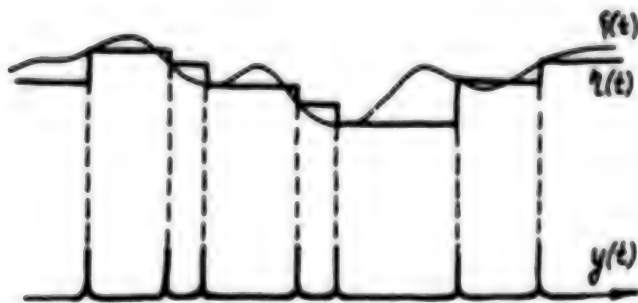


Fig. 2. Discretization of the process  $S(t)$  by a random pulse sequence  $y(t)$ .

Thus, the measurements of  $\langle P_g \rangle$ ,  $\langle P_g^2 \rangle$ ,  $\langle P_g^3 \rangle$  make feasible to determine the sea cross-section  $\sigma$ , the invariant  $A_3$ , and the mean moduli of the curvature and of its reciprocal:

$$\sigma = (\langle P_g \rangle / P_0) 4\pi^{-1} (H/DO)^2, \quad A_3^{1/2} = \alpha / 2\pi P_0, \quad (72, 73).$$

$$\langle |\alpha| \rangle = \frac{a \langle P_s^2 \rangle}{S \langle P_s \rangle} \cdot \langle |\alpha^{-1}| \rangle = \frac{\langle P_s^2 \rangle P_s^2}{a \langle P_s \rangle} \int_0^\infty \int_0^{2\pi} I_s(r, \theta) r dr d\theta^{-1}, \quad (10)$$

respectively.

### 3. PHASE PROFILOMETRY WITH A NARROW BEAM

In the case of phase profilometry, the laser beam is amplitude-modulated with some frequency  $f_o$ . The return is formed by specular points mentioned above. To monitor the profile continuously, the lidar surface spot should be widened, thereby degenerating spatial resolution and averaging surface elevation over the spot. Oceanographers are primarily concerned in the sea spectrum or other statistical quantities rather than in isolated sea elevation records. The problem is, therefore, to reconstruct the statistics of an unknown random sea from an experimental discreet sample corresponding to the specular points.

Let  $\xi(t)$  be a stationary random function of the surface elevation in time (or in space). The discretization of  $\xi(t)$  (cf. Fig. 2) by a random sequence  $y(t)$  produces a new random  $n(t)$ . If  $n(t)$  is of the Poisson distribution with a mean pulse period  $T_o$ , the spectrum  $S_2(\omega)$  of  $n(t)$  depends on the spectrum  $S_1(\omega)$  of  $\xi(t)$  as [10]:

$$S_2(\omega) = \frac{1}{1 + \omega^2 T_o^2} [S_1(\omega + S_o)] \cdot S_o = \frac{2\pi^2}{\pi} \int_0^\infty \frac{(\omega')^2 S_1(\omega')}{1 + (\omega')^2 T_o^2} d\omega'. \quad (11)$$

It is evident from (11) that the discretization of a random process by a pulse Poisson sequence is equivalent to incorporation of a high-pass filter of a cut-off frequency  $\omega_o = \gamma^{-1}$ , which is connected in parallel with the source of 'white' noise of the spectrum  $S$ .

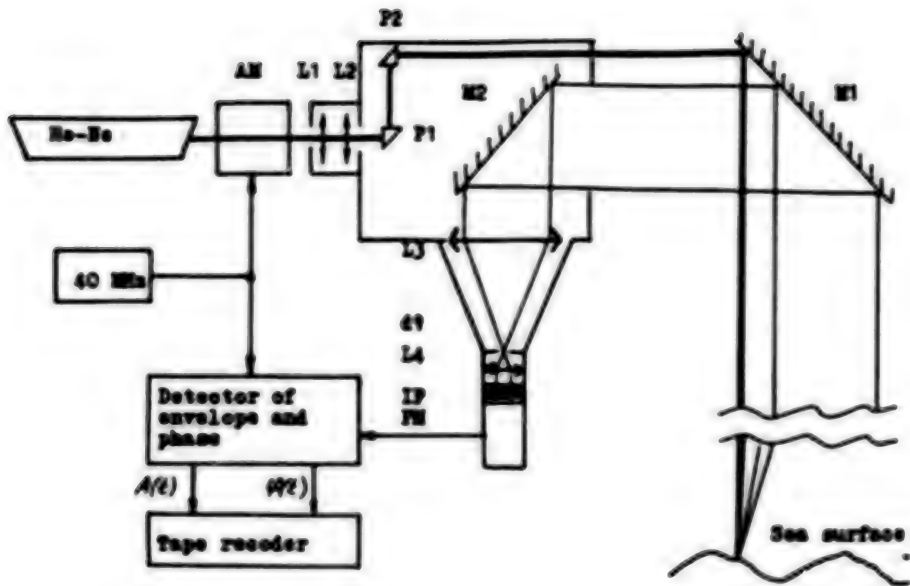


Fig. 3. Experimental set-up.

For an initially limited sea spectrum, where  $S_1(\omega) = 0$  at  $\omega > \omega_m$ , we reconstruct  $S_1(\omega)$  by the following: (i)  $S_2(\omega_1)$  is evaluated at  $\omega_1 > \omega_m$ ; (ii) the 'white' noise spectrum  $S_3(\omega(1 + \omega^2/\tau_b^2))$  is found; and (iii) the initial spectrum  $S_1(\omega) = S_2(\omega(1 + \omega^2/\tau_b^2)) - S_3$  is reconstructed. When probing is carried out from a stable platform, we can show that the sea specular glitter is described rather well by the Poisson statistics, that allows us to apply the suggested algorithm for reconstructing the sea spectrum.

#### 4. EXPERIMENTAL SYSTEM AND SITE

To study the statistics of the laser return from the sea surface, we have designed a lidar shown schematically in Fig. 3. The source was a 15mw CW He-Ne red (633nm) laser LG-79/1. The sounding beam was amplitude-modulated by an electrooptical modulator. The modulation frequency (40 MHz) corresponded to the 2n-uncertainty range of 3.75m. The modulated beam was focused by a system of lenses, L1, L2, and directed vertically downwards through prisms, P1, P2, and an output mirror, M1.

The return reflected by the sea surface and transmitted through mirrors, M1, M2, was focused by a lens, L3, onto a diaphragm, d1, inserted in the image plane to limit, for the sake of better sensitivity, the receiver field of sight. The input aperture, D, was defined by the L3 diameter of 4.7cm, while the d1 diaphragm diameter was from 0.04 to 0.3mm. So the receiver visual angle was 10', i.e., the linear dimension of the sea

site visible through the diaphragm was from 0.7 to 5 cm. The return beam cut-off by the field diaphragm was made to pass through a collimator, L4, and an interference filter, IF, then it was registered by a photomultiplier, PM. The radiopulses of frequency 40 MHz from the PM output were fed to a detector of envelope and phase. The analog envelope and phase signals from the detector were recorded by a Brüel and Kjaer 7005 tape recorder. The signals were also processed using a DISA 56 N11-type mean-value meter, a Brüel and Kjaer 7005 spectrum analyzer, and a CLANP 0270 computer.

The lidar experiments were conducted during May-June 1987 at an oceanographic platform located in the Black Sea 500m off the Crimea coast. Under various hydrometeorological conditions, we carried out 70 series of 20-minute measurements. The distance between receiving telescope and the sea was 16m. Some of the experimental series were accompanied by in situ measurements with a standard wire waverecorder.

## 5. DATA ANALYSIS AND DISCUSSION

After processing the return envelope in accordance with (7)-(10), we evaluated  $\sigma, \Delta_z = (\bar{A}_x \bar{A}_y)^{1/2}$ ,  $\alpha = \langle |\alpha| \rangle^{1/2}$ , and  $R = \langle |R| \rangle^{1/2}$ , then analyzed their dependence on the wind velocity,  $W$ . Spectral processing of the phase signal and its correction (11) allowed us to determine the sea spectra under various winds. The results were checked partly by wire waverecords and compared to the data reported elsewhere. The sea cross-section versus the wind velocity for different sounding spots is plotted in Fig. 4. The value of  $\sigma^2$  for vertical incidence falls rapidly with the wind strength and it varies from 0.5 to 0.01, when  $W$  changes from 1 to 12 m/s. For comparison, we show here the data [5] obtained with an airborne green (530 nm) Nd: TAG lidar.

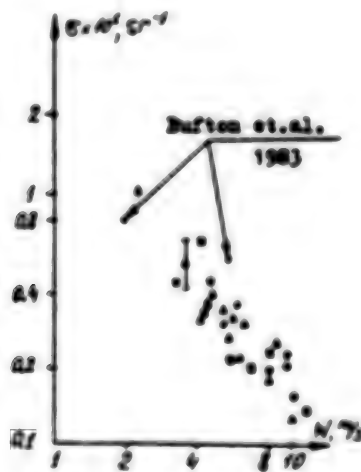


Fig. 4  $\sigma$  versus  $W$ .

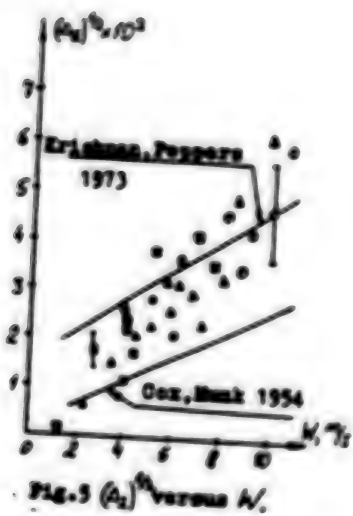


Fig.5  $(P_d)^{1/2}$  versus  $N/\%$ .

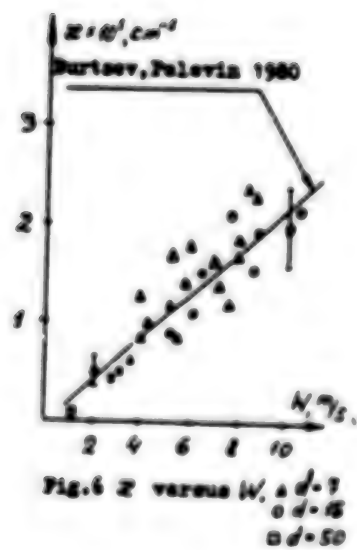


Fig.6  $Z$  versus  $N, \times 10^3$

$\circ d=15$   
 $\square d=50$

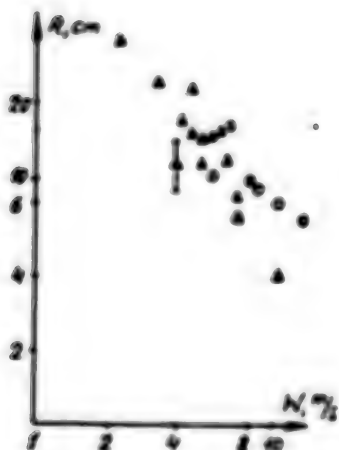


Fig. 7  $R$  versus  $W$ .

Assuming the Gaussian sea statistics, we can readily evaluate the product  $\sigma_x \sigma_y$  of slope variances from  $\sigma^2$ . Fig. 5 sketches the relation  $p$  between  $\sigma_x \sigma_y$  and  $W$ , as well as  $\Delta^{x,y}_{\text{CWD}}$ , which is derived from semiempirical [11] relations  $\sigma_x^2$ <sub>CWD</sub>,  $\sigma_y^2$ <sub>CWD</sub> and evaluated from a model [12] spectrum. As seen, our data are in a satisfactory agreement with the results cited. Figs. 6,7 show the experimental graphs  $\mu_{\text{CWD}}$  and  $R_{\text{CWD}}$ , respectively. Fig. 6 also gives the semiempirical [13] relationship  $\mu_{\text{CWD}}$ . The errors present in Figs. 4 through 7 are related to the imperfect lidar graduation. The variations in experimental data may be partly attributed to several uncontrollable factors, i.e., to duration and length of wind fetch, wind turbidity, differing temperatures of the air and sea, etc. Notice also that, at the widest sounding spot of 5 cm dia, correct measurements of  $X$  and  $R$  are possible only under rather slight ( $W < 4$  m/s) winds because under stronger winds the specular point density increases sharply and the condition (v) of narrow spot (Sect. 2) is no longer fulfilled. Figs. 8a,b exemplify different sea spectra, where we demonstrate: (i) the spectrum of an initial phase signal; (ii) the phase spectrum corrected in accordance with (11); and (iii) the waverecorder surface elevation spectra, respectively. A comparison of all the spectra exhibits good coincidence of the rough lidar and recorder data up to frequency of 1.25 Hz. After correction the upper limit of the coincidence shifts to around 2.5 Hz.

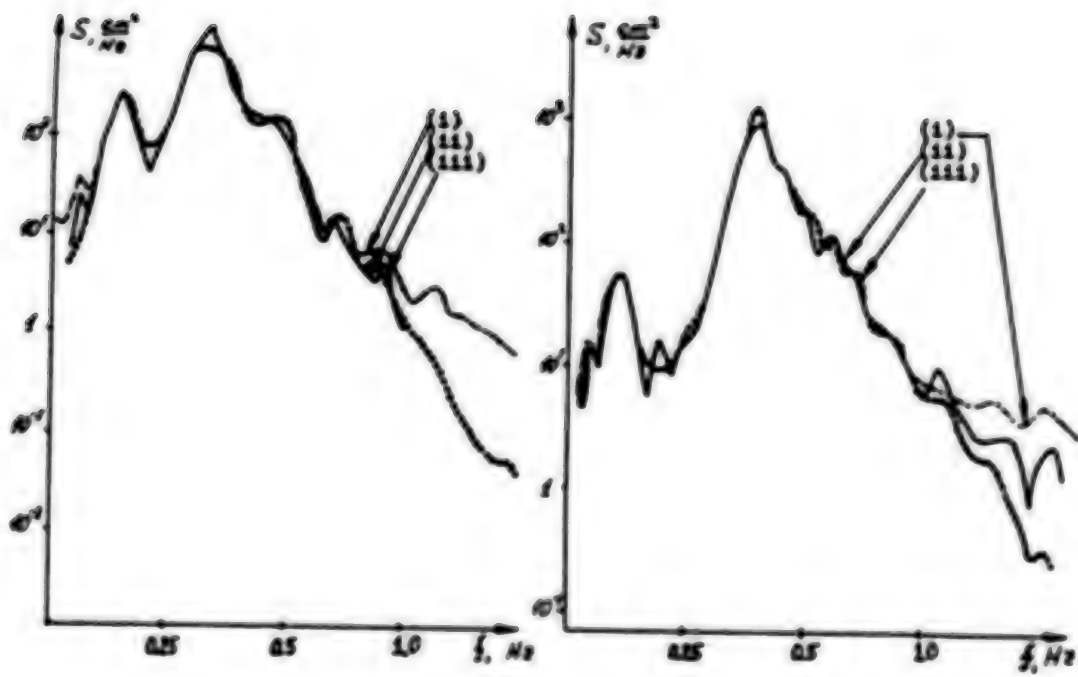


Fig. 8 Examples of the spectrum reconstruction.

Thus, the suggested method enables a noticeable progress to be made in lidar remote measurements of the high-frequency sea waves and of the slope variance and the curvature of a disturbed sea.

#### References

1. Vesely J.F. and Stewart R.M. The observation of ocean surface phenomena, using imagery from the SEASAT synthetic aperture radar: An assessment. *J. Geophys. Res.* C87, 3397-3430, 1982.
2. Alpers W.R., Ross D.B. and Rufenach C.L. On the detectability of ocean surface waves by real and synthetic aperture radar. *J. Geophys. Res.* C86, 6481-6498, 1981.
3. Skolnik M., Ed. *Radar Handbook*. McGraw-Hill, N.Y., 1970.
4. Prokhorov A.M., Ed. *Laser Handbook*. Sovradio, Moscow, 1978.
5. Buffon J.L., Hoge F.E. and Swift R.N. Airborne measurements of laser backscatter from the ocean surface. *Appl. Opt.* 22, 2603-2618, 1983.

applications in tropical countries such as India where perennial cloud cover in many parts of the country precludes the utility of optical/IR sensors. Owing to these advantages India also is planning at present for its own space borne microwave remote sensing mission (with the Synthetic Aperture Radar (SAR) forming an important component by 1993-94).

## 2. DATA PRODUCTS GENERATION AND DEMAND:

When the distribution of data products began in early 1980, the remote sensing technology in India was in its initial promotional phase. Satellite data products generation and supply were a few hundreds in 1980.

In the last few years, the number of users requiring the data products increased at a fast pace. Initially, the major users were from within the Department of Space, which is the nodal agency in India for developing and promoting remote sensing technology. Gradually, the other Central Government agencies also started using data products. During this period, to bring out the user awareness, seminars were organised, presentation made, workshops held, courses conducted, pilot projects completed, results presented to decision makers, etc. These promotional efforts have had a telling effect on the growth of demand. Now Central and State Government agencies are the major users. Many of the universities have started teaching remote sensing and have post-graduate diploma courses on the subject. The growth in the number of users also has been substantial.

With this large growth in users, the demand for data products also increased substantially. While in 1980, about 30-40 products requests per month were processed, the number increased to more than 900 products per month in 1987. The demand in the last few years and the corresponding supply is shown in Fig. 1.

## 3. SATELLITE DATA PROCESSING:

With such a multiple satellite data processing program, hundreds of gigabytes of data are to be handled every day. The processing steps involved in handling satellite data are reception, archival, storage of 'information on data', and its retrieval, processing of the data to convert it to a usable form using computers, photo processing equipments; distribution, application/analysis of such data, maintenance of such facilities, etc. Allied steps are training of personnel, conception and execution of national level projects to use the data. (Fig. 2 and 3)

TABLE 1. COMPARISON OF SATELLITE/SENSORS VOLUMES

| Satellite/<br>Sensor                | Type                                   | No. of Pixels X<br>No. of scan-<br>lines (Apprx.) | Pixel<br>size<br>(in mts) | Area<br>cover-<br>age<br>(Apprx.<br>in Kms) | No. of<br>Bands | No. of scenes<br>acquired/day<br>(Average)<br>(Land Area) | No. of<br>MB/Scene<br>/Band<br>(Apprx) |
|-------------------------------------|----------------------------------------|---------------------------------------------------|---------------------------|---------------------------------------------|-----------------|-----------------------------------------------------------|----------------------------------------|
| Landsat/<br>MSS                     | Electro-<br>Mechani-<br>cal<br>Scanner | 3240 x 2400                                       | 56x79                     | 105 x 185                                   | 4               | 25 - 30                                                   | 7.5                                    |
| Landsat/                            | Electro-<br>Mechani-<br>cal<br>Scanner | 6320 x 6000                                       | 30x30                     | 105 x 170                                   | 7               | 25 - 30                                                   | 36                                     |
| SPOT<br>(Panchro-<br>matic)         | CCD                                    | 6000 x 6000<br>to 8500                            | 10x10                     | 60 x 60<br>to 85                            | 1               | 15                                                        | 36                                     |
| SPOT<br>(Multi-<br>spectral)        | CCD                                    | 3000 x 3000<br>to 4250                            | 20x20                     | 60 x 60<br>to 85                            | 3               | 15                                                        | 9                                      |
| IRS<br>LISS-I                       | CCD                                    | 2048 x 2400                                       | 72.5x72.5                 | 148.5 x 174                                 | 4               | 35                                                        | 4                                      |
| IRS<br>LISS-II                      | CCD                                    | 2048 x 2400                                       | 36.25 x<br>36.25          | 74.25 x<br>87                               | 4               | 140                                                       | 4                                      |
| NOAA<br>series<br>Met.<br>Satellite |                                        | 2048 x 4096                                       | 1 Km x<br>1 Km            | -                                           | 5               | 4                                                         | 8                                      |

To handle the large increase in products supply, a multi billion dollar program is under execution at NRSA, which envisages going in for newer, technologically advanced, faster systems. Firstly, large volume data calls for a well thought out archival policy where only useful data are archived.

Next, an integrated information management system in the form of an electronic data base is planned to be implemented which serves as an external user interface while at the same time controlling the internal data flow and production. This system is designed such that it serves as the master assigning jobs to all the slave work centres.

The data processing systems so far have been using the 'Conventional' approach where in the data is first transferred from high density tapes to disk and then the data is corrected in Array Processors. This poses limitations in throughput and utilizes system resources less efficiently. To overcome this, using an I/O computer connected to the conventional processor, the input/output speed is enhanced and more efficient utilization of resources achieved. In yet another innovation, a Master Flexible System (MFS) is being designed and implemented, which shall have the capability to process all types of sensor data. This is

essential in our environment, where the demand for different types of products from different sensors may vary over time and such a MFS can act as a 'load' balancer.

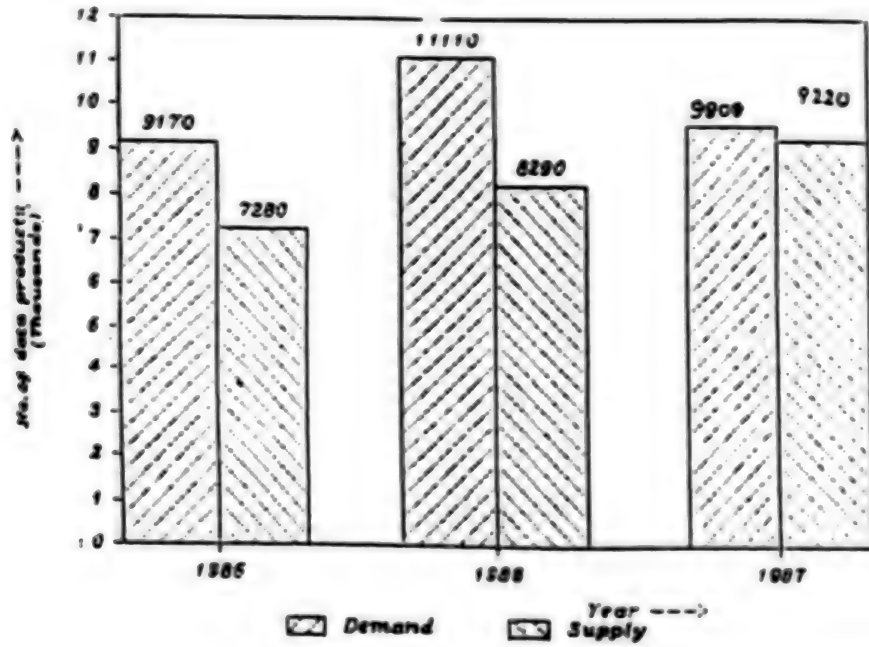


Fig. 1 Demand and Supply of Data Products

Large percentage of the data products required are photo products; hence the program envisages going for large volume production using roll film recorders, automatic photo-processing machines and the building of a modern, controlled, dust free photo processing laboratory.

### 3.1 POLICY FOR THE ARCHIVAL OF DATA:

The archival of satellite data has been in the form of raw data on High Density Tapes, quick look Video Cassettes, Quick Look Films, User Computer Compatible Tapes (CCTs), 240mm Negative/Positive B/W or Color master films.

The High Density Tapes (HDTs) contain data from Landsat MSS, RBV, TM, SPOT, Metsat as well as IRS data.

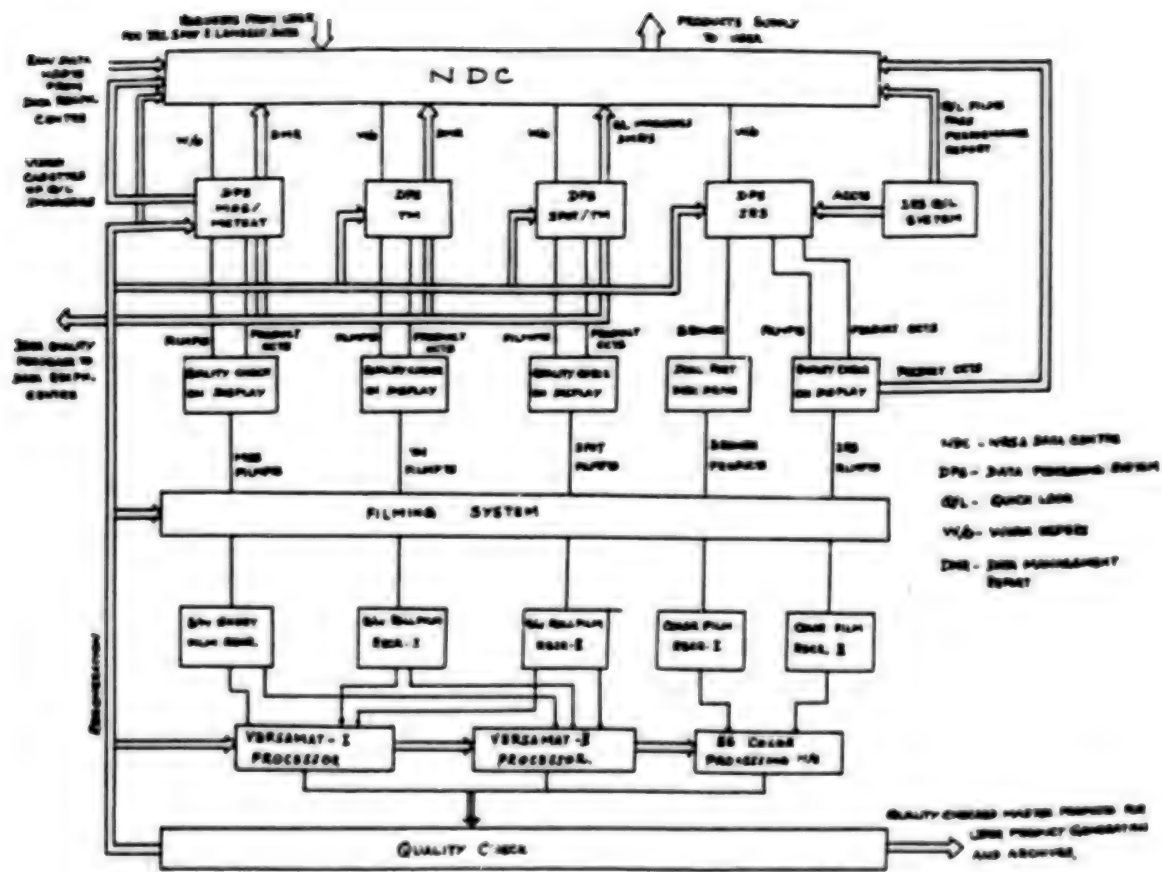


**Fig. 2 Master Data Products Generation: Data Processing, Filming and Photoprocessing**

Enormous amount of data had been archived in the last 5 years. (Table 2 and 3) The policy so far, had been to acquire and archive as much data as possible. With the increasing volume of data, it became apparent that a suitable archival policy had to be worked out and implemented. Accordingly, after wide consultations, a draft archival policy has been worked out, which when implemented will

- ensure that an archive of representative and useful satellite imagery of India exists, is maintained and is accessible;
- ensure that selected scenes from the existing data set are not lost;
- reduce the tape storage and tape consumption to manageable proportions.

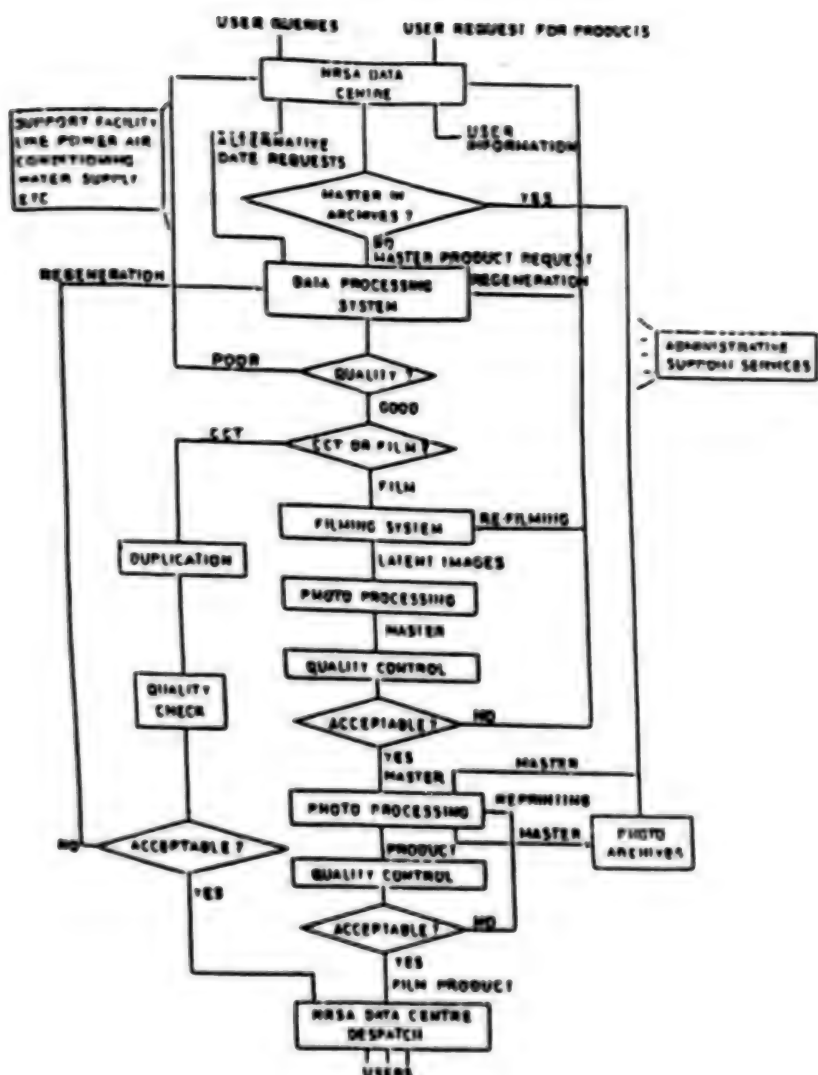


Fig. 3 Data Products Generation Flow

The three tier criteria for archival is as follows:

Tier 1: Within a week of acquisition, the HDTs having technical reproduction problems will be identified. These will not be considered at all for archival.

Tier 2: After a year of acquisition, data to be retained will be subject to the criteria that only when 5 or more scenes in a pass have less than 40 percent cloud cover, the data of that pass shall be retained in the archives. Before destroying the weeded out HDTs adequate notice will be given to the user community to indicate whether they have any need for the data identified to be removed. During such weeding process it will also be ensured that sufficient data for Target Sites are available.

Tier 3: After 5 years of acquisition the following data only will be retained:

- i. One pre-monsoon coverage of India
- ii. One post-monsoon coverage of India
- iii. Disaster affected areas
- iv. Data at the required frequency for Target Sites

Table 2. ARCHIVED LANDSAT QL AND CCT DATA

| Satellite & Sensor | Archive Medium & Data Format  | Date Range of Archive Data   | Approx.No. of Frames |
|--------------------|-------------------------------|------------------------------|----------------------|
| Landsat 4&5<br>MSS | 70 mm<br>Film rolls           | Sept.1982 to<br>Mar.1985     | 33,500 frames        |
| Landsat 4&5<br>MSS | Quick Look<br>Video cassettes | April 1985 to<br>August 1985 | 5,900 scenes         |
| Landsat 4&5<br>MSS | Quick Look<br>Video cassettes | Feb.1986 to<br>Oct.1986      | 20,800 scenes        |
| Landsat 2,3<br>MSS | 1600 bpi<br>Digital Tape      | Nov.1979 to<br>Dec.1982      | 650 scenes           |

### 3.2 INTEGRATED INFORMATION MANAGEMENT SYSTEM:

NRSA Data Centre is the focal point of data products generation activity. It is the interface between the user agencies and NRSA. It handles the data products requirements of all the users both internal and external. The primary function of NDC are User assistance, data archival, User order processing and data dissemination in response to user requests. The user interface with NDC typically includes both general enquiries about the data availability and ordering procedures as well as requests for data covering specific areas. NDC also provides to

any user, on request, the information on the status of his order or account. It enables the visitors to view Quick Look data and make use of reference facilities such as catalogues, orbital calendars, etc.

Table 3. ARCHIVED LANDSAT HDDTs

| Satellite & Sensor | Archived Medium & Data Format | Date Range of Archive Data | Approx.No. of Frames |
|--------------------|-------------------------------|----------------------------|----------------------|
| Landsat 4&5 MSS    | HDDT                          | Aug.'82-Oct.'84            | 1,50,400 scenes      |
| Landsat 5 TM       | HDDT                          | June'84-Nov.'84            | 6,250 scenes         |
| Landsat 5 TM       | HDDT                          | Mar.'85-Nov.'85            | 15,600 scenes        |
| Landsat 5 TM       | HDDT                          | Jan.'86-Oct.'86            | 17,000 scenes        |

The volume of information being handled is enormous. Currently, NDC is operating in a semi-automatic, semi-annual mode. Because of large growth in demand, it is planned that the entire activities of NDC is computerised and handled through the data base. This can be achieved through a multi satellite, Integrated Information Management System (IIMS). IIMS is a system to store, manage and retrieve information of several Users of the system as a resource for their mutual benefit and for several purposes. IIMS will also be used as a production controlling, monitoring system work centre wise and also create job orders for various work centres. The system will be based around two VAX processors. NDC data base operations are very critical. The information to be dealt with is voluminous and prompt information retrieval is desirable to answer the Users queries within reasonable time. To meet this criticality, it is necessary that system should have no 'down time' virtually. To ensure this, the system has a redundant processor, redundant intelligent I/O server and sufficient number of disk drives. Data processing computer system will be connected to this system through Ethernets Local Area Network. The Gateway will connect Decnet nodes on the Ethernets network to Remote Users for information retrieval. This system will store and retrieve data kept in by several Users such as DATA RECEPTION, DATA PROCESSING UNITS, PHOTOLAB and DATA CENTRE. Using the Ethernets link; information such as type and details of the products to be generated, HDT No., priority of products, products generated, quality of products, acquisition and data processing information, system status, etc., can be exchanged between this system and the various Data Processing Computers, Photoprocessing, Filming System, Quality Control, Data Acquisition, Data Archival, etc.

#### 4. CONCLUSION:

With the completion of the activities relating to the augmentation programme the Data Products supply is expected to be streamlined and will have a Turn Around Time (TAT) of within 7 days for 50 percent of

the products and within 21 days for the balance. It will also be possible to cater to increase in user demand for any one type of sensor products with the corresponding decrease in any other sensor products. It will also ensure guaranteed supply of products in case of emergency and the data products quality is also to be better. While, going through this programme it will also be ensured that future expansion can be easily done.

Till about a couple of years back, the facility available for digital analysis of the Remote Sensing data was practically not existent in the country. To overcome this situation, 5 Regional Remote Sensing Service Centres along with two Associate Centres which can perform high throughput digital analysis have been established. It is likely that in the next few years the digital analysis of satellite data will increase manifold and Remote Sensing will be used in an operational mode regularly.

/08309

### Real Time SAR Processing Techniques

43070008b Kyoto Selections from INTERNATIONAL ARCHIVES OF PHOTOGRAMMETRY AND REMOTE SENSING in English Vol 27 1988 Part 89 pp 184-190

[Article by Roland Schotter, DORNIER SYSTEM GmbH, P.O.B. 1360 D-7990 Friedrichshafen, Federal Republic of Germany]

#### [Text] Abstract

Spaceborne Synthetic Aperture Radar systems provide raw radar data information at high data rates of 10 Mwords per second. Real time SAR processors, therefore, must perform more than 1 giga-operations (multiplications, additions) per second in order to generate images from the raw data. Since conventional computer systems are not able to cope with these requirements DORNIER has developed real time SAR processors on the basis of a modular pipeline concept.

The processing pipeline is built up to standardized hardware modules which are required for digital signal processing of two-dimensional data. These modules show identical electrical and mechanical interfaces so that each hardware module can be used in any place of the pipeline.

The paper presents the basic principles of the real time modular pipeline concept and its processing rate requirements for real time SAR processing applications. The implementation of some of the most important modules like Fast Fourier Transformation, correlation, interpolation and data memory is described.

Finally, a short outlook on further applications of the pipeline processing concept is given.

## Introduction

Synthetic Aperture Radar images (SAR images) of the earth are an important tool for many scientific ranges and application related problems. Due to the fact that radar waves are able to penetrate even though strong clouds at very low attenuation, SAR images are available day and night independent of weather conditions.

SAR data can be applied in a multiple way. In oceanography theories on the origin and extension of ocean waves can be investigated. Limits between iced and iceless areas can be detected by means of SAR images as well. This facilitates for example finding optimum ship navigation courses and the operation of ocean platforms in polar areas. Since icebergs are detectable in SAR images, SAR information is also predestinated to be applied in iceberg warning.

The scattering coefficient for radar waves mainly depends on the water content of the illuminated objects. Therefore, conclusions on the growth conditions of vast agricultural areas can be derived from the radar images (wheat and tobacco fields, detection of forest damages). Geological structures are often clearly visible in SAR images so that radar images can be used in this field, too. This applies mainly for the exploration of hardly accessible areas.

Further applications can be found in overall ship control (200 miles zones, environmental oil pollution monitoring on sea), in archeology and glacier research.

Most of the above mentioned applications require real-time conversion of SAR raw radar data into images for its efficient use. For this reason DORNIER has implemented a digital real-time SAR processor for earth exploration in the framework of a BMFT/DFVLR contract. The missions ERS 1 (C-band) and X-SAR (X-band) are intended to be the first applications of the developed SAR-processor.

## The SAR System

The complete SAR system consists of a sidelooking radar and a SAR processor which converts raw radar data into SAR images. The basic geometry of the SAR is shown in Fig. 1. The radar antenna travelling at uniform speed illuminates a certain swath on ground which returns radar echos to the antenna according to its reflectivity. These signals are converted in several steps from the carrier frequency band into the baseband by the receiver. The SAR processor transforms the raw radar data into images which have to be analysed according to the relevant application. The system control data (orbit altitude and velocity, disturbances of the antenna trajectory, etc.) are also used by the processor during the generation of SAR images.

Fig. 2 shows a block diagram of the most important components of a SAR system. These components are basically used both for airborne as well

as for onboard SAR systems. However, there are some differences concerning the processing of the raw radar data which can either take place onboard the carrying aircraft or in a ground station. In the latter case the radar data have to be transmitted by means of a telemetry system, as it will be done for ERS 1 and X-SAR.

### The Real Time SAR Processor

The signal processing task of a real-time SAR processor is characterised both by complex algorithms to be implemented as well as by high input data rates. Even the most advanced computer systems are presently not able to solve this task by means of software programs.

Fig. 3 shows the block diagram of a SAR processor. In a first step the demodulated radar signals are converted into digital information. Usually, real and imaginary I/Q data are used in the baseband for the representation of the amplitude and phase of the radar signal. Afterwards, the range compression of the raw data is performed. The linear range migration effect of the signal energy has to be compensated before the azimuth compression and look summation can take place. The "corner turn memory" converts the processing direction from range into azimuth. The azimuth processing is succeeded by the "post-processing." In this unit the processing is changed to range direction, again. Additionally, the correct pixel mapping of the compressed radar data is done in this unit.

The "Doppler Estimator" and "FM Estimator" units derive the characteristics of the azimuth reference function either from the radar data itselfs or from the orbit and attitude data of the antenna.

Concerning processing rate requirements in terms of millions of arithmetic operations per seconds (MOPS) under real time conditions, range and azimuth compression (see Fig. 3) are the most demanding units within the processor. Given the ERS 1 SAR parameters, roughly 900 MOPS are necessary for range compression in the frequency domain, whereas 350 MOPS must be performed for azimuth compression using the SPECAN algorithm.

### Processor Implementation

A pipeline architecture as shown in Fig. 4 is most suitable for realtime digital SAR processing. The raw radar data enter the pipeline at the left hand side and are transformed--step by step--into the focussed image. This structure can be well compared to a manufacturing line in which the final product is assembled at different stations working at the same time on products which show different degrees of completeness.

The processing pipeline consists of digital hardware modules like Fourier transformation, interpolation, lowpass filter, twodimensional data memory, complex multiplication etc., the sequence and number of which are determined by the algorithm to be implemented by the processor. Several identical pipelines can be used in parallel if the

requirements in terms of processing speed cannot be met by a single channel.

The processing parameters of each pipeline module are provided by the assigned pipeline controller. These controllers compute local module control parameters from some global control information which is received and distributed by the supervisor controller.

The processor hardware was implemented under the aspect that each specifically designed hardware module must include enough commonality and flexibility to make it a part of a more general signal processing hardware family. This concept allows the functional modules to be used at several places of the processor or even supports the implementation of different image processing tasks (e.g., other SAR algorithms, pattern recognition, etc.) at very low development cost by using the same hardware modules in different arrangements.

All hardware modules incorporate identical electrical and mechanical interfaces in order to guarantee full modularity within the pipeline. Power saving CMOS technology has been chosen as far as possible to cover applications which suffer from lack of electrical energy (e.g., mobile processing in aircrafts, etc.). 16 bit word length of both the real and imaginary data channel is offered by all modules allowing the hardware to handle the full dynamic range of present SAR systems.

Some features of the more important modules of the pipeline SAR processor are described in detail in the subsections below.

#### High speed storage unit:

Intermediate storage of data frames is a most important function of any kind of image processing. In a SAR processor these memories are used during corner turning, look summation, recorner turning and test pattern generation. In order to cover the above applications a universal memory board has been developed which allows for writing and reading line based data in both azimuth and range direction. The length of a line can be programmed within the limit of 256k words. The memory boards can easily be cascaded if more than 256k words of memory size is required for a specific application.

Dynamic NMOS memory chips and Advanced Low Power TTL control circuits are used for the board the mechanical size of which conforms to double eurocards. A read/write speed of up to 3 Mwords/sec could be achieved at a power consumption of 3.2 Watt only. Refresh circuits for the dynamic NMOS chips are included on the board.

A complete memory system (e.g., corner turn memory) for data frames of  $1024 \times 256$  words is built up of three memory boards and a simple controller board which provides the correct input/output interface and some trigger signals, which tell the memory boards when to read or write data frames.

### Finite impulse response (FIR) filter:

FIR filters are widely used for low pass filtering, bandpass filters in combination with a complex premultiplication, digital interpolation and correlation. In a SAR processor all functions mentioned above are required at different places of the pipeline.

A FIR filter offering programmable length of up to 256 samples has been developed using CMOS multiplier/accumulator circuits and CMOS/TTL control logic. The board is able to perform all functions described above. In case of low pass filtering the output data can be subsampled by noninteger factors. The filter coefficients can be downloaded from the assigned pipeline controller. Up to 256 different filter sets can be stored at a time.

The maximum input data rate is given by the internal 20 MHz computation clock and the selected filter length.

### Fast Fourier transformation (FFT) module:

A radix 2 decimation in time algorithm has been chosen for the high speed FFT module. This unit shows the following features:

- complex input/output 16 bit I / 16 bit Q
- programmable FFT length (2 up to 4096)
- FFT or inverse FFT selectable
- data weighting function loadable from external source
- programmable gain
- complex butterfly operating at 15 MHz
- full CMOS technology

A 4k FFT can be performed at a rate of 600 Hz whereas a shorter length of 32 runs at almost 140 kHz.

There is a wide range of applications for this module. Within the SAR processor both range and azimuth compression rely on this function in case of longer replica lengths of the respective reference function. For shorter replica lengths also a time correlation solution might be selected as the proper hardware choice.

A prototype real time SAR processor for 1024 range samples of range compressed SAR data has been built on the basis of the pipeline architecture as described above. This processor is able to handle both ERS 1 and X-SAR data by simply initializing the processor according to the specific requirements of the actual SAR. The power consumption of the complete processor amounts to 120 watt thus demonstrating the

efficiency of the hardware concept also in terms of electrical power requirements.

#### Further SAR Processor Activities

The developed SAR processor has proven the feasibility of digital real-time SAR signal processing. An operational SAR processor including range compression and the Mean Doppler and FM Estimator units is presently being developed for the ground station of the X-SAR project.

A Quicklook processor for airborne SAR processing (DOSAP) is also being designed and developed within 1988. This processor will include additional functions for motion compensation.

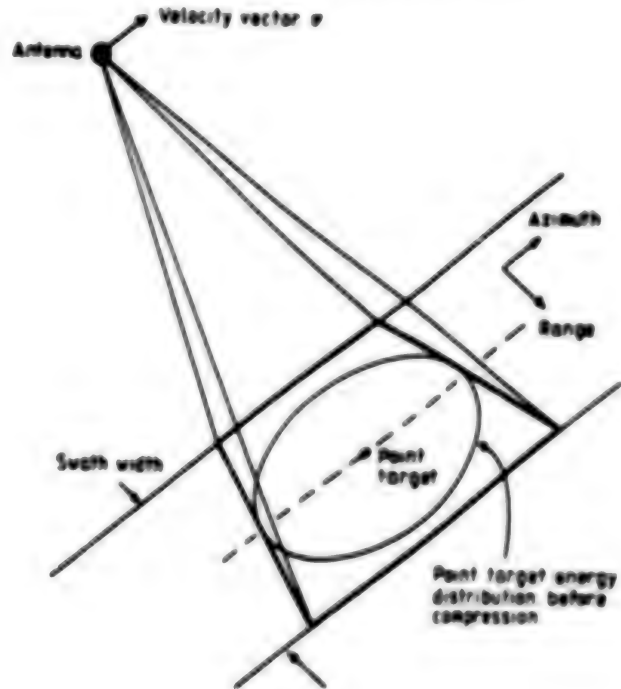


Fig. 1. Basic SAR Geometry

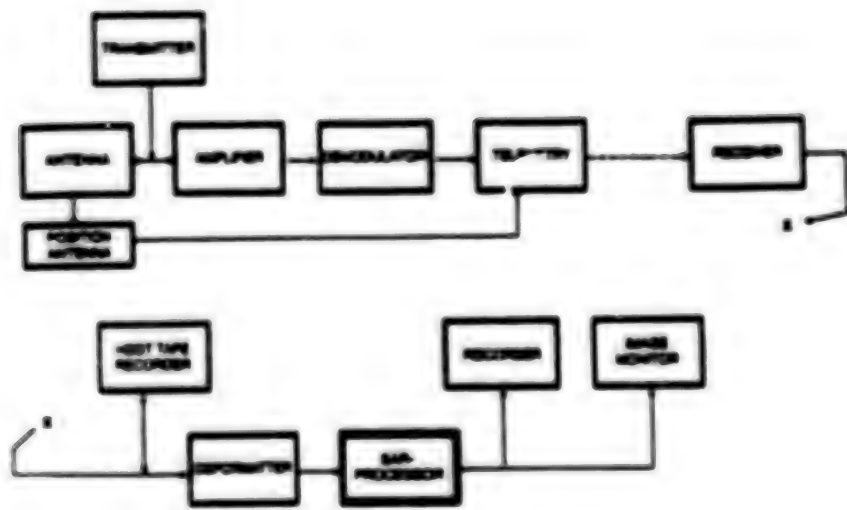


Fig. 2. Block Diagram of SAR System

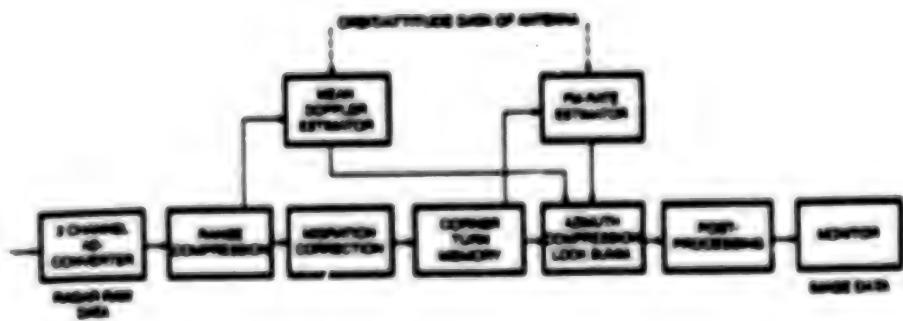


Fig. 3. SAR Processor Functions

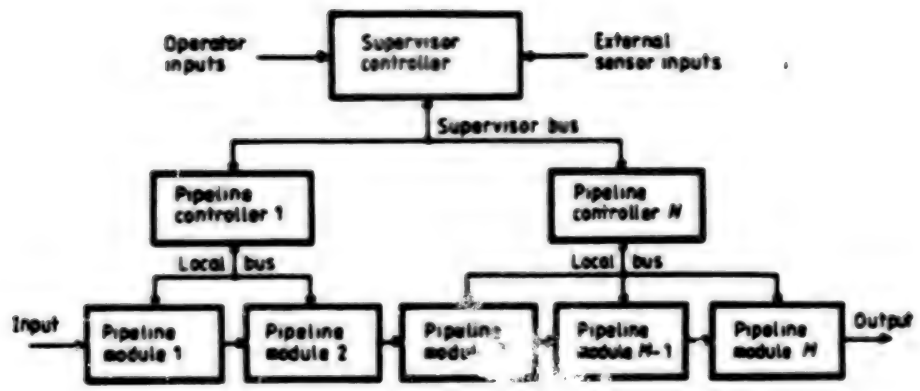


Fig. 4. Block Diagram of Pipeline Architecture

/08309

Simulation of ERS-1/OPS by the Use of Airborne Spectroradiometer

43070008c Kyoto Selections from INTERNATIONAL ARCHIVES OF PHOTOGRAMMETRY AND REMOTE SENSING in English Vol 27 1988 Part B9 pp 277-286

[Article by H. Watanabe, T. Osanai, Japex Geoscience Institute, Inc., 2-17-22. Akasaka, Minato-ku, Tokyo Japan, Commission Number VII]

[Text] 1. Introduction

Several sets of OPS (Optical Sensor) bands to be mounted on Japanese ERS-1 (Earth Resources Satellite-1) were simulated and evaluated. Simulated data were produced by the use of ASR (Airborne SpectroRadiometer) of GER (Geophysical Environmental Research, Inc., USA). Data acquisition was conducted in Death Valley, California and in Comb Ridge, Utah. Evaluation of these simulated data contributes to the finalization of OPS specification. In this study, ground truth using field spectrometer IRIS was also conducted to check ASR data.

2. Acquisition of ASR data and ground truth by IRIS

(1) Description of ASR

ASR that we used in this study is capable to measure radiance, along the track line (Image data is not available for this sensor). Major parameters of ASR are listed in Tab. 1.

(2) Description of data acquisition

Aircraft is AZTEC-E, and the two test sites, Death Valley and Comb Ridge, were selected, considering the degree of vegetation cover and the types of soil/rock. Major parameters of data acquisition are listed in Tab. 2. Airborne data acquisition was conducted from May 24 to May 27 for Death Valley, on May 31 and June 1st for Comb Ridge, both in 1986. During the flight radiance, data on the ground surface were measured by the use of IRIS with equal time interval in order to correct the incident solar energy. After preliminary check of ASR data, ground truth using IRIS was conducted for the targets which are located at the

cross points of two track lines and also for the targets including interesting spectral curves.

### (3) Analysis of rock sample

Some rock samples, against which we measured on site-spectra by IRIS, were sent back to Japan. Samples including clay minerals or carbonates rock were analysed by XRD; carbonate and evaporites, by X-ray fluorescence analysis; and volcanics, micro scope using thin section.

### (4) Comparison between ASR data and field spectra by IRIS

For ASR data, only radiance data were available. so, all the data were divided by the spectra that is supposed to have no spectral absorption. They will be called pseudo-reflectance data hereafter, and they are compared with a set of IRIS spectra for the corresponding site. One example is shown in Fig. 1. This site is basically an outcrop of limestone partially covered by low vegetation. However, absorption at 2.35 um is well expressed both on ASR and IRIS spectra.

### (5) Comparison between IRIS spectra and analysis of rock samples

Example for limestone is shown in Fig. 2. As shown in this figure, IRIS spectra, XRD and X-ray fluorescence analysis indicate the existence of calcite. In almost all the results, IRIS spectra and analysis of rock samples are consistent.

## 3. Simulation of ERS-1/DPS

### (1) Flow chart for simulation

Flow chart is shown in Fig. 3. In this flow, the attenuation of the solar energy from the aircraft to ERS-1 is supposed to be negligibly small, based on the results by the LOWTRAN 5 simulation.

### (2) Analysis of ASR data

#### 1) Check of level of radiance data

DN values of ASR data were converted to radiance data by the conversion table supplied by GER. For the short wavelength infrared (SWIR) region, radiance spectra by ASR, IRIS and LOWTRANS 5 are shown in Fig. 4. ASR and IRIS spectra show similar curves and LOWTRAN 5 is also very similar except the regions of water absorption.

#### 2) Estimation of noise

GER measured the dark current of ASR by shutting out incident light. From these results, noise for ASR is estimated negligibly small in comparison with ERS-1.

### 3) Correction of solar energy difference caused by data acquisition time

Data acquisition of ASR were conducted between 10 a.m. and 3 p.m. in local time. This caused the difference in incident energy to ASR. so, by the use of IRIS measurement of solar energy during the flight, ASR radiance data were fitted to that at 10 a.m. in mean solar time.

### (3) Execution of simulation

After above mentioned procedure, simulation was executed by the flow chart in Fig. 3. The 256 ( $2 \times 2 \times 2 \times 4 \times 4 \times 2$ ) sets of simulation parameters were tried for 6 categories listed in Tab. 8. The supervisors were selected as they show respectively characteristic spectra. Classification was executed for the data showing typical spectral features, and also for those showing intermediate features. Two examples of the results are shown in Tab 4-a and 4-b.

### (4) Evaluation of the results

#### 1) Number of bands

Rate of correctly classified data significantly decreases when the number of band changes from 5 to 3.

#### 2) Band width and noise

Rate of correct answer is higher for narrower band width for the cases of no noise data. However, if the noise for ERS-1 level is added, this rate shows the highest value for the band width of 100nm through 150nm. This tendency becomes unclear for the case of 3 bands or for the 6 bits data.

#### 3) Data acquisition time

For the data with noise, the rate of correct answer is lower at 10 a.m. than noon. This tendency is more significant for 5 band case than for 3 band case.

#### 4) Data with typical spectra and miscellaneous data

For miscellaneous data, the above-mentioned tendencies become ambiguous.

#### 5) Number of bits

Decrease in bit number from 8 to 6 is equivalent to noise addition

### (5) Recommendation for ERS-1/OPS

From the above evaluation, following specification is recommended:

1) Band width: 100nm (for the actual S/N)

2) Central wavelength

5 bands [2.08, 2.15, 2.20, 2.33, 2.38 $\mu$ m]

4 bands [2.08, 2.20, 2.33, 2.38 $\mu$ m]

3 bands [2.08, 2.20, 2.33 $\mu$ m]

5 bands are the most recommendable, because the rate of correct answer decreases significantly in other cases.

3) Bit number

8 bit data are preferable

#### (6) Discussion

1) In this study, we have not discussed visible and near infrared (VNIR)

2) ASR data were limited to VNIR and 2 $\mu$ m region. However, this region is also important.

3) Actual specification of ERS-1/OPS is slightly different from the recommendable specification. So, continuous evaluation effort of this specification will be needed.

#### (7) Acknowledgement

This study was funded by Technology Research Association of Resources Remote Sensing System (RRSS). We would like to express our thanks to RRSS.

Table I. Major Parameters of ASR

VNIR                   $0.4\mu\text{m}$  -  $1.00\mu\text{m}$   
 number of bands      512  
 band width             $1.5\text{nm}$   
 detector              31

SWIR 1.952 $\mu$ m - 2.494 $\mu$ m  
 number of bands 64  
 band width 8.6 $\mu$ m  
 detector PbS

**IFOV**

|             |          |
|-------------|----------|
| Along track | 0.172deg |
| Cross track | 1.72deg  |

Interval of Data Acquisition  
0.033sec      10 data are integrated to be 1 record for along track  
                  (0.33sec interval for 1 record)

Aerial Photo for Tracking  
One shot for every 10 records by 35mm film

Table 2. Specification of Flight Lines and Altitude for ASR Data Acquisition

**Death Valley**

| Abs Alt<br>[ft] | Alt. fm<br>ground<br>[ft] | Spatial<br>resolution<br>[mxm] | No. of<br>Lines | Total Line<br>Length<br>[km] |
|-----------------|---------------------------|--------------------------------|-----------------|------------------------------|
| 4,000           | 2,000                     | 20.1 x 18.3                    | 33              | 408.0                        |
| 10,000          | 8,000                     | 25.6 x 73.2                    | 15              | 129.6                        |
| 18,000          | 16,000                    | 32.9 x 146.4                   | 14              | 185.6                        |
| Total           |                           |                                | 62              | 732.2                        |

**Comb Ridge**

| Abs Alt<br>[ft] | Alt. fm<br>ground<br>[ft] | Spatial<br>resolution<br>[m xm] | No. of<br>Lines | Total Line<br>Length<br>[km] |
|-----------------|---------------------------|---------------------------------|-----------------|------------------------------|
| 6,500           | 2,000                     | 20.1 x 18.3                     | 23              | 259.2                        |
| 12,500          | 8,000                     | 25.6 x 73.2                     | 5               | 64.0                         |
| 20,500          | 16,000                    | 32.9 x 146.4                    | 12              | 19.2                         |
| Total           |                           |                                 | 40              | 342.4                        |

Table 3. Parameters of Simulation

1. Supervisors only (195) , Data including misc data (396)

2. with / without noise

3. 8 bits / 6 bits

4. bandcombination (central wavelength, in  $\mu\text{m}$ )

case1      2.05, 2.15, 2.20, 2.33, 2.38

case2      2.08, 2.20, 2.33, 2.38

case3      2.08, 2.20, 2.33,

case4      2.06, 2.19, 2.34 (RRSS plan)

5. band width

50 / 75 / 100 / 150 [nm]

6. data acquisition time

10 A.M./ 12 A.M.

Table 4-a. Example of Simulation

Central wavelength    2.08 / 2.15 / 2.22 / 2.33 / 2.38  
 Band width            50  
 Bit number            8  
 Time                12 AM  
 (Supervisors only, without noise)

| A \ B | 1  | 2  | 3  | 4  | 5  | 6  | 7  | 8  | 9* |
|-------|----|----|----|----|----|----|----|----|----|
| 1     | 24 | 0  | 0  | 0  | 0  | 0  | 0  | 0  | 0  |
| 2     | 0  | 36 | 0  | 0  | 0  | 0  | 0  | 0  | 0  |
| 3     | 0  | 0  | 42 | 0  | 0  | 0  | 0  | 0  | 0  |
| 4     | 0  | 0  | 0  | 24 | 0  | 0  | 0  | 0  | 0  |
| 5     | 0  | 0  | 0  | 0  | 21 | 0  | 0  | 0  | 0  |
| 6     | 0  | 0  | 0  | 0  | 0  | 16 | 0  | 0  | 0  |
| 7     | 0  | 0  | 0  | 0  | 0  | 0  | 15 | 0  | 0  |
| 8     | 0  | 0  | 0  | 0  | 0  | 0  | 0  | 17 | 0  |

A : Actual Class

B : After Classification

9\* : unclassified

rate of correct answer for all data      100%

rate of correct answer for limestone      100%

Table 4-b. Example of Simulation

Tab.4-b Example of Simulation

Central wavelength 2.06 / 2.19 / 2.34  
 Band width 100  
 Bit number 6  
 Time 10 AM  
 (Misc data, with noise)

| A \ B | 1  | 2  | 3  | 4  | 5  | 6  | 7 | 8  | 9* |
|-------|----|----|----|----|----|----|---|----|----|
| 1     | 32 | 8  | 1  | 5  | 1  | 1  | 0 | 0  | 2  |
| 2     | 13 | 26 | 7  | 13 | 0  | 21 | 0 | 12 | 1  |
| 3     | 0  | 0  | 37 | 3  | 0  | 2  | 0 | 0  | 0  |
| 4     | 5  | 4  | 8  | 38 | 0  | 3  | 0 | 0  | 0  |
| 5     | 0  | 2  | 0  | 1  | 22 | 4  | 0 | 5  | 11 |
| 6     | 0  | 4  | 4  | 3  | 0  | 27 | 0 | 3  | 0  |
| 7     | 11 | 6  | 2  | 12 | 0  | 0  | 7 | 0  | 2  |
| 8     | 0  | 0  | 0  | 0  | 1  | 0  | 0 | 23 | 3  |

A : Actual Class

B : After Classification

9\* : unclassified

rate of correct answer for all data 53.5%

rate of correct answer for limestone 28.0%

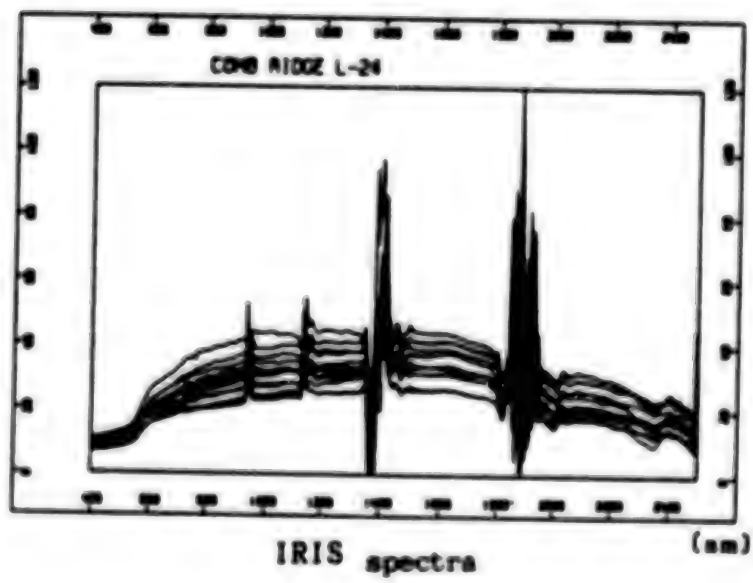
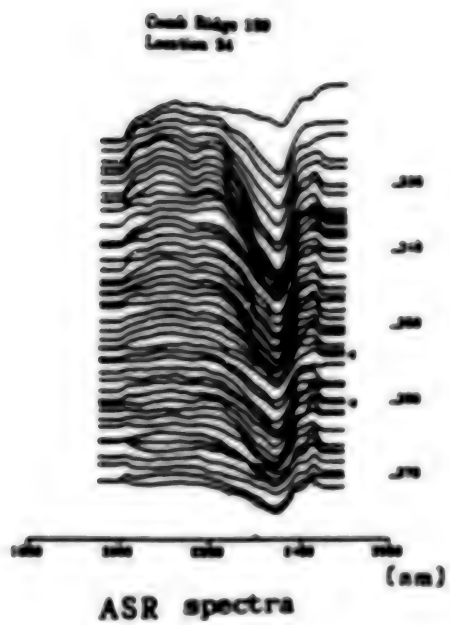


Fig. 1. ASR Pseudo-Reflectance Data and IRIS Reflectance Data for the Site Including Limestone

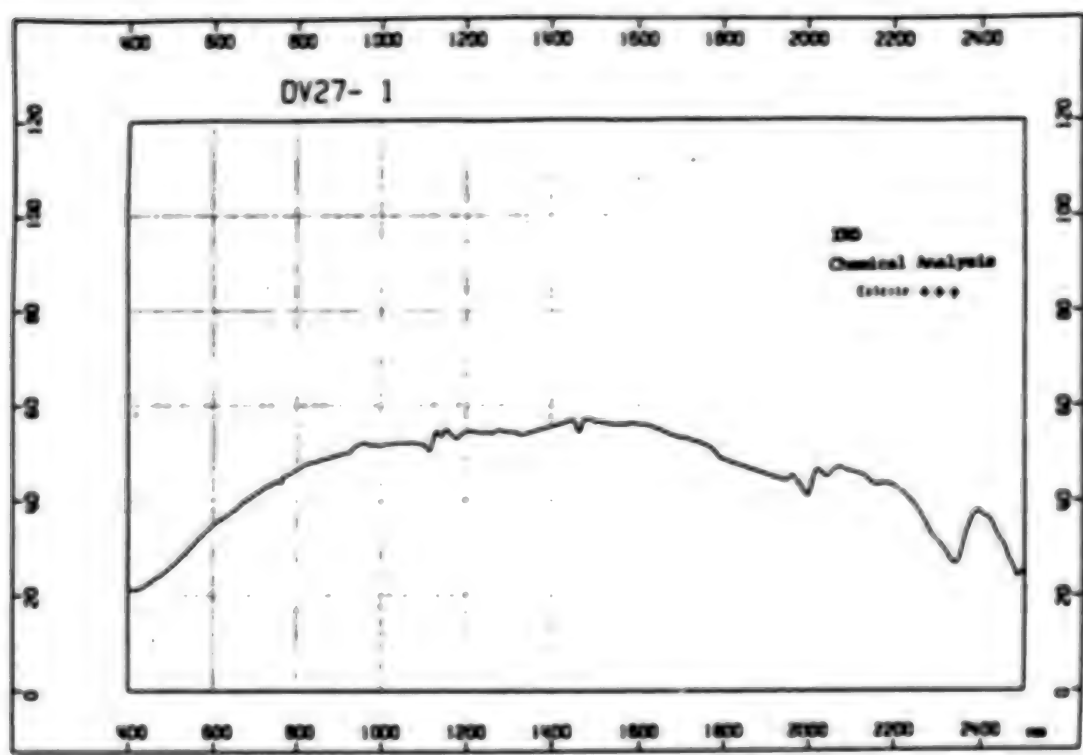


Fig. 2. IRIS Reflectance Data of Limestone and Results of Rock Analysis

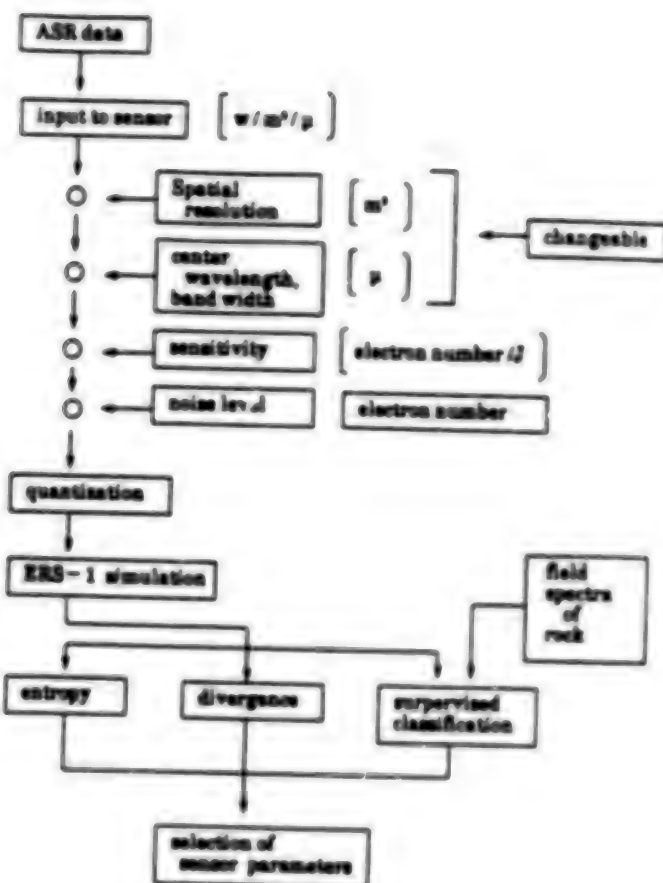


Fig. 3 Flow Chart for the Evaluation of ERS-1/DPS Specification

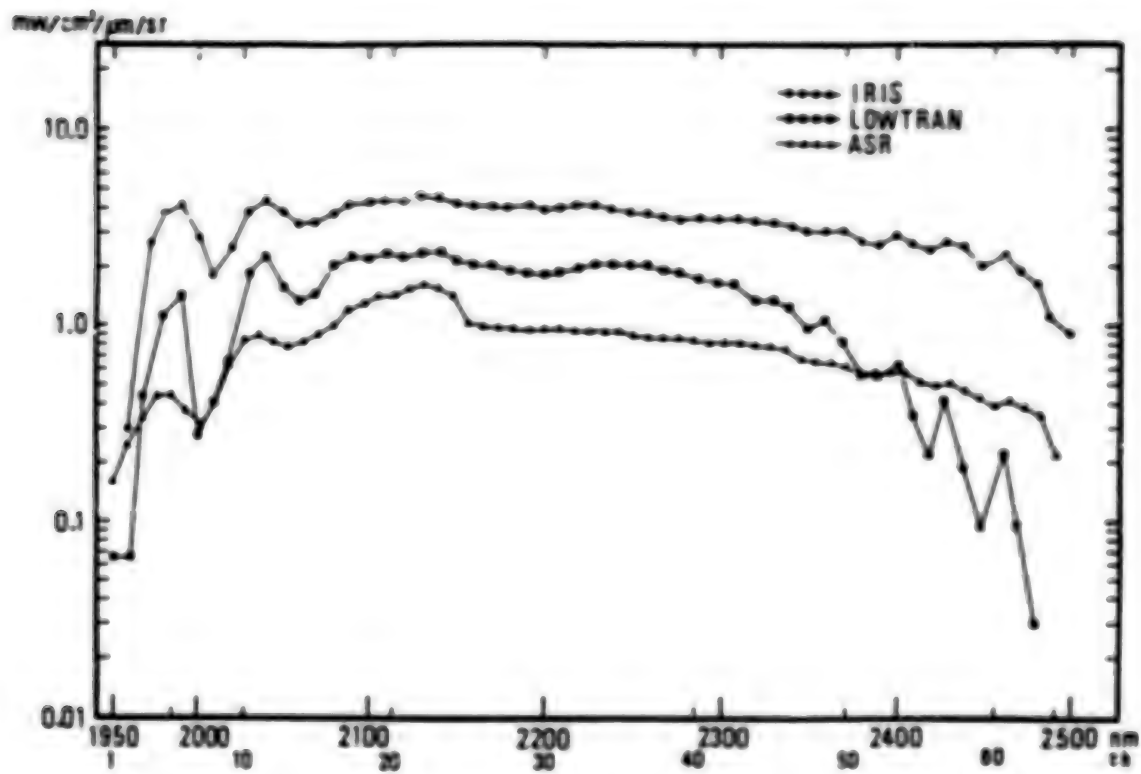


Fig. 4 Radiance by ASR, IRIS, and LOWTRAN 5

/08309

Noise Reduction From Synthetic Aperture Radar Imagery

43070008d Kyoto Selections From INTERNATIONAL ARCHIVES OF PHOTOGRAHAMTRY AND REMOTE SENSING in English Vol 27 1988 Part B9 pp 329-336

[Article by Olli Sirkia, Helsinki University of Technology, Institute of Photogrammetry and Remote Sensing , Otakaari 1 02150 Espoo Finland, Commission VII]

[Text] ABSTRACT

The characteristic of the noise in SAR images differs quite much from that of more conventional digital spaceborne or airborne images. Removal of such usually high-amplitude speckle noise without losing too much high-frequency information requires at least some kind of adaptiveness from the filter. In this paper some adaptive spatial filters are described and results of their use are compared.

1. INTRODUCTION

Speckled noise in SAR (Synthetic Aperture Radar) images is usually found as a problem when thinking of interpretation or segmentation and classification. The noise appears as heavy granularity even in homogeneous areas containing no natural texture. Adaptiveness of the filter is required to reduce this granularity sufficiently while preserving meaningful edges and objects. These objects can be very bright (strong reflectors) because the dynamic range in SAR images is usually much wider than in images in visible or infrared regions. Adaptiveness is usually carried out by taking into account in different ways statistical or spatial properties of the image and objects on it.

2. FADING AND SPECKLE

Inside a ground element (ground cell, resolution cell) there are usually many individual scatterers contributing to the signal received by the radar antenna. The signals from these individual scatterers have different phases and the summation of the individual signals varies because of the relative motion between the radar and the scatterers.

Fading is a concept connected with this variation. Fading frequency means the interval on the frequency scale after which the total signal decreases down to null value. The fading frequency of the imaging system depends on the spacing between individual scatterers, speed of the radar platform, used wavelength and the distance from object to radar. In homogeneous areas containing no dominant individual scatterers certain noiselike statistics apply for fading.

Speckle is the visual effect of those random fluctuations in the return signal caused by the summation of the randomly phased phasors inside one ground element. Actually speckle is not really noise but usually disturbing and useless information related to particular SAR imaging system and target. Speckle can carry some interpretable information about the object surface but Gaussianly distributed speckle doesn't do it. In Figure 1 two grey level histograms of different homogeneous areas are shown as an example. The areas are from the Seasat-A test data used for making this article.

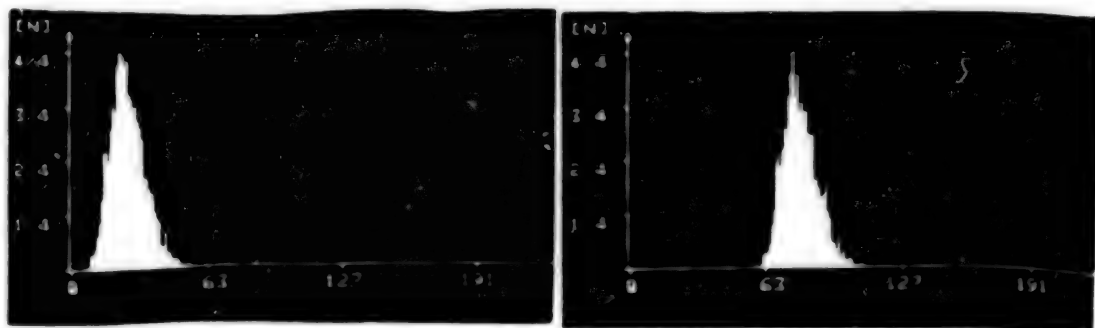


Fig. 1. Two histograms of different homogeneous areas.

Multiplicative speckle (noise) model is mostly used because the intensity value of a pixel is the sum of many independent random variables. It has been found that the signal voltage due to backscattering from a distributed target may be described in terms of Rayleigh statistics. Hence in homogeneous areas holds theoretically

$$\text{dev} = 0.523 * \text{mean} / N^{1/2}, \text{ for amplitude images} \quad (1a)$$

$$= \text{mean} / N^{1/2}, \text{ for intensity images} \quad (1b)$$

where mean is the mean voltage corresponding to the average scattering coefficient of a ground cell and dev is the standard deviation associated with the measurement (estimate) of that cell. This knowledge has been made use of in some of the adaptive filtering methods described later.

The test data used in this article was originally an intensity image (square law detection during observing followed afterwards in SAR processing stage by incoherent averaging). Later it had been square-rooted thus becoming a square-root intensity image. In this case the normalized standard deviation of a ground cell measurement should be

approximately the same as in amplitude images in which the observations are made in linear detection mode before averaging. Here the incoherent averaging means averaging of smaller resolution cells to form a final pixel in the image and it is done to reduce the worst speckle effect. Unfortunately this incoherent averaging (increasing the number of independent samples per pixel) reduces the spatial resolution respectively.

In the test data here the pixel size is  $12.5 \times 12.5 \text{m}^2$  each pixel consisting of four ( $N=4$ ) independent samples about  $6.6 \text{m}^2$  each. From this data eight different homogeneous areas were chosen and the standard deviation to mean value ratios (dev/mean) were computed. The average value for this ratio was 0.261 while minimum was 0.230 and maximum 0.293. The theoretical value would be according to Rayleigh statistics for amplitude images  $0.2615 (0.523/4^{1/2})$ , so the ratio values with this data seem to fit well to the theory. In homogeneous areas with multiplicative noise model the mean to standard deviation ratio (m/s) can be used directly to approximate signal-to-noise ratio. This has been done later in this paper to compare different filtering methods.

### 3. DIFFERENT METHODS

Quite many studies have been presented about the filtering of multiplicative noise both in frequency domain (e.g., homomorphic filtering, Wiener filtering) and in spatial domain. In this paper only spatial domain methods are described. Often in practice signal-to-noise ratio in SAR images is low, too low, e.g., for Wiener filtering to achieve good results. The window size used in the following methods has been either 5 or 7. In adaptive filtering the window size is not very critical factor.

In reference [3] 10 different filters, four of which adaptive, have been compared for noise reduction and classification. There the non-adaptive methods were simple averaging and its logarithmized variant to transform the multiplicative noise into an additive one (and exponentiation after), median filtering and iterative median filtering. To some extent adaptive but without any speckle model was a method of choosing the average value of the most homogeneous subwindow (the one with smallest variance among four subwindows).

One adaptive method was Frost-filtering which assumes that the useful information in a small neighbourhood has an exponential autocorrelation function. Here the image is filtered with an exponentially shaped weighting function and the midpixel value of this window is estimated (the weighted sum)

$$y' = k * a * e^{-a(|x-x_0|+|y-y_0|)} * z(x,y)$$

where  $z(x,y)$  is the image pixel value and  $(x_0, y_0)$  is the location of the window's central pixel. So the weighting of the window is

$$w(x,y) = k * a * e^{-a*D}$$

where  $k$  is a normalizing constant (filter weights sum to unity) and

$$a = (4/(n*s^2)) * \text{dev}^2/\text{mean}^2 \quad (n \times n - \text{window})$$

where  $\text{dev}$  is the standard deviation of the image pixels inside the window and  $\text{mean}$  is the mean value respectively. So the weighting of the midpixel increases when the standard deviation to mean ratio inside the window increases. The value of  $s$  (reference, assumed real speckle standard deviation) can be computed from (1) by setting the mean value to 1 for multiplicative noise. It can also be estimated from homogeneous areas by collecting (normalized)  $z/\text{mean}$  values.

Another method was a maximum likelihood filtering where the most likely estimate  $y'$  for  $N$ -look intensity images is the actual positive root of the equation.

$$y'^3 - \text{mean}^2 * y'^2 + N * s_y^2 * y' - N * s_y^2 * z = 0$$

where  $z$  is the window's midpixel value in the image to be filtered and

$$s_y^2 = (\text{dev}^2 - \text{mean}^2 * s^2) / (1+s^2).$$

The third method aims at minimizing the mean square error for each pixel value assuming that the noise is additive with a mean value equal to zero. Thus logarithmic transformation is needed before and exponential after filtering. Now the estimate  $y'$  for a pixel value is

$$y'_{\log} = \text{mean}_{\log} + (z_{\log} - \text{mean}_{\log}) * (\text{dev}_{\log}^2 - s_{\log}^2) / \text{dev}_{\log}^2$$

where the speckle variance  $s_{\log}^2$  can be estimated from homogeneous areas as described earlier or be set values  $1.645/N$  or  $0.465/N$  for intensity and amplitude images respectively.

The fourth method is like the previous one but assuming the multiplicative noise model with the mean value of 1. Now the filtering midpixel value estimate

$$y' = \text{mean} + (z - \text{mean}) * (1 - \text{mean}^2 * s^2 / \text{dev}^2) / (1 + s^2).$$

The last method was found best in [3] and it is tested in this work too named here method 1. Here the value  $s$  for speckle was first computed from (1a). With  $N=4$  it gives  $s=0.523/2$ . The filtered image (window size  $n=7$ ) and the greyvalue profile of the marked image row are shown in Fig. 2 middle row while the original image and the row profile are shown on the upper row. The m/s ratio of the whole image increased

from the original 1.53 to 1.78 and in homogeneous areas averagely from 3.26 up to 6.26. So the improvement was much larger in homogeneous areas. Also the row profile shows that edges and details are well preserved.

Method 2 in this study is introduced by the writer and is very much like the previous one. Here (1a) again is used to conclude whether and how homogeneous the area is inside the window. From (1a) the reference speckel standard deviation is 0.261. The filtered midpixel value

$$y' = \text{mean} + k*(z-\text{mean}), \text{ where the factor } k \text{ is simply } k = \lfloor 1-\text{dev}/(0.261*\text{mean}) \rfloor \text{ cut into interval } [0,1].$$

In homogeneous areas the dev/mean ratio should be near the value 0.261 and then  $k$  is about zero and averaging is done inside the window. The more the dev/mean differs from 0.261 the more obviously window area contains an edge, details or some texture and less averaging is done. With this method the m/s ratio of the whole image was a little smaller (1.71) than with method 1 and in homogeneous areas it increased from 6.26 to 6.61. Also the row profile shows that some details are better preserved while e.g., the water area is a little more flattened (lower row in Fig. 2). (Figure 2 omitted)

A variant of method 2 was also tested here where the reference noise standard deviation was computed from a big water area to get a statistically reliable practical estimate. The new reference value was then 0.310. The result of filtering is shown in Fig. 3 upper row. The m/s ratio in homogeneous areas increased up to 6.97 and in the whole image the ratio increased slightly. So the filter was more effective but seemed to blur a little originally unsharp edges.

A second variant of this method was to use window sizes 7, 5 and 3 for every pixel choosing the window with smallest dev/mean ratio. The aim was to filter effectively areas also quite beside edges. Unfortunately the unreliability of small window statistics caused the loss of some details although, e.g., edges between water and land areas were sharpened. There were no significant changes in m/s ratios. The result is shown in Fig. 3 middle row. (Figure 3 omitted)

Method 3 was presented in reference [4] and is much like the Frost-filter described earlier. Here the weighting function is also exponential and made narrower in areas with higher dev/mean ratio;

$$w(x,y) = k * a * e^{-a|x-y|}$$

where  $|x,y|$  is the distance from a window element to window's central pixel and the decay constant  $a$  is approximated  $a = \text{dev}/\text{mean}$ . In this case a sufficiently effective filtering seems to cause more blurring than the previous methods. The result with  $n=5$  is shown in Fig. 3 lower row.

Method 4 [5] is in some sense also adaptive but without noise model. This Symmetric Nearest Neighbour filter takes pixel pairs symmetrical to the window's central pixel and chooses the pixel with greyscale nearer to central pixel's value. Finally mean or median value is computed from chosen pixels. This filter tends to flatten local variations (including small details) while preserving and even emphasizing more significant edge structures. The filter can be used iteratively as shown in Fig. 4 ( $n=5$ ). In Fig. 4 lower row is shown the result of applying Symmetric Nearest Neighbour filter with  $n=5$  to the filtered image in Fig. 3 upper row. The effects of area flattening, small detail weakening and edge sharpening can be seen especially from the profile image. (Figure 4 omitted)

#### 4. SUMMARY

In this paper some filtering methods for noise reduction in SAR images were described. Adaptive spatial filters using local first order statistics showed fairly good performance. The reference standard deviation for speckle can be theoretically evaluated or it can be estimated from homogeneous areas. In the case of  $N$  (number of looks used to generate the image) being unknown  $N$  can be inferred from the comparison of theoretical and actual speckle distribution in homogeneous areas.

#### REFERENCES

- [1] Ulaby, F., Moore, R., Fung, A., "Microwave Remote Sensing, active and passive," Addison Wesley, Artech House, 1981-86.
- [2] Ouchi, K., Tajbakhsh, S., Burge, R., "Dependence of Speckle Statistics on Backscatter Cross-Section Fluctuations in Synthetic Aperture Radar Images of Rough Surfaces," IEEE Transactions on Geoscience and Remote Sensing, No 5/1987.
- [3] Durand, J., Gimonet, B., Perbos, J., "SAR Data Filtering for Classification," IEEE Transactions on Geoscience and Remote Sensing, No 5/1987.
- [4] Frost, V., Stiles, J., Shanmugan, K., Holtzman, J., "A Model for Radar Images and Its Application to Adaptive Digital Filtering of Multiplicative Noise," IEEE Transactions of Pattern Analysis and Machine Intelligence, No. 2/1982.
- [5] Harwood, D., Subbarao, M., Hakalahti, H., Davis, L., "A New Class of Edge-Preserving Smoothing Filters," Report CAR-TR-59, CS-TR-1397, University of Maryland, May 1984.

/08309

The New Generation SPOT Satellites SPOT 4 and 5

43070009a Kyoto Selections From INTERNATIONAL ARCHIVES OF PHOTOGRAVIMETRY AND REMOTE SENSING in English Vol 27 1988 Part B10 pp 113-123

[Article by Michel Arnaud and Marc Leroy, Centre National d'Etudes Spatiales, 18 Avenue Edouard Belin - 31055 Toulouse Cedex, France, Commission Number 1]

[Text] ABSTRACT

This paper presents the main characteristics of the new generation SPOT 4 and 5 satellites, the improved version of a series of high resolution imaging remote sensing satellites constituting the SPOT family. The main objectives of the SPOT 4/5 mission concern:

- i) the continuity of the SPOT 1/2/3 services and products,
- ii) the extension of the high resolution mission, in particular, through the addition of a new band in the middle infrared region,
- iii) the development of a new optical instrument called Vegetation, characterized by a wide field of view and a high radiometric resolution for the purposes of agricultural forecasts and environmental studies,
- iv) the extension of the satellite life duration,
- v) the capability to offer an embarkment to new passengers, and
- vi) the reorganization and new development of the ground segment.

I. INTRODUCTION

The SPOT 1 satellite, the first of a series of high resolution imaging remote sensing satellites, has been successfully launched by the ARIANE launcher on 22 February 1986. After more than 2 years of operation, the SPOT 1 operational behaviour appears quite satisfactory, at the exception of some anomalies in the tape recorder operations which

resulted in a definitive failure of one of the two tape recorders in July 1986. Moreover, the SPOT 1 image quality fulfills the original system specifications as explained in Ref. 1. General information about the SPOT 1 system may be found in Refs. 2 to 5.

The basic mission of the SPOT program being to establish a continuity of the SPOT data and services, it has been decided:

--to produce two recurrent models named SPOT 2 and SPOT 3;

at the time of writing (May 1988), SPOT 2 has completed its integration phase and is planned to be launched in early 1989. The industrial phase of SPOT 3 has already started and SPOT 3 should be ready to be launched in early 1990.

--to develop two improved satellites named SPOT 4 and SPOT 5.

The design phase (phase A) of SPOT 4/5 is over, and its preliminary industrial definition phase (phase B) will be completed at the end of 1988. The industrial development and realization phases (phases C and D) will start in early 1989, the goal being to be ready to launch SPOT 4 at the beginning of 1993 and SPOT 5 in 1995.

The main objectives of the SPOT 4/5 mission are the following:

--provide the continuity of the SPOT 1/2/3 services,

--ensure the extension of the high resolution mission, essentially through the addition of a new spectral band in the middle-infrared region and the on-board registration of the 10m/20m resolution channels in the high resolution instruments HRVIR,

--add a new payload named Vegetation, a wide field of view, low spatial resolution instrument for high repetitivity observations in the visible and middle infrared range,

--increase the life duration of the satellite,

--offer new possibilities of embarkment of passengers,

--improve the ground segment.

This paper describes these objectives, the main technical choices adopted for the space and ground segments, and their evolution relative to the SPOT 1 system.

## 2. CONTINUITY OF THE SPOT PROGRAM SERVICES

The SPOT 4/5 system must provide the continuity of the SPOT services up to the year 2000 at least.

The SPOT 4/5 system appears as an extension of the SPOT 1/2/3/ system, hence the main system parameters have remained unchanged. Thus the orbit parameters, the local time and the main high resolution instrument characteristics (spatial resolution, swath, spectral bands in the visible and near infrared region, etc...) have not been modified.

The continuity of the SPOT 4/5 system is also apparent at the ground station interface level. The ground stations belonging to the SPOT 1/2/3 system will be able to receive and process the SPOT 4/5 telemetry emission without any other modification than proper equipment adjustment. In other words, it will be possible to program the SPOT 4 satellite in a mode compatible with the SPOT 1 modes with a telemetry format identical to that of SPOT 1 (see also section 3.3.).

Moreover the preprocessing of raw data as well as the use of system parameters to elaborate higher level products will be made possible with minor modifications with the type of hardware and software currently used in the ground stations belonging to the SPOT 1/2/3 system.

### 3. EXTENSION OF THE HIGH RESOLUTION MISSION HRVIR PAYLOAD

The SPOT 4/5 system will allow an improvement of detailed thematic inventories through the addition of a new band in the middle infrared region (this is why the HRV instruments have been renamed HRVIR, standing for High Resolution in the Visible and Infrared Range) and the ability to register on-board the 10 meter resolution and the 20 meter resolution channels.

#### 3.1. Use of a middle infrared band (MIR) 1.58-1.75 microns

In agronomy and natural vegetation studies, the MIR band will permit an estimation of the ground humidity and will improve agricultural inventories, particularly those of cereals. The objective in this latter domain is to increase the performance of cultures identification with a monotemporal or multitemporal set of data, first, by bringing an information on the differences of water content in the vegetation cover either in time or between different parcels of a given agricultural zone, and second, by offering a better sensitivity than that of the near infrared channel B3 to the covering rate of the ground by the vegetation.

In hydrography, it will be possible with the MIR band to perform a detailed cartography of the snow mantle (since this band discriminates easily snow and clouds) and to inventory the various types of snow.

In geology, the 1.58-1.75 microns band can improve significantly the possibilities of discrimination between various types of minerals; it can also give an access to the notion of ground humidity, and indirectly to anomalies of metal content of the ground.

### 3.2. Registration of 10m resolution and 20m resolution channels

The panchromatic 0.49-0.73 microns SPOT 1 band operating at 10 meter resolution has been replaced on SPOT 4 by the B2 band (0.61-0.68 microns). The 10m resolution channel is of strong interest in urbanism, forestry, small parcels inventory, texture analysis, etc.... Many applications of the 10m resolution channel require its combination with the 20m data. The adoption of the same band B2 for the 10m and 20m resolution channels has made possible an instrument concept where both channels are registered on-board, which is most convenient in the production of data for such applications.

### 3.3. Main characteristics of the HRVIR payload

The HRVIR payload contains two identical HRVIR instruments. As those of SPOT 1, the instruments are pointable in the across track direction up to plus over minus 27 degrees (plus over minus 460 km on ground) to provide accessibility and stereo coverage capability. The HRVIRs operate independently with the capability to produce monospectral (M), multispectral (X), and/or SPOT 1 compatible multispectral (XS) images whose swath width is 60 km at Nadir.

In the monospectral mode, the HRVIR generates a black and white image in the B2 band with a ground resolution of 10 meters by 10 meters.

In the multispectral mode, the HRVIR generates a multispectral image in 4 bands B1, B2, B3, MIR whose ranges are 0.50-0.59, 0.61-0.68, 0.79-0.89, 1.58-1.75 microns respectively at 20 meter resolution.

In the SPOT 1 compatible multispectral mode XS, the HRVIR generates a multispectral image in 3 bands B1, B2, B3 at 20m resolution.

The X and M data are compressed on-board using Delta Pulse Code Modulation techniques (8-5-5-8), while the XS mode is not compressed on-board. The pixel is restituted on ground on 8 bits.

Each HRVIR can deliver two 25 megabits/sec. data streams corresponding to the monospectral (M) and multispectral (X or XS) modes. Only two among the 4 bit streams available are transmitted to the ground or recorded on-board, the total telemetry data rate being 50 megabits/sec. The recording capability of each of the two tape recorders has been increased from 20mn (SPOT 1) to 40 mn on SPOT 4. The transmitted data are ciphered on-board.

The radiometric and geometric image quality criteria are listed in Table 1. Note that the instrumental radiometric resolution and dynamic range are obtained from the Table 1 ground reflectance data and from the assertion that the solar incidence angle be in the range 15-60 degrees. Note also that while the localization and length alteration criteria apply to rectified images using system corrections only (no ground control point), the photogrammetric restitution criterium applies to the processing of stereo pairs with the use of ground control points.

We mention finally two interesting improvements of the SPOT 4/5 system relative to SPOT 1. First, it will be possible to program each HRVIR independently regardless of any possible motion of the pointable mirror of the other HRVIR, whereas on SPOT 1 such motion on one HRV invalidates the image acquisition of the other HRV due to pointing inaccuracies, resulting in significant programming difficulties. Second, there will exist at any time 3 operational analog gains per spectral band and per HRVIR; the SPOT 4/5 mission center will program the appropriate gain out of the 3 gains available on different segments of a given orbit from criteria elaborated in advance with an histogram data base made of all histograms of cloud free scenes acquired by SPOT 1/2/3. Such a measure should be most appropriate in bands B1 and B2 where the scene radiometric dynamic range may vary significantly with season, latitude and the type of scene considered (sand, vegetation, etc...).

#### 4. A NEW PAYLOAD: VEGETATION

##### 4.1. The VEGETATION mission

The HRVIR instruments provide very detailed images of the Earth surface but their repetitivity of observations is sometimes insufficient for applications relative to renewable resources or environmental studies.

Table 1. HRVIR Image Quality

| RADIOMETRY                       |                                           |                                     | GEOMETRY                                                     |                                        |
|----------------------------------|-------------------------------------------|-------------------------------------|--------------------------------------------------------------|----------------------------------------|
| Ground reflectance resolution    | Wavelength                                | $3 \cdot 10^{-3}$                   | Localization                                                 | 1500m rms<br>4500m max                 |
| Ground reflectance dynamic range | min                                       | 8                                   | Length alteration<br>on image $\Delta l$                     | $10^{-3}$ rms<br>$3 \cdot 10^{-3}$ max |
|                                  | max                                       | 0.5(B1) 0.3(B2)<br>0.7(B3) 0.6(MIR) | Sampling regularity                                          | 0.1 pixel rms                          |
| Calibration accuracy             | absolute<br>band to band<br>multitemporal | 10% max<br>3% max<br>10% max        | Multispectral<br>registration                                | 0.3 pixel max                          |
| RTF                              | at Nyquist<br>frequency                   | <0.3                                | Photogrammetric<br>restitution<br>(planimetry/<br>altimetry) | 1m rms                                 |

The Vegetation instrument, named also VGT, is conceived as a high radiometric resolution instrument with a wide field of view, with consequently a high repetitivity observation capability allowing a continuous monitoring of evolutive phenomena. The first priority objective of VGT is the worldwide operational monitoring of evolutions of crops and natural vegetation for the purposes of agricultural forecasts and environmental studies. The second priority objective of VGT is the observation of oceans mainly for scientific purposes. These two objectives are detailed hereafter.

#### 4.1.1 Estimate of crops and natural vegetation monitoring

The possibility to estimate crop yields relies on the capability of VGT to monitor temporal evolutions of the ground reflectance. Hence the VGT instrument will deliver data which will eventually permit:

- i) to retrace at any point the evolution of biomass and of the vegetal cover structure to detect possible growth anomalies or hydrous stresses,

- ii) to cartography the disparities of evolution, in a given agricultural or climatic zone, by a multiday measurement over this entire zone,
- iii) to provide an indication of the amount of biomass at its maximum.

The VGT data will also permit, besides the biomass evaluation, the estimation of the proportion of given species in large homogeneous regions. Such estimate, wherever possible, should be performed through a spatial extension of detailed classifications elaborated from HRVIR data.

These varicus informations will be obtained with a combination of the VGT informations at any point in the bands B1, B2, B3, MIR, the same bands as those of HRVIR.

#### 4.1.2. Oceanography

The addition of a "blue" band B0 (0.43-0.47 microns), centered on the main absorbtion band of phytoplankton pigments, makes possible the monitoring of the amount of vegetal biomass in water, with the following potential applications:

- i) cartography of spatio-temporal variations of the distribution of phytoplankton and archive,
- ii) quantitative estimation of worldwide primary production of phytoplankton,
- iii) climatologic and biogeochemical studies (carbon fixation, CO<sub>2</sub> cycle),
- iv) use of biomass as a tracer of the dynamics of superficial water masses,
- v) assistance to fishing by fast localization of zones of high phytoplankton concentration.

The bands P1 and B2 can also be used, in addition to B0, to perform a mesoscale monitoring of water turbidity, in particular along the coast lines. All these applications require careful atmosphere corrections which will be taken care of by the system.

#### 4.2. The VGT operations

The VGT instrument can generate 2 channels at 500 kbit/sec. data rate each.

The first channel is called "direct" or "regional" channel and transmits data in real time with a spatial resolution at nadir of about 1 km. This operating mode is called "Regional Observation" and provides information from the region in which the station (Toulouse or another ground station) is located. The working zone for the Regional Observation is subject to the condition that the sun incidence angle be lower than 60 degrees.

The second channel is called "recording" or "worldwide" channel and transmits data which have been recorded at 4 km resolution at nadir. The 4 km resolution is obtained by agglomerating onboard 4x4 neighbouring image elements at 1 km resolution. The production of 4 km resolution recorded data is called "Worldwide Observation" and can be obtained only at the Toulouse station. The working zone for the Worldwide Observation is nominally located between 60 degrees North and 40 degrees South.

A very high repetitivity of observations is achieved, taking into account the orbit characteristics, by a wide field of view of the instrument (+ over - 50 degrees) corresponding to a swath width of 2200 km. With this configuration, a given point on ground is seen every day by VGT above a latitude of 35 degrees, and seen 3 days out of 4 at the Equator.

#### 4.3. The VGT instrument

The VGT instrument contains a radiometer made of 5 objectives (one for each spectral band B0, B1, B2, B3 and MIR) and an electronic chain which amplifies and codes on 10 bits the signal.

An array of 1728 CCD detectors is located in the focal plane of each objective.

The main characteristics of the VGT payload are displayed in Table 2, while the VGT geometric and radiometric image quality criteria are listed in Table 3.

Note in Table 3 that the local distortion on an image remains sufficiently small that 2 images taken at different dates be superimposable to a 1 pixel rms accuracy and to within a translation of an integer number of pixels (less than 5 by virtue of the localization performance).

#### S. EXTENSION OF LIFE DURATION AND MODIFICATIONS OF THE SATELLITE

A number of improvements have been inserted in the satellite design, in order to improve its performances and increase its life duration from 2 years (SPOT 1 concept) to 5 years.

Table 2. VGT Main Characteristics

|                     |                            |
|---------------------|----------------------------|
| Weight              | 160 kg                     |
| Volume              | 0.7 x 1 x 1 m <sup>3</sup> |
| Power               | 200 watts                  |
| Data rate           | 2 x 500 kbytes/sec.        |
| Pixel coding        | 10 bits                    |
| Telemetry frequency | 8.2 GHz                    |
| Recording memory    | 256 Megabits               |

Table 3. VGT Image Quality

| RADIOMETRY                       |                                                        |                                                           | GEOMETRY                   |                                |
|----------------------------------|--------------------------------------------------------|-----------------------------------------------------------|----------------------------|--------------------------------|
| Ground reflectance resolution    | NoAp                                                   | $10^{-3}$ (B0)<br>1 to $3 \cdot 10^{-3}$<br>(other bands) | Localization               | 2400m rms<br>5000m max         |
| Ground reflectance dynamic range | pMIN                                                   | 0                                                         | Local distortion on image  | 0.3 pixel rms<br>0.6 pixel rms |
|                                  | pMAX                                                   | 0.1(B0) 0.5(B1)<br>0.7(B3) 0.6(MIR)                       |                            |                                |
| Calibration accuracy             | absolute<br>band to band<br>multitemporal<br>VGT/HRVIR | 10% max<br>3% max<br>10% max<br>3% max                    | Multispectral registration | 0.3 pixel max                  |
| HTF                              | at Nyquist frequency                                   | >0.3                                                      | Localization<br>VGT/HRVIR  | 1500m rms                      |

The increase of life duration will be ensured by an appropriate choice of elementary components and by a new thermal design in order to lower the average operating temperature and hence reduce the failure rate of the electronic components.

The flexible solar arrays of the solar generator have been replaced by a solar array with rigid panels, a concept both simpler and more reliable, and the available power end of life has been extended from 1100 watts (SPOT 1) to 1800 watts. Moreover the 3 x 24 A.h batteries have been replaced by 4 x 40 A.h batteries to accommodate to a higher demand of power and to provide a reduced depth of discharge.

The mechanical concept has been changed by adding an "equipment case" between the platform and the payload. Such equipment case is needed to

accommodate the new tape recorders and to provide a mechanical support to the HRVIRs and VGT payloads as well as to a number of passengers of the SPOT 4/5 platform.

The in orbit configuration is shown on Figure 1.

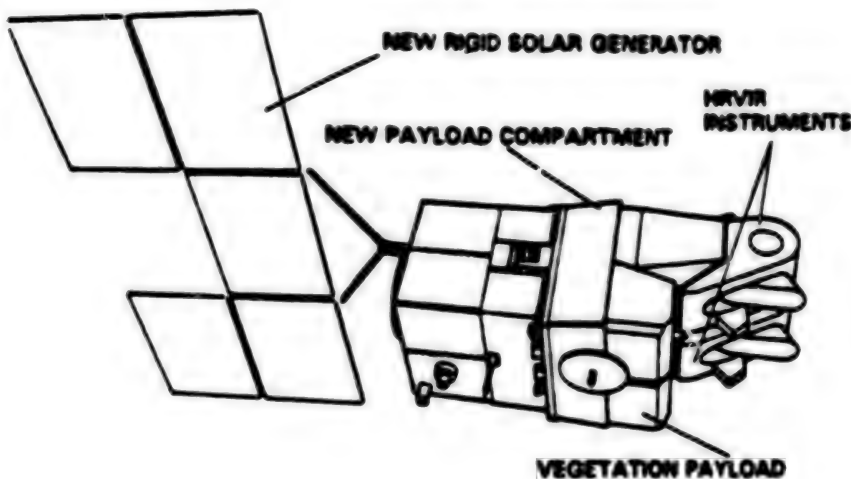


Fig. 1 SPOT 4 in Orbit Configuration

## 6. THE SPOT-4 PASSENGERS

The extended capabilities of the SPOT 4 satellite allow to embark the following additional experiments:

--PASTEC (PASSager TECnologique) which is a group of experiments for studying orbital environment,

--DORIS (Doppler Orbitography and Radiopositioning Integrated by Satellite) which will be used for precise orbit determination and localization of ground platform,

--a Radar Transponder which will be used to calibrate the ground radar of the Guyana Space Center and to train the operators,

--PASTEL (PASSager Spot de TELEcommunication Laser)

The PASTEL package is part of an European Space Agency program for the experimentation of an optical link between a low orbit spacecraft (SPOT 4) and a geostationary satellite. This optical link will be used for transmitting the SPOT 4 payload data stream at a rate of  $2 \times 25$  Mb/sec.

These data will demonstrate the feasibility and performance of optical communication and will be used on a pre-operational basis to relay image data.

Using these facilities will bring about a fundamental change in the capabilities and management of the system. As an example, Figure 2 shows the visibility on earth between SPOT 4 and a geostationary satellite located at 19 degrees E. As seen in Figure 2 the visibility is restricted mainly by the Earth and the SPOT 4's body which may obscure the optical link.

The operational SPOT services will still use the tape recorder and ground station network, while the optical link will be used to extend image transmission capabilities in the event of lack of tape recorder capability or failure.

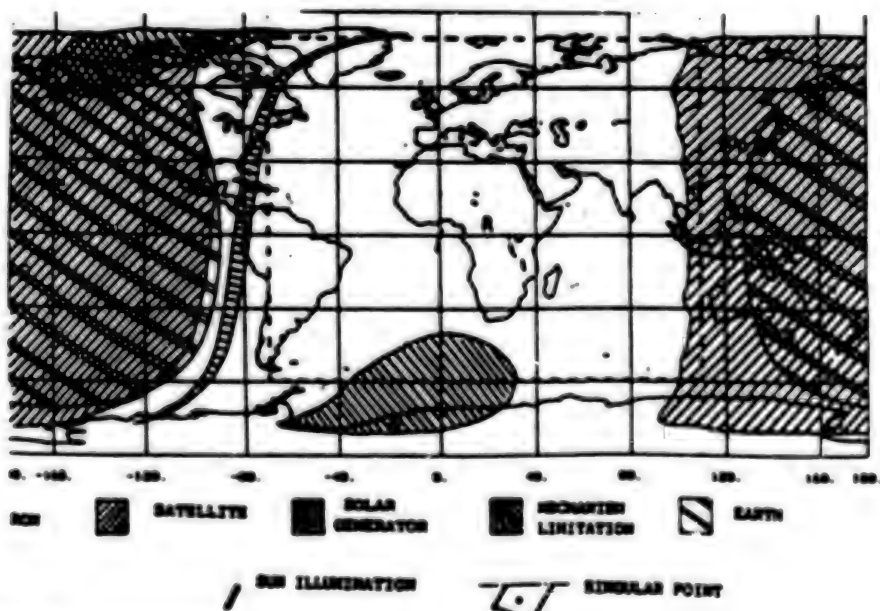


Fig. 2 PASTEL Ground Coverage

## 7. THE GROUND SEGMENT

### 7.1. The image ground segment - Products

Two stations--Toulouse and Kiruna--will be used to ensure a large direct and playback transmission capacity of the HRVIR data. Night passes and some day passes will be used to collect recorded VEGETATION data on the Toulouse station.

Apart from these stations direct read-out X band stations can be implemented worldwide to acquire HRVIR and VGT data.

The Toulouse and Kiruna stations contain an HRVIR Archiving and Preprocessing Center which archives all the HRVIR data and processes level 0 and level 1 products. These centers are also capable to process images issued from the SPOT 1/2/3 archive.

The level 0 product is an exchange level product with geographically arranged pixels and a raw radiometry.

The level 1 is a radiometrically corrected (level 1A) and geometrically corrected (level 1B) product. Only system corrections are applied to perform the geometric rectification. Note that contrary to SPOT 1 the level 1B scenes can be mosaiced along the track without further processing and centered upon request at any point along the track. Note also that the cloud cover notation at the inventory step (catalogue) of the image processing will be significantly improved relative to the SPOT 1 system, by the addition of automatic and semi-automatic analysis methods (analysis of the reflectance and reliability, graphics facilities, etc...).

The Toulouse station includes also a Preprocessing Center of VGT images which produces and archives level 1 data. The level 1 VGT product is characterized by radiometric and systematic geometric corrections, as well as a systematic correction of atmospheric effects. The VGT level 1 product contains also reduced data such as the vegetation or turbidity indexes, and a simplified classification map (snow, cloud, water, ground).

The products delivered by the Toulouse VGT Center will be available within 8 hours in the Regional Observation mode, 36 hours in the Worldwide Observation mode after their acquisition by the satellite, as soon as VGT enters its fully operational phase.

## 7.2. Organization of the ground segment

In the operational phase, after the post launch assessment, the responsibilities will be shared between the various entities as follows.

The satellite operator (CNES) will be in charge of the Control Center and the Platform and Payload Management Center. These centers perform all satellite management functions, monitor the satellite operations, generate the necessary commands and determine the orbital parameters.

The commercial operator (SPOT IMAGE) has the exclusive license to organize the promotion, the distribution and sale of SPOT data. It will be in charge, moreover, of the Mission Programming Center and of the Toulouse image ground segment. The Mission Programming Center is responsible for mission management regarding the HRVIR and VGT payloads. It programs the on-board image acquisition and storage in accordance with user requirements, and also sends the data necessary for image acquisition and processing to the ground stations.

## 8. CONCLUSION

CNES has undertaken an ambitious earth observation and data distribution program. This ambition is obviously already apparent since SPOT 1 has been giving most satisfactory results for more than 2 years of operational life, and since the following satellites SPOT 2 and SPOT 3 have been either built or fully decided. The aim now is to ensure a continuity and an improvement of the SPOT services and products up to the year 2000 and beyond. The SPOT 4/5 system has been designed to fulfill this requirement. This generation of satellites represents a technological challenge (in particular, the development of CCDs in the MIR band, the wide field of view objectives with CCD arrays of Vegetation, the development of a new polar platform) and widens the field of potential applications of earth remote sensing, especially through the use of the new payload Vegetation.

## REFERENCES

1. BEGNI G., HENRY P., "SPOT 1 Image Quality : 2 years of experience," this issue.
2. BEGNI G., BOISSIN B. and PERBOS J., 1985, "Image Quality Assessment Methods," Advances in Space Research, Pergamon Press, New York.
3. BEGNI G., BOISSIN B., LEROY M., "SPOT Image Quality" - Progress in imaging sensors, Proc. ISPRS Symposium, Stuttgart, 1-5 September 1986. (ESA SP-252, November 1986).
4. CHEVREL M., COURTOIS M., and WEILL G., August 1981, "The SPOT satellite remote sensing mission," Photogrammetric Engineering and Remote Sensing, Vol 47, 1163-1171.
5. COURTOIS M. and WEILL G., 1985, "The SPOT satellite system," Progress in Astronautics and Aeronautics Series, Vol 97, published by the American Institute of Aeronautics and Astronautics, Abraham Schnapf Editor.

/08309

**Design Aspects of a System for Geocoding Satellite SAR Images**

**43070009b Kyoto Selections From INTERNATIONAL ARCHIVES OF PHOTOGRAMMETRY AND REMOTE SENSING in English Vol 27 1988 Part B10 pp 135-143**

[Article by G.Schreier, D. Kosmann, A. Roth; DFVLR, German Aerospace Research Establishment, D-8031 Oberpfaffenhofen, West Germany; Commission I]

**[Text] Abstract**

The concepts in algorithmic design and operational use of the German Processing and Archiving Facility Geocoding System for ERS-1 are presented. The System will produce non-terrain corrected and terrain corrected products. The latter require complex algorithms in terrain height consideration and ground control pointing.

The Geocoding System will be implemented on UNIX workstations and programmed within an image processing system. To guarantee operational throughput and flexibility, new software tools will be implemented.

**2. Introduction**

In 1990, the first European Remote Sensing Satellite (ERS-1) will be the first step towards a scenario of satellites carrying a Synthetic Aperture Radar (SAR) as a prime sensor (SIR-C, RADARSAT, J-ERS-1). For the 90's and beyond, SAR-sensors--then upgraded in terms of wavelength and polarization--will be the basic source of image information besides optical sampling techniques.

To cope with the large amount of data and to benefit from its intrinsic information, the data processing and data evaluation techniques must keep pace with the development of space-segment hardware.

Especially for SAR-data processing, powerful hardware and sophisticated software concepts will be realised, to generate digital raster image data out of the holographic information gathered by the sensor (Noack, 1987).

The microwave image information is now basically interpretable by digital or visual means, but suffers from the lack of geographic context. Therefore, scientists, engaged in remote sensing, first try to rectify or geocode the satellite images (for optical images as well) to ease the interpretation and to utilize further existant geocoded information for data synergism, covering several aspects (spectral wavelength, time, polarization, look-angle) of the investigation area.

Rectification and geocoding algorithms are more or less a standard feature of many remote sensing image processing systems, but are time-consuming (by manual tiepoint search and raster data resampling) and produce often unsatisfactory and uncomparable (with other systems) results.

This is one reason, why many potential commercial and governmental users hesitate from using satellite borne images due to the complex procedures, which must be performed, before getting useful information.

For optical scanner images, a few national remote sensing organisations and commercial distributors are already offering geocoded satellite images. For the future microwave satellite scenarios mentioned above, such geocoded products should become a standard user service and is therefore planned by several facilities (JPL, CCRS, ESA).

The German Aerospace Research Establishment (DFVLR) is currently building up--in contract with ESA--a Processing and Archiving Facility (PAF) for ERS-1 SAR images.

One major sub-system besides the processing of the radar raw data by the new Intelligent SAR processor ISAR is the SAR Geocoding System GEOS. The major design aspects of the Geocoding sub-systems will be described in the following chapters.

### 3. Algorithmic Needs for Future Satellite SAR Image Data Geocoding Systems

The future remote sensing satellite scenario can be characterized by the amount and variety of data. The SAR processing systems must cope with this data by increasing the processing speed up to near real time. The variety of the data for different satellites and sensors must be properly obeyed in the SAR cases, where orbit, wavelength and satellite technical parameters determine the SAR image generation process and its quality. Thus, the input data needs a flexible structure in hardware and software of the SAR processing system.

The target where all SAR and also optical sensors can be referred to, is the imaged body itself--the earth. All sensor views of the same physical ground element and all sensor data can be geometrically re-ordered to a pre-defined cartographic presentation. The latter task is subject of Geocoding Systems.

Satellite image Geocoding Systems can be characterized by the following attributes:

- kind of sensor and its imaging physics
- parametric or tiepoint rectification (or intermediate)
- consideration of terrain height displacements
- support of different cartographic projections
- data throughput capabilities

The imaging physics (which intentionally substitutes "geometry" in this case) of Synthetic Aperture Radar sensors determines the geocoding algorithm to compute the proper geo-location of each output pixel. The orientation of one image pixel in a SAR image and its correspondence to an earth location can be established by solving three equations (Curlander, 1982):

- The range timing (the absolute travel time between sensor to target)
- The azimuth Doppler reference (depending on the SAR Processing algorithm applied)
- The actual terrain shape (ellipsoid or Digital Elevation Model if terrain height is considered).

In remarkable contrast to optical sensors, the pointing accuracy of SAR systems do not depend on angle measurements, but on time and frequency analysis of the radar echo. These parameters can be extracted with better accuracy than satellite angle control.

Having the necessary parameters at hand, a geocoding approach with parametric rectification using the sensor/processor entities is obvious for SAR systems and gives sufficient results for many application areas.

Unfortunately, SAR images and its geometry are affected by the local earth surface elevation more heavily, than it is the case for sensors. For ERS-1 (look angle 23 degrees at mid swath) 1000 m elevation come along with mis-registration of about 425 m. For areas with moderate to hilly terrain, these mis-registrations can cause pixel geocoding errors which are considerably higher than the possible system pointing accuracy mentioned above. The most common way to tackle with this problem is to introduce the terrain height of each earth point target by using a Digital Elevation Model (DEM).

In principle, an absolute mapping accuracy could then be achieved within the bonds of the system parameter accuracy. However, the introducing of a "foreign" data set like DEM, which has no direct relationship to the SAR mission data or even to remote sensing geometry, can cause "scaling" problems. These problems will come from:

--the remaining uncertainty of the SAR pixel location.

--shifts and scalings in reference to the common ellipsoid.

--errors and uncertainty in DEM generation.

Having this in mind, it is obvious, that some ground control must be incorporated in the geocoding process, when precision mapping is aspired. In any case, the quality control of geocoded SAR products must use ground control to verify the achieved accuracy.

Following the principles of geocoding stated so far, SAR geocoded products can roughly be divided into two categories:

--Geocoded without terrain correction, using an ellipsoid as reference earth surface and referenced to the system initial geometric accuracy. These products are abbreviated here GEC (Geocoded with Ellipsoid Correction).

--Geocoded with terrain correction, using a DEM as reference earth surface with more precise accuracy introduced by ground control points. These products are abbreviated GTC (Geocoded with Terrain Correction).

The algorithms for generating these two basic products at the German-PAF are described in the following chapters.

#### 4. Geocoding Without Terrain Correction

Due to the spare availability of DEM data, the GEC-data are considered to represent the major throughput of the Geocoding System. As already mentioned above, the SAR systems inherent pointing accuracy can be used to rectify SAR images without any foreign control or tiepoint information. Using this scheme, the geodetic location of each SAR image pixel could be estimated and resampled to the desired map projection. Of course, this approach would be rather time consuming and ineffective. Instead, the correct SAR image pixel to ground correspondence of four corner pixels of an appropriate rectangular frame is calculated precisely. The area and pixels in between the rectangle are transferred using a lower degree polynominal, estimated from the four corner pixels mapping function.

The deviation of the geocoded pixel location using polynominal interpolations instead of the correct transformation formula depends on the mesh-size and the used interpolation formula. For SEASAT images this approach, with a 500 pixel mesh size gives only deviations of one pixel with respect to correct mapping. Due to the increased data throughput without considerable loss of accuracy, this rectification scheme is used in many geocoding algorithms.

Considering that geocoding of satellite borne imagery consists mainly of a rotation towards grid north and some rectification of internal

distortions of the image, the rotation of points within the mesh frames can be written:

$$\begin{pmatrix} x' \\ y' \end{pmatrix} = \begin{pmatrix} \cos\theta & \sin\theta \\ -\sin\theta & \cos\theta \end{pmatrix} \begin{pmatrix} x \\ y \end{pmatrix}$$

In re-arranging the transformation matrix and splitting in two steps, the formula reads (Curlander, 1987a).

$$\begin{pmatrix} x' \\ y' \end{pmatrix} = \begin{pmatrix} 1 & 0 \\ -\tan\theta & \sec\theta \end{pmatrix} \begin{pmatrix} \cos\theta & \sin\theta \\ 0 & 1 \end{pmatrix} \begin{pmatrix} x \\ y \end{pmatrix}$$

A further initial step can be involved to avoid aliasing when rotating and resampling the image. This step oversamples the image in y-direction. The oversampling factor nf is derived from the rotation angle (Friedmann, 1981).

$$nf = 1 + \tan\theta$$

Although the initial 1-step formula seems to be more convenient than the derived 3-step formulas, the re-arranged resampling scheme has important advantages. The step-by-step rectification touches only one coordinate direction per step and needs only 1-dimensional resampling kernels. Considering a  $4 \times 4$  cubic convolution 2-dimensional kernel, 16 points must be touched, whereas only 8 in the modified 1-dimensional scheme (plus 4 additional in the initial oversampling step). This remarkably increases data throughput. The line/column access scheme fits to the data needs of array-processors and simplifies address calculation. Figure 1 shows a schematic sketch of the gercoding process.

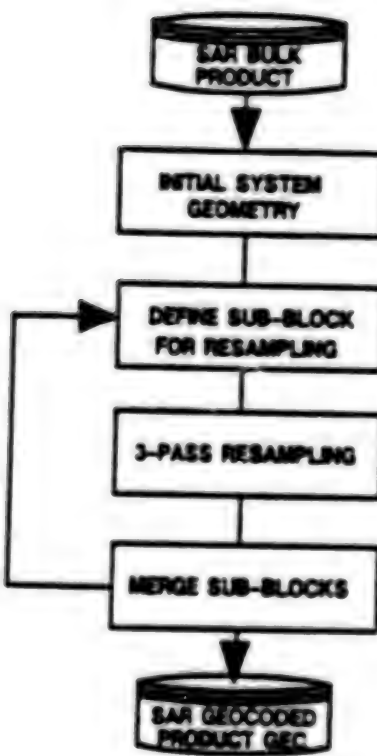


Fig. 1 Geocoding Process Without DEM Correction

Because no ground control information or control and merging of DEM data is required for this geocoding process, it can run without operators interaction.

Therefore, the flexible architecture of the D-PAF Intelligent SAR Processor (ISAR), consisting of a huge hardware memory, a powerful 100 MFlop array processor and a UNIX workstation host, is used as an implementation target for generating the SAR geocoded GEC product in one standard map projection (e.g.: UTM).

The direct coupling of SAR image generation and SAR geocoding within one process will make it possible to use the complex intermediate data for geocoding input rather than the look summed and detected slant range image.

## 5. Geocoding With Terrain Correction

When terrain correction is involved in the geocoding process, the computing algorithm becomes more complicated, due to additional raster data sets needed (DEM), which requires data handling and geometric model adjustment.

Together with contracted institutes, DFVLR has performed a phase-B study to identify the required algorithms and to introduce and test new approaches. According to the gained results, the operational processing scheme for GTS-products will be as follows:

The terrain elevation data, which is necessary for GTS-product generation will be stored on-line in raster format in a large disk database. Before adding DEM data to this database, quality tests will be performed to ensure a minimum accuracy of the DEM data used. Although, it must be aspired that DEM generating organizations might perform a quality test, the results we have gained with different height data from different sources, unveiled a variety of errors--some severe and some neglectable for geocoding--which are partly derived from the generation process of the DEM data.

From the DEM database, the required part of the DEM is resampled to the cartographic projection demanded by the geocoding process. This resampling of DEM data will use a comparable fast algorithm as outlined for the SAR GEC-Geocoding mentioned in the previous chapter.

As stated earlier, the utilisation of the resampled DEM for terrain correction might give erroneous results, because the estimated SAR point location accuracy (ERS-1 about 100 m) and the DEM accuracy (FRG: approx. 25 m raster size) might not fit on a pixel by pixel basis. Hence, both geometry models need to be adjusted and refined. Due to the origin of most DEMs from maps, the height model itself will be used as a geometry adjusting reference.

This can be achieved by considering the strong influence of hilly topography to the backscatter of SAR images. Using the imaging geometry and simple backscatter assumptions, a simulated image can be generated out of hilly parts of the DEM, showing the backscatter behaviour of the SAR with an exact cartographic reference. After some pre-processing, the original SAR image can be correlated with the template, giving an "artificial" tiepoint. The phase-B study results (Wiggenhagen, 1988) showed that the process can work automatically and gives better results for considerably good DEMs than matching SAR with Landsat TM images.

The "artificial" tiepoint with DEM-derived information has several advantages:

--No other external data set (like Landsat or Spot) is needed, which

might introduce inconsistent geometric adjustment. Instead, the DEM data itself, which is used for terrain correction is the geometric reference.

--The search for "candidate" hilly regions for simulation and matching can be done in advance. Using the pre-known geometry of ascending and descending ERS-1 orbit, candidate regions can be found and flagged in the DEM database. Operationally, it will only be necessary to simulate small regions, around hilly areas, rather than simulating the whole image.

--Test show (Curlander, 1987b) that the DEM to SAR image geometry derivation is mainly driven by linear effects. Thus, only few tie-points (2-3) will be needed for the adjustment, which can be found even in moderate hilly terrain.

By introducing these few tie-points, an adjustment calculation will fit the geometry estimation of the processor to the needs of the DEM data and cartographic accuracy (Raggam, 1987). The number of necessary tie-points and the degree of adjustment will depend on the sensor behaviour. For ERS-1 the orbit will be known very accurately and the SAR processor will produce considerable location estimates. Thus, only a few tiepoint might be necessary.

Having the adjusted imaging model and the resampled DEM data, a backward resampling to generate the GTS-product can start. There, each DEM point, corresponding to the pixel size in the final output image, is transferred to a common cartesian system, as well as the satellite orbit. A slant-range vector from DEM point to an estimated orbit position is defined, giving a relationship between slant-range length and Doppler-azimuth reference. The orbit point is now iterated to fulfill the range-Doppler relation given by the system geometry. The calculated range and orbit position gives the line and column location in the SAR slant range image which is used to resample the appropriate gray value of the output pixel of the GTS-product, located at the initial DEM point (Meier, 1985). Figure 2 shows a schematic flow chart of this process.

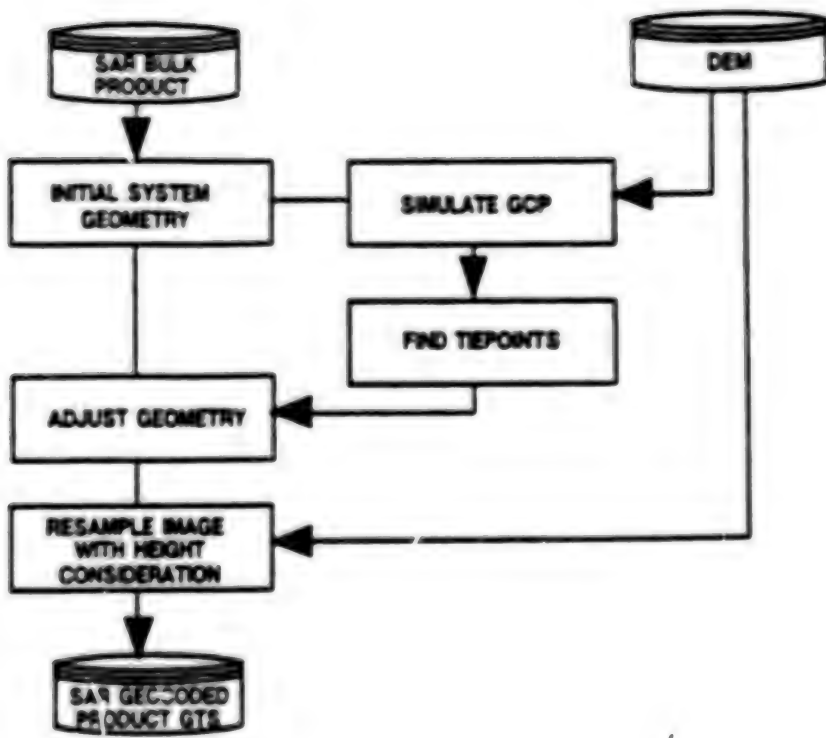


Fig. 2 Geocoding Process With DEM Correction

In contrast to the GEC-product generation, the GTS-product generation must touch each DEM point for the exact location computation of the geocoded SAR pixel. Hence, the utilisation of fast geocoding algorithms, mentioned earlier, is more complicated to realise. A polynomial interpolation of the correct imaging geometry for small sub-frames must also treat the DEM geometry transfer and terrain height dependant adjustment. This resampling scheme will increase data throughput and is modified to meet the requirements of pixel location accuracy within the magnitude of the DEM raster size used.

#### 6. The Software Environment of the Geocoding System

The sketch of the geocoding algorithms explained in the previous chapters reveals the diversification of the necessary data and input/output interfaces for this task.

Obviously, geocoding is tightly coupled to the output of the SAR processor and its computed parameters. As far as more accuracy in location is aspired, geocoding has also to tackle with digital elevation data, ground control points and precise map projections. Finally, all

these data sets must be visualised, at least for quality control. For the D-PAF, geocoding is a set of modules to be integrated in a remote sensing image processing system, which is modified to the special needs of an operational production environment. Since several years, DFVLR, together with a software company, develops and uses the UPSTAIRS image processing software running on the VAX-VMS operating system. The UPSTAIRS software is dedicated to process remote sensing images and supports program development with pre-defined user/machine interface calls and simple access to a sophisticated image database. A magnitude of application programmes covers the area of radiometric and geometric processing of satellite borne raster images.

For the geocoding system, the UPSTAIRS kernel was ported to UNIX and partly rewritten in C (see Figure 3). Along with the software transfer, some important modifications, which enhances operationality of the Geocoding System have been integrated. These upgrades support operational data throughput, new data like DEM and GCP and a new user interface based on the bit-mapped screen of UNIX workstations. They are described in more detail as follows.

#### Data Throughput Upgrades and Upgrades for Operational Use

In contrast to an image processing systems as a "scientific tool," the operational Geocoding System has to store only the SAR input and the geocoded output image as a minimum. This data must be accessed and transferred as fast as possible. Therefore, software tools are integrated, which manage large pixel sets for fast data I/O by considering disk resources and HW/SW capabilities, especially the data transfer to the attached array processor.

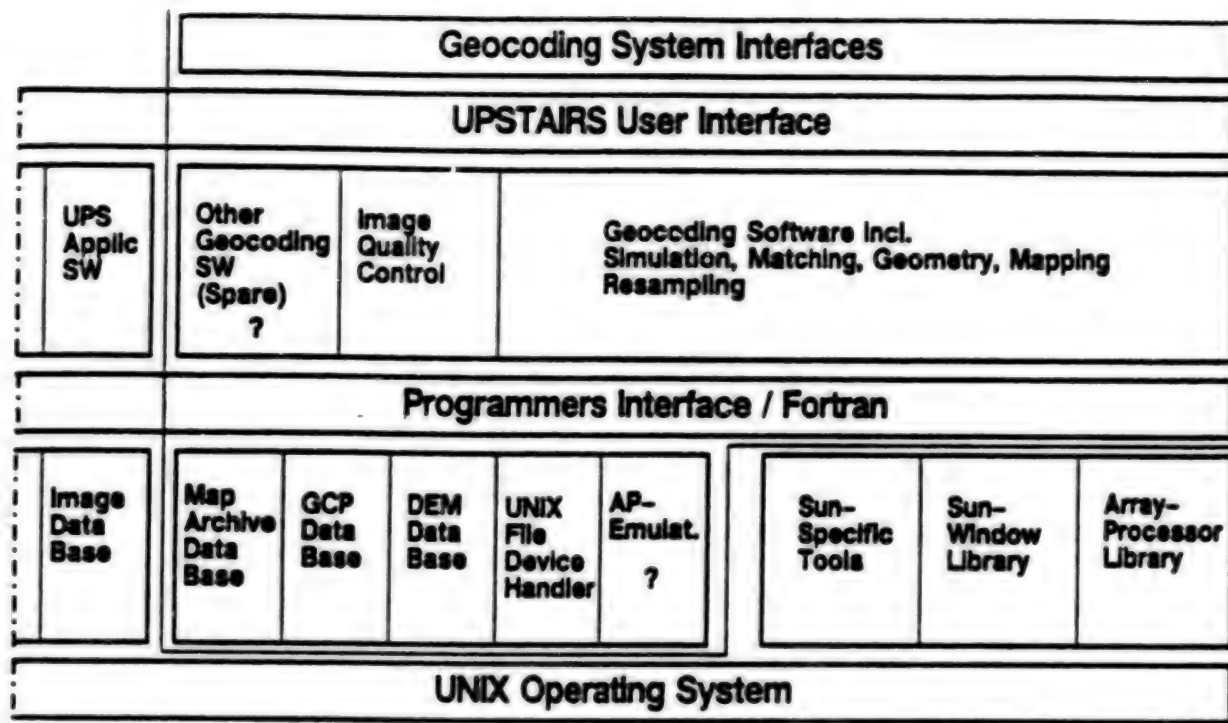


Fig. 3 Geocoding Image Processing System Software Layers

To exchange data and parameters between different modules of the geocoding system, a "parameter pool" is integrated, which resides in the computer memory and delivers access via write and read functions. This feature will support the programming and the flexibility of the modules, rather than exchanging parameters by files.

#### The Databases for DEM

Although the Digital Elevation Model raster data could be stored like image data, its handling within the Geocoding System is organised in a DEM database. The database is structured according to a geographic binary reference tree. Each branch in the tree defines a reference area. The final data-tile on the earth surface is able to store DEM raster sizes of about 10 m x 10 m resolution plus additional annotation data. These include flags for candidate simulation areas for artificial tie-points stated earlier. All DEM data will be stored on-line on magnetic disks. The capacity of the DEM database is only limited by disk capacity and--in principle--allows to store DEMs covering the whole globe. With subroutine calls, the DEM data can be accessed and resampled to the format required by the geocoding process.

### The Operators Interface for the Geocoding System

The geocoding system will run on a UNIX workstation with "bit-mapped" screen. This screen allows to display concurrently graphics, images (up to 256 different colours out of 16 million) and alphanumerics in different "windows" and utilizes a "mouse" as a fast and versatile user input device. Whereas the normal menu screen is managed in alphanumerics and gets its input via keyboard, the system will have some tasks, which directly benefit from the advanced user interface. Among these tools in the final image quality control, which will be performed using the normal colour screens, capable of displaying 900 x 1152 pixels in 256 shades of grey.

There, features in the geocoded SAR image--displayed on the screen--will be compared with homologue points on map paper sheets on a digitizer table. Knowing the geocoded coordinates of the product the cursor on the screen will move, controlled by the movement of the digitizer pen.

### 7. The Hardware Environment of the Geocoding System

The revolutionary development in computer techniques gave smaller systems the capabilities of former mainframe hosts. Due to their reasonable costs, small workstations can be dedicated to one task and equipped with special hardware like bit-mapped screens, fast and large disks and array processor.

Nevertheless, such dedicated systems are not isolated as far as they are coupled via communication links to other workstations, building up a computing system with one (or even more) computing units for each task, but with the transparency of a large mainframe. Together with the UNIX operating system, supported by more and more manufacturers, these computer networks can easily be adopted to different needs.

The Geocoding System is part of a larger workstation network with dedicated software and hardware for each function like SAR processing, data management and facility control.

A sketch of the Geocoding System is given in Figure 4. The server workstation controls the Geocoding System and is the physical storage for the DEM and GCP database, as well as the I/O interface to SAR data stored on optical disks.

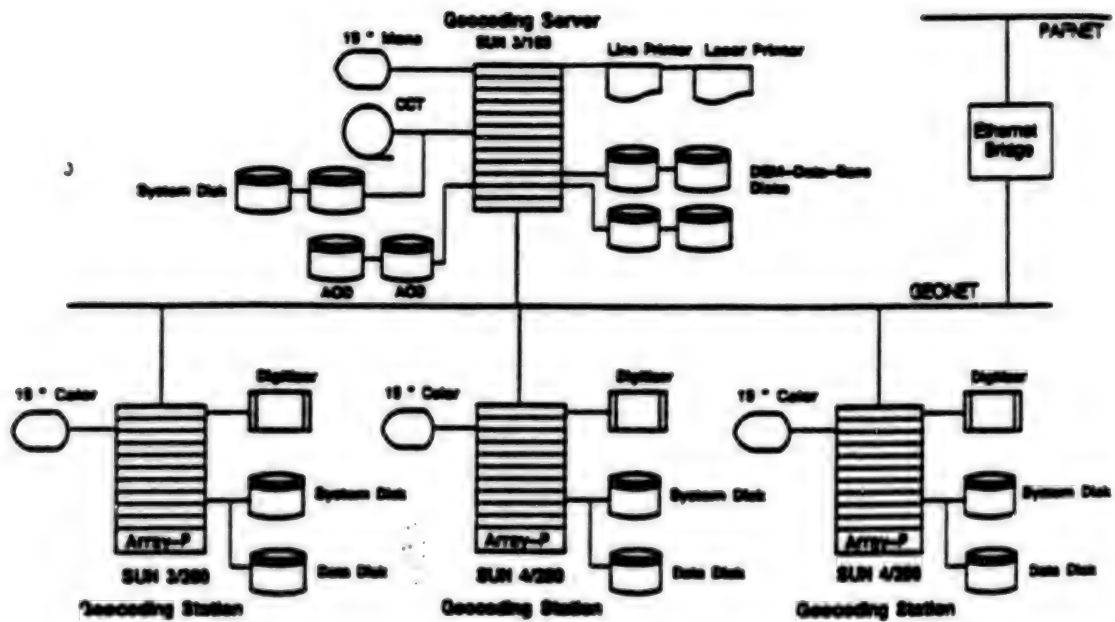


Fig. 4. Hardware Configuration of the Geocoding System

To cope with the variety of products, the expected data throughput and to perform manual quality control and experimental processing without interfering the operational throughput, three identically equipped workstations are foreseen for the system. As stated earlier, the geocoded product without terrain correction will mainly be produced by the SAR processor. This processor is also based on the workstation concept but equipped with special hardware like huge corner turn memory

and a fast array processor (Noack, 1987). The Geocoding System mentioned above, will produce geocoded products without terrain correction for required special map projections and all geocoded products which need Digital Elevation Models for precise mapping.

## 8. Conclusions

Aspects for an operational system for geocoding SAR images with and without terrain rectification have been discussed and the design for the German Processing and Archiving Facility Geocoding System (D-PAF GEOS) for ERS-1 SAR images was presented. Though, this system is dedicated to ERS-1, it will also cope with SIR-C/X-SAR images and has the capability to process other satellite SAR images as well.

Further, our aim was not only to build up a mission dedicated number cruncher, but to define a basis in terms of concepts in software, hardware and methodology for advanced user needs to geocoded SAR products for the polar platform area.

## 9. References

1. Curlander, J.C.: Location of Spaceborne SAR Imagery; IEEE-GRS, Vol. GE-20, No 3, July 1982.
2. Curlander, J.C., Kwok, R., Pang, S.B.: A Post-processing System for Automated Rectification and Registration of Spaceborne SAR Imagery, Int. J. Remote Sensing, Vol. 8, No 4, 1987.
3. Currlander, J.C., et. al.: An Algorithm for Generation of Geocoded Data Products From Spaceborne SAR Imagery, JPL D-4801, Technical Publication, 1987.
4. Friedmann, D.E.: Two-Dimensional Resampling of Line Scan Imagery by One-Dimensional Processing, Photogrammetric Eng. and Remote Sensing, Vol. 47, No 10, 1981.
5. Meier, E., Nuesch, D.: Registration of Spaceborne SAR Data to Large-scale topographic maps, 79th Int. Sym. of Remote Sensing on Environment, Ann Arbor, 1985.
6. Noack, W., Popella, A., Schreier, G.: Knowledge-Based SAR Processing and Geocoding IEEE-GRS, Vol. GE-25, No 6, 1987.
7. Raggam, J.: Relevant Parameters in the Reconstruction of the Analytical SAR Sensor Model Institute for Image Processing and Computer Graphics, Graz, Austria, Technical Publication, 1987.
8. Wiggenhagen, M., Sasse, V.: Praktische Anregungen zur geometrischen Korrektur von SAR-Bildern, eingereicht fur BuL, 1988.

/08309

### A Survey of Aerial Image Quality Assessment Methods

43070009c Kyoto Selections From INTERNATIONAL ARCHIVES OF PHOTOGRAHMTRY AND REMOTE SENSING in English Vol 27 1988 Part 810 pp 144-154

[Article by Anders Boberg, MSc, The Royal Institute of Technology, Department of Photogrammetry, S-100 44 Stockholm, Sweden, Commission I]

#### [Text] 1. Abstract

The accuracy of photogrammetric mapping, as well as the reliability of image interpretation, strongly depend upon the quality of the images used. It is therefore important to assess or describe image quality. Different areas of application and various methods of evaluation imply quality demands that differ considerably. An investigation into the nature of these demands and into the differences between them is necessary as a basis for further investigations of image quality criteria. Image quality measures must be relevant with respect to subjectively experienced image quality or image usefulness. At the same time the measures should be based on objective measurements of image properties.

In this survey, subjective as well as objective image quality criteria are studied. Methods for evaluation of image information are investigated from an image quality point of view. Special emphasis is put on the adjustment of objective assessment methods to subjectively experienced image quality with respect to certain applications.

#### 2. Background

The results of an application of aerial photographs, either in the form of photogrammetric mapping accuracy or in the form of image interpretation reliability, is highly dependent on the image quality of the photographs used. An example of this is the accuracy and reliability improvement of photogrammetric mapping from low altitude aerial photographs, resulting from the introduction of aerial cameras using forward motion compensation (Ackerman 1986, Boberg 1986). Image quality affects not only the result of the mapping or interpretation

project, but also the time consumed for image evaluation and subsequent field completion, and therefore the costs involved in the project. It is therefore important, not only to produce aerial photographs of the highest possible quality, but also to be able to assess or describe the quality of the images produced.

The main objective of the project, of which this is a status summary, is to find methods for assessment and description of the image quality of existing aerial photographic negatives. The quality of the image-forming process, or of the parts thereof, is thus not stressed. Also, the presence of imaged test objects cannot be presupposed. The study is restricted to near-vertical photographs, taken with 15/23x23 cm aerial mapping cameras on black-and-white film, disregarding, e.g., geometrical quality and color balance. In this paper, a number of image quality descriptors and assessment methods will be reviewed from the point of view of their relevance and practical applicability. The review is based upon a literature survey and upon a few preliminary experiments.

### 3. The concept of image quality

#### 3.1. Image interpretability

An imaging system translates an object's spatial and spectral radiation characteristics into a density (or color) distribution over an image plane. The imaging process is an information channel, the end product of which is a memory for information. Information is retrieved from the memory by interpretation of the image. The amount and quality of information that can be retrieved, is dependent upon the quality of the image, expressed in a relevant way with respect to the human ability to interpret the image. Therefore, the interpretability of images will be the basis of a discussion of the relevance of different quality descriptors. It is at this stage important to bear a few things in mind:

--Image interpretation is a very complex process, the result of which is dependent not only of the detail definition of the image and of the visual properties of the eye, but also of the psycho-physical interactions between the eye and the brain.

--Image interpretation, e.g., mapping, is normally performed stereoscopically. The mechanism of stereoscopic vision is in this respect not fully known. According to Konecny, et al. (1982), features could be interpreted stereoscopically with only half the resolution required to interpret the same features on single images. Trinder (1986) claimed that the boundaries of the objects rather than the areas are the important properties used by the visual system to detect the stereoscopical disparity. These questions, as well as the effect of different image quality for the left and the right eye, should be further investigated.

--Most interpretation tasks are based upon a priori knowledge or expectation of the existence, location or shape of objects. This may affect object detectability and recognizability.

The two main approaches to image quality description are the subjective and the objective one. Both are at the same time weak and strong. Combining the strength of the methods while avoiding their weaknesses has been the more or less explicit aim of many image quality studies.

### 3.2. Image quality demands

Aerial photographs are used for many different applications, utilizing many different types of instruments. This implies that image quality demands may differ considerably. One reason for this is that image quality may mean different things for, and is described in different ways by, different categories of image users. For example, stereo-plotting in analog or analytical plotters, photo interpretation in instruments with high image magnification, orthophoto production, image coordinate measurement for block triangulation, image digitizing for automatic image matching measurements, and digital mono-plotting from image coordinates measured on a digitizing table all may put different demands on the quality of the images used. An investigation into the nature of these different quality demands is necessary.

## 4. The influence of the photographic process

### 4.1. Exposure and dodging

The photographic process has a determining influence on image quality. The reason for mentioning this again is the availability of aerial mapping cameras with forward motion compensation (FMC), which have increased the possibilities to optimize film exposure and made fine-grained, low-sensitivity films possible to use also for low altitude aerial photography. As reported before (Boberg 1986), image quality as assessed by the National Land Survey of Sweden (NLS) has improved using this technique.

Image resolution varies with exposure (Brock 1952, Corten 1960, Zeth 1984). This restricts the useful log brightness scale and the exposure latitude. Exposure should bring also the darkest parts of the subject to the straight part of the D/logH curve. Corten used  $D_{min} = D_{fog} + (0.1-0.3)$ , while Graham and Read (1986) indicate best resolution at  $D = D_{fog} + (0.4-0.6)$  and Istomin (1961) at  $D = D_{fog} + 0.6-1.0$ . Gerencser (1979) recommends  $D_{fog} < 0.2$ ,  $D_{min} = D_{fog} + (0.2-0.4)$  and  $\Delta D = (0.8-1.5)$ . The NLS uses  $D_{min} = 0.5$  and  $D_{max} = 1.4$ , giving a density range of  $\Delta D = 0.9$ , according to practical experience.

Istomin (1961) used the amount of exposure range, within which a photographic material provides for a pre-determined resolution, as an information capacity criterion.

Corten (1960) investigated the resolution of transparencies and paper prints of different gradation and exposure, as function of the copy density. With the aim to optimize the copy resolution, he recommended the use of density compression (dodging) to an apparent density range of  $\Delta D = 0.6$  and a high contrast copying material. Since then, the silver content of photographic materials has decreased, and air pollution has changed the haze conditions. Tone reproduction studies of today's conditions would therefore be of great interest.

#### 4.2. Photographic tone reproduction

Tone reproduction diagrams show how densities and contrasts are transferred from the object to the positive copy. A limited, preliminary measurement and construction of photographic tone reproduction curves of aerial photographs of the NLS quality marks 7 (which is the very best), 5 and 3 (which is barely accepted) has been made (see Figure 1). The  $D/\log H$  curves were constructed with the help of the step tablets in the Zeiss Jena LMK camera frame. The solid parts of the curves represent the object range. From the graphs, the values in Table 1 were derived.

The following, very preliminary conclusions can be drawn from the figures and the table:

- The negatives are nicely linear, but only a limited part thereof is used--apparently the best part from resolution point of view, though!
- Negative gradation is relatively high for film 2412, which could be expected.
- Negative density difference  $\Delta D_n$  varies with NLS quality mark approximately as  $NLS\# = 5 \times \Delta D_n$ .
- Positive gradation is very high for copies from film 2405. As automatic dodging has been used, diminishing the positive exposure range  $\Delta log H_p$ , this is in accordance with Corten's (1960) recommendations.
- The gamma product is very high, and inversely proportional to the quality mark.
- The negative density range partly falls below the linear part of the  $(D/\log H)_p$  curve, resulting in a similar result for the final tone reproduction curve. This is especially evident in the NLS#5 curve, and is probably the result of copy underexposure.
- An increased exposure and a shorter development time of the copies seem preferable.

Summing up, photographic tone reproduction curves seem to be an interesting source of information on reasons for image quality differences. The effect of dodging on them should be further investigated. To use them for image quality assessment, they have to be coupled to other quality descriptors.

## 5. Subjective image quality descriptors

### 5.1. Resolving power

A resolution test means a subjective decision whether imaged test patterns, normally three-bar targets of increasing line frequency, are resolvable or not. The test leads to resolving power values in lp/mm for the imaging system. The subjectivity of the method is limited to the judgment whether the three-bar target is possible to resolve or not.

Although resolving power measures the combined effect of all the information transmitting or degrading parameters in the imaging system, it has no absolute or permanent significance, derived from physical optics, but simply means the ability of a camera system to reproduce fine details of the type of the test object (Brock 1952, 1969).

Resolving power is an incomplete description of image quality, although it is reported to show strong correlation to subjectively experienced aerial image quality. Resolution is different for objects of different shape, size, arrangement and contrast (Rosenberg 1971, Overington 1974). A high-contrast pattern limits the usefulness of the method, as the landscape normally imaged in aerial photographs consists of different, mainly low contrasts. Brock (1952) is clearly in favor of an annulus target, with target contrast  $\Delta D = 0.2$ . Further, as the method presupposes the imaging of man-made targets, it is not applicable for routine airphoto production.

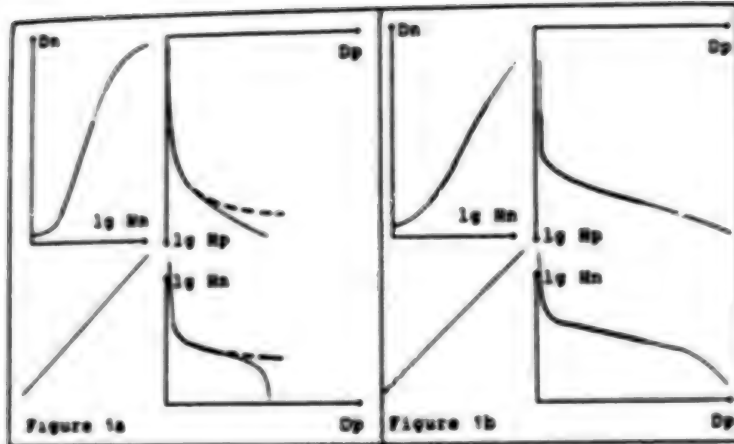


Figure 1a

Figure 1b

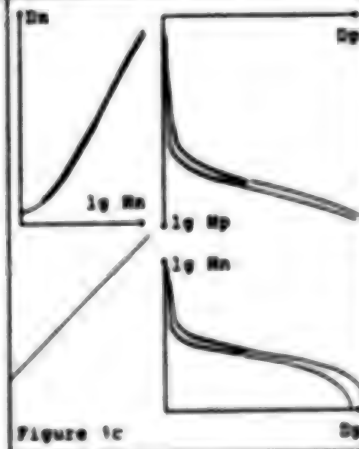


Figure 1c

**FIGURE 1** Tone reproduction diagrams for MLS aerial strips of different subjective image qualities (MLSQ).  
Aerial camera: Zeiss Jena LMK 15/23 with INC

**Fig MLSQ Film F1b a**

| ls | 7 | 2412 | 2300 |
|----|---|------|------|
| ls | 5 | 2405 | 1600 |
| ls | 3 | 2405 | 1500 |

| MLSQ | algmn | Adn | Adp | Adp/algmn | vn  | vp  | vnpvp | MLSQ/Adn |
|------|-------|-----|-----|-----------|-----|-----|-------|----------|
| 7    | 0.8   | 1.3 | 1.6 | 2.0       | 1.8 | 1.6 | 2.9   | 5.4      |
| 5    | 0.9   | 1.1 | 1.5 | 1.7       | 1.1 | 3.3 | 3.7   | 4.5      |
| 3    | 0.7   | 0.7 | 1.0 | 1.4       | 1.1 | 3.9 | 4.4   | 4.3      |
|      | 0.5   | 0.5 | 1.1 | 2.2       |     |     |       | 6.0      |

**Table 1.** Photographic density values for negatives of different subjective image quality (MLSQ), and for the corresponding diapositives.

Thus, resolving power is useful for comparison of the performance of different imaging systems, but not for quality description of images in hand.

## 5.2. Quality mark assessment

The National Land Survey of Sweden (the NLS) performs nearly all aerial photography for mapping purposes in Sweden. The assessment of image quality must not delay the production, and therefore must not be too elaborate. For this reason, a relatively simple, subjective image quality assessment method is used. Every photographed strip, as a unit, is given a subjective quality mark in a seven-step scale, expressing the mean photographic image quality of the negatives in the strip. The assessment is based upon criteria on illumination, gradation, haze and image motion, using a few density readings and ocular examination with a magnifying glass. The method was explained more in detail in (Boberg 1986).

The method works fairly well, according to experience on how the images are received by the users. However, a more thorough investigation into the relevance of the quality marks for different categories of image users is needed. E.g., Biedermann (1978) has experienced that quality judgment depends on object detail and contrast and on the attitude of the observer to the imaged subject. Also, the NLS method should be calibrated in a more objective way than via a yearly review of the routines by the personnel responsible for the assessment. Measurements of objective parameters and calculation of quality descriptors of the negatives would thus improve the method.

## 6. Objective image quality descriptors

### 6.1. Image acutance

Acutance is a measure of image sharpness, using the gradient of a microdensitometer trace across an edge, which has an infinitely steep gradient in the object. Istomin (1961) reports of the acutance measure used by Jones and Higgins, namely the ratio of the RMS mean gradient of an edge response curve and the contrast of the edge, expressed as log exposure height of the edge. Contrast as information carrier for image interpretation is however better expressed as a density difference,  $\Delta D = D_{max} - D_{min}$ . If density is used instead of log intensity, and the photographic process is considered practically linear, acutance could be expressed as

$$A = \frac{1}{N} \sum_{n=1}^N \left( \frac{dD}{dx} \right)^2 \Delta D$$

in which the gradient  $dD/dx$  might be determined as the mean slope, like a gamma value.

Acutance is a complement to resolving power. The two might even be complementary, as high acutance often means low resolution and vice versa. The definition of acutance (in logH values) is related to edge gradient analysis for modulation transfer function determination.

## 6.2. The modulation transfer function

If an object is regarded to be composed of sinusoidal line patterns of different frequencies, an analysis of the degradation of the imaged object contrast, as a function of the spatial frequencies of the composing line patterns, leads to the modulation transfer function (MTF). This means, that if the line pattern frequencies are regarded as a measure of the sizes of image details, the MTF will describe the reproduction quality of imaged object details. Although this is not generally true, the MTF has been shown to be a good starting point for derivation of image quality measures.

MTFs could be determined for each step of the imaging process, as well as for the process as a whole. In our case, this is of certain interest, because the positive copy is the end user product, while the image quality assessment should refer to the negative. Knowing the MTF of the copying process, it could be reduced from the MTF of the copy, to get the function for the negative.

MTFs of images in hand must be determined from microdensitometer traces of natural image details. Normally, Edge Gradient Analysis (EGA) of natural sharp edges has been used for this purpose. Gerencser (1972, 1974, 1976) has gathered some experience from the EGA method, using the graphical method of Scott et al (1963) as well as an automated system. The accuracy requirements on the microdensitometer's length measurement was found to be very high. Using known contrast panels, the MTF curves don't have to be normalized to 100 percent modulation at 0.1 p/mm frequency, which makes it possible to evaluate the contrast reduction of the atmosphere. This experience is of interest for this study, as an image quality descriptor should encompass the whole imaging chain. The possibilities to use natural, known contrasts should be investigated. Gerencser expected difficulties in finding suitable edges and to define the trace length.

Especially in large scale aerial photography, the definition of the imaged object edge has to be considered carefully. Gerencser (1976) as well as Ackermann (1986) encountered great problems in finding suitable edges. In some cases, line objects for direct measurement of the Line Spread Function (LSF), may be easier to find, e.g., in built-up areas with road-markings. Figure 4 shows an example of this. Generally, image scale must be considered when suitable targets are chosen.

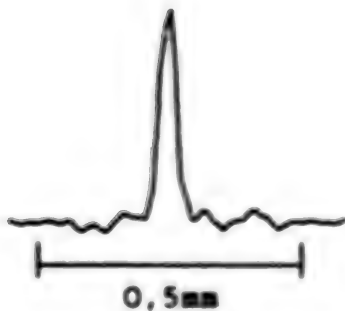


Fig. 4. An example of a microdensitometer trace across a white marking line on an airport runway. Image scale 1:15,000

A basic prerequisite for MTF analysis is that the imaging system is linear. The photographic emulsion is principally not, however. Welander (1968) has put together results that show that within reasonable limits of contrast, gamma product, frequencies and negative exposure range, the photographic process may be considered linear for practical purposes. Hendeberg (1967) showed that in the absence of adjacency effects, the MTF of the negative is independent of contrast and exposure within wide ranges. These results are of great importance if the total system result is to be assessed and related to subjective image quality. The negative quadrant of the tone reproduction curves shown above seems to fulfill the linearity well, but the positive quadrant does not, if copy exposure is insufficient.

#### 6.2.1. MTF condensation

A MTF is normally expressed graphically. Moreover, many MTFs are needed to fully describe all quality aspects of an image. It is therefore natural, that much effort has been devoted to try to condense the MTF into a single figure of merit. Computing the logarithm of the integrated area beneath the curve, or of a part thereof, has been the most commonly used method.

A Threshold Modulation (TM) curve for a specific emulsion and development describes the image modulation needed to resolve an object, as a function of object spatial frequency. The intersection of the appropriate MTF and TM curves gives a frequency threshold, which is a measure of the system resolving power. This threshold is often used as upper limit of the MTF condensation integration. The method is suited for prediction of the performance of imaging systems (Rosenbruch 1986).

A more promising form to use with images in hand is based upon integration of a frequency weighted MTF curve, as described below.

### 6.3. Granularity

Image interpretability is strongly influenced by graininess, especially when detail contrast is low. This could be expressed as a signal-to-noise ratio (S/N), where the object image contrast is the signal, and the graininess is the noise. According to experience, S/N = 4 is needed for object detection, and S/N = 10 for recognition (Welander et al 1972).

Graininess is measured as granularity, defined as the standard deviation  $\sigma_D$  of a large number of density readings, each covering a very small area of the image. Typically, a 24μm diameter aperture is used, but Gerencser (1972) used a 1,6x200μm microdensitometer slit. The Kodak method for granularity measurement, leading to RMS granularity ( $10^3 \sigma_D$ ), is supposed to indicate the impression of graininess perceived at 12x magnification of the sample. The Selwyn granularity measure G is standardized to a unit measuring area a as

$$G = \sigma_D / \sqrt{2a}$$

Granularity increases with the square root of the density value, and roughly in proportion to the contrast of the printing material (Welander 1968). This reduces its value as quality measure for images at hand.

Granularity could be investigated with the help of Fourier analysis, in which noise strength is expressed as a function of its spatial frequency. This form of description, a Wiener spectrum, is closely related to the MTF. Trinder (1980) has investigated this in detail, and found it important to consider the S/N in attempting to relate visual performance to image quality parameters.

## 7. Relations between objective and subjective criteria

Attempts have been made to correlate physically measurable figures of merit to subjectively perceived quality of photographic images. Biedermann (1967, 1978) tried in his thesis to relate subjective assessments of image quality via weighting functions to measurements of modulation transfer functions of the images. Biedermann's study concerned mainly "normal" images like landscapes, portraits, etc., but also an aerial photograph, at a viewing distance of 40cm. He found good correlation with subjective quality G (running from 1 "excellent" to 7 "useless") using the following function of MTF, denoted M(v):

$$G = C_1 + C_2 \log \int_0^\infty \frac{M(v)B(v)dv}{B(v)dv}$$

Different weighting functions B(v) were tested, of the form

$$B(v) = \frac{1}{1 + (Fv)^4}$$

where F could be varied. Thus, image quality was related to the logarithm of the area under the weighted MTF.

Rosenbruch (1986) proposes the agreement on a standard weighting function. However, frequency weighted MTFs, or derivatives thereof, as descriptors of aerial image quality, require weighting functions adapted to the image application and to the image evaluation situation at hand. As a base for the choice of frequency weighting functions, a study of the importance of different frequencies and contrast distributions for different applications is needed. The base for this should be an investigation into image quality demands of different categories of aerial image users, e.g., stereo operators, image interpreters, topographic map makers, forest taxators and physical planners. The judgment should be done in their real working situation, with the images oriented in evaluating instruments.

The result of such a study might be a suggested calibration procedure, or a replacement method, for the NLS subjective image quality assessment method.

## B. References

Ackermann F. 1986. Improvement of Image Quality by Forward Motion Compensation--A Preliminary Report. ISPRS Archives Vol 26, Part 1. ESA SP-252, Noordwijk, the Netherlands.

Boberg A. 1973. Nagra synpunkter pa begreppet bildkvalitet (Some Views on the Concept of Image Quality. In Swedish) Svensk Lantmäteritidskrift 3:1973, Stockholm, 22p.

Boberg A. 1986. Image Quality Problems in Practical Aerial Photography. ISPRS Archives, Vol 26, Part 1. ESA SP-252, Noordwijk, the Netherlands. Fotogrammetriska Meddelanden No 53, Department of Photogrammetry, the Royal Institute of Technology, Stockholm, 8p.

Biedermann K. 1967. Ermittlung des Zusammenhanges zwischen der Subjektiven Gute und den physikalischen Eigenschaften des Photographischen Bildes. Phot Korr, Band 103, Nr 1,2,3, pp 5-14, 26-31, 42-48.

Biedermann K. 1978. Subjective Quality and Modulation Transfer Function of Photographic Images. Physikalisch-Technische Bundesanstalt, PTB-Bericht PTB-Opt-7, pp 96-104. Braunschweig.

Brock G.C. 1952. Physical Aspects of Air Photography. Longmans, Green & Co, London. 267p.

Brock G.C. et al 1969. Photographic Considerations for Aerospace. Itek Corporation, Lexington, Mass. 122p.

Corten F.L. 1960. Image Quality in Air Photography. Degradation and Conservation of Details in Positive Copying. ITC Publications, Series A/B, No 5. Delft, 17p.

Gerencser M. 1972. Comparative MTF Tests of Entire Aerial Photographic System in Black-and-White and Color. ISP Archives, Vol 19, Commission I. Ottawa, Canada, 20p.

Gerencser M. 1974. Comparative MTF Evaluation of Aerial Photographic Systems by Simultaneous Using of RP, Spread Functions, MTF's, CTF's and Information Capacity. ISP Archives, Vol 20, Commission I, Stockholm, Sweden. 19p.

Gerencser M. 1976. Automated Edge Gradient Analyse (EGA) for Testing Photogrammetric Systems. ISP Archives, Vol 21, Commission I. Helsinki, Finland. 14p.

Graham R, Read R.E. 1986. Manual of Aerial Photography. Focal Press, London. 346pp.

Istomin G.A. 1961. Objective Evaluation Criteria in Image Photographic Quality. XIII Congr Intern della Tecn Cinematografica, Torino Sept 1961, pp 83-89.

Jensen N. 1968. Optical and Photographic Reconnaissance Systems. John Wiley and Sons, New York. 211p.

Konecny G, Schuhr W, Wu J. 1982. Investigation of Interpretability of Images by Different Sensors and Platforms for Small Scale Mapping. Proceedings ISPRS Commission I Symposium, pp 11-22.

Overington I. 1974. Visual Efficiency--a Means of Bridging the Gap between Subjective and Objective Quality. Proc SPIE, Vol 46, pp 93-102.

Rosenberg P. 1971. Resolution, Detectability and Recognizability. Phot Eng Vol 37, No 12, pp 1255-1258.

Rosenbruch K-J. 1986. OTF-based Quality Criteria for Aerial Cameras and Imaging Systems. ISPRS Archives, Vol 26, Part 1. ESA SP-252, Noordwijk, the Netherlands.

Scott F, Scott R.M., Shack R.V. 1963. The Use of Edge Gradients in Determining Modulation-Transfer Functions. PS&E, Vol 7, pp 345-349.

Trinder J.C. 1980. Aerial Film Granularity and Its Influence on Visual Performance. ISPRS Archives, Vol 23, Commission I, pp 167-181, Hamburg.

Trinder J.C. 1986. Precision of Stereoscopic Height Measurements. Phot Eng & RS, Vol 52, No 1, pp 75-79.

Welander E. 1968. Modulation Transfer Functions for Photographic Emulsions and Their Applications in Aerial Photography. Meddelande Nr A37, the Geographical Survey Office of Sweden, Stockholm.

Welander et al 1972. Photographic Modulation Transfer Functions. Report by ISP Commission I WG. ISP Archives, Vol 19, Part 1, Meddelande Nr A39, The Geographical Survey Office of Sweden, Stockholm.

Zeth U. 1984. Exposure Metering and Control in the LMK Aerial Survey Camera System. Sensing the Earth, Photogrammetric Instruments 1984/II, VEB Carl Zeiss Jena, pp 21-26.

/08309

The Processing of SPOT Imagery in Brazil

43070009d Kyoto Selections From INTERNATIONAL ARCHIVES OF PHOTOGRAHAMETRY AND REMOTE SENSING in English Vol 27 1988 Part B10 pp 300-307

[Article by Machado e Silva, Antonio Jose Ferreira d'Alge, Jollo Cesar Lima Bezerra, Paulo Cesar Rego Barbosa, Osvaldo Caldas; MCT - MINISTERIO DA CIENCIA E TECNOLOGIA, INPE - INSTITUTO DE PESQUISAS ESPACIAIS, Rod. Presidente Dutra, km 40 12630 - Cachoeira Paulista, SP Brazil, Commission II]

[Text] ABSTRACT

The purpose of this paper is to show the present situation of the Brazilian SPOT Direct Receiving Station, involving both the SPOT Receiving and Recording Station and the SPOT Image Processing Center. One of the main functions of the Processing Center is to perform the radiometric and geometric treatments in order to eliminate system distortions inherent to the HRV-SPOT images generation process. Nowadays, the station is capable to process images in the 1A and 1B levels, in both digital and analogical domains. In addition, new developments are being carried for the generation of HRV-SPOT images in the levels 2A, 2 and 3, where extra information obtained from ground control points and digital terrain elevation models are used to refine the geometric system corrections.

1. INTRODUCTION

The Brazilian SPOT Direct Receiving Station (BSDRS), set up by INPE, begun its operational phase in December, 1987. It comprises the SPOT Receiving and Recording Station (SRRS), located at Culaba, Mato Grosso State, and the SPOT Image Processing Center (SIPC), situated at Cachoeira Paulista, Sao Paulo State.

The antenna of SRRS is shared with the Landsat Receiving and Recording Station (LRSS), and its location allows full coverage of Brazil and most of South America. SIPC makes use of hardware facilities of INPE's Image Generation Department (DGI) which were primarily configured in view of TM data processing, and are still used also to this end.

Figure 1 shows the present hardware configuration both for SRRS and SIPC, while Figure 2 presents the software already implemented. Together, they give an overview on the complete SPOT data manipulation cycle performed at BSDRS.

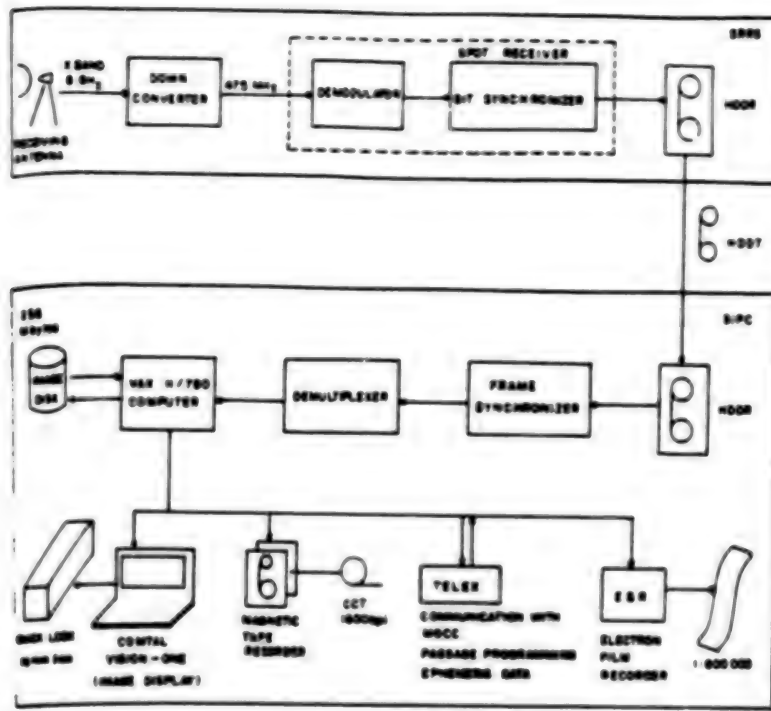


Fig. 1. BSDRS Hardware Chain

Nowadays, the station is capable of producing images in the 1A and 1B preprocessing levels, and new efforts are being carried by INPE in order to enable the processing at higher levels. These efforts are oriented into two directions:

--Development Project SPOT2, whose objective is to implement a processing subsystem corresponding to levels 2A and 2 before the end of 1988.

--Research Project SPOT3, where experiments with Digital Terrain Elevation Models are being made with the aim of giving subsidies to a future development project.

The differences between the various levels are concentrated on software functions GEO and COR, and so the following sections are dedicated to describe the different mathematical models associated with them.

## 2. PREPROCESSING LEVELS 1A AND 1B

As stated earlier, these are the levels at which SPIC is presently capable to generate SPOT images. Thus, in the scope of the software package already implemented, the aim of GEO is to determine the geometric correction parameters for the image generation at level 1B; for all scenes recorded during one pass of the satellite. COR is applied for the generation of each scene, both on level 1A and 1B; if the level is 1A only radiometric corrections are done, while if it is 1B the geometric corrections are also taken into account, based on the parameters computed by GEO.

### 2.1. GEO FUNCTION

On level 1B, one-dimensional geometric corrections are used, which allows one to write the inverse mapping equations as follows:

$$L = f(I) \quad (1)$$

$$C = g(J) \quad (2)$$

$$\Delta J = h(I) \quad (3)$$

where  $(L, C)$  and  $(I, J)$  correspond to (line, column) in raw and corrected images, respectively.

The applied geometric correction model, known as photogrammetric model, relates each point in a raw image to another one in a tangent plane to the reference ellipsoid, with the tangency point corresponding to the raw image center.

Due to the HRV-SPOT sensor characteristics, all the pixels belonging to a given raw line are acquired at the same time. Because of this, the sight directions relative to these pixels determine a plane, and thus the intersection of this plane with the projection plane defines a straight line, which validates the hypothesis related to equation 1. Nevertheless, it is important to observe that the direction of this line will be variable if the heading velocity and the yaw are not constant.

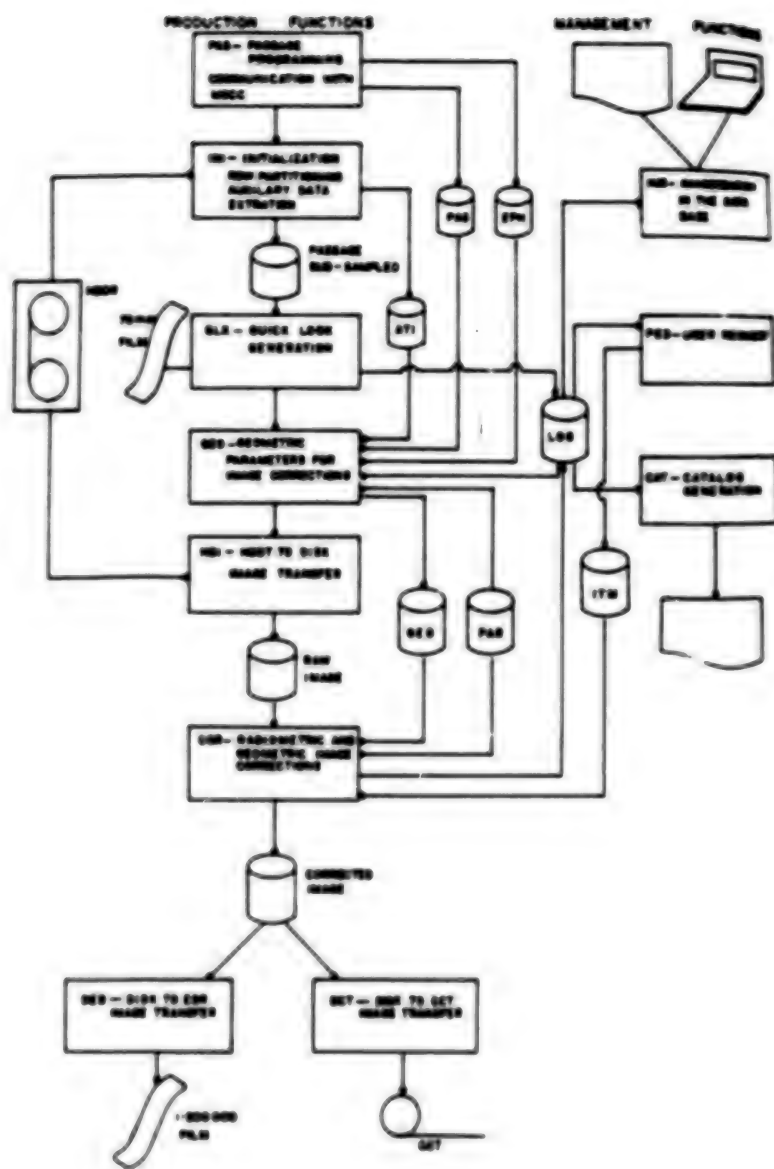


Fig. 2. SPIC Software Chain

Otherwise, the pixels belonging to a given raw column are sampled at different times, being submitted to different effects coming from attitude and heading velocity changes and, above all, from Earth's rotation. These effects give rise to displacements between consecutive lines, causing discontinuities in the columns; these displacements are taken into account by equation 3.

Functions  $f$ ,  $g$  and  $h$  were specified as third order polynomials, being left to GEO the determination of their coefficients ( $f_1$ ), ( $g_1$ ) and ( $h_1$ ), as well as the computation of geodetic coordinates (latitude  $\theta$  and longitude  $\lambda$ ) of the scene center and of its corners.

The polynomials coefficients are determined by applying the photogrammetric model to two sets of 61 breakpoints each, one regularly spaced along the center line ( $(g_1)$ ) and the other along the center column ( $(f_1)$  and  $(h_1)$ ).

The photogrammetric model can be depicted by a two equations system, the first one corresponding to the straight line defined by the satellite position and some sight direction, and the other one corresponding to the reference surface.

Initially, the position of the satellite and the reference surface are entailed to the Greenwich geocentric system, and the sight angles are related to the HRV imager reference system as a function of operation mode, mirror position and detector number. Transformation from the latter to the former system is done in three steps, through boresight and attitude angles, and ephemeris data.

Attitude angles are determined by integrating attitude rate data broadcasted by the satellite. This integration is first carried out assuming a null attitude for the first received attitude rate record; later, when the geometric parameters for each scene are to be computed, the attitude at scene center time is subtracted from the integrated data corresponding to that scene, thus zeroing the scene center attitude. Ephemeris data obtained via telex link are interpolated through a seventh order Lagrangian polynomial.

The projection plane has its tangency point to the ellipsoid defined by the application of the photogrammetric model over the ellipsoid for the scene center. The photogrammetric model is then applied over this plane for every breakpoint, leading to a set of points with coordinates referred to the Greenwich geocentric system.

Afterwards, a projection system is defined with origin in the tangency point to the ellipsoid, Y axis corresponding to the center line on the projection plane, eastward oriented, and X axis orthogonal to Y, southward oriented. Using the origin coordinates and the unitary vectors X and Y, both related to the Greenwich geocentric system, it is possible to perform the transformation from this system to the projection system for all the breakpoints.

The lines and columns of the corrected image are oriented along the Y and X axis, respectively; for this reason, the conversion from metric projection coordinates to discrete coordinates (I,J) is easy and conditioned only to the nominal spatial resolution and the corrected dimensions.

The coordinates  $L_k$ ,  $l_k$  and  $J_k$  ( $J_k = J_k - J_{61}$ ) of the center column points are then related, and the coefficients  $\{f_i\}$  and  $\{h_i\}$  determined. In the same way,  $C_k$  and  $J_k$  of the center line points are related, and the coefficients  $\{g_i\}$  computed.

The geodetic coordinates of the scene corners are obtained by applying the photogrammetric model over the reference ellipsoid for the four raw image corners.

## 2.2. COR FUNCTION

This function is applied when an HRV-SPOT scene is to be generated, both on level 1A and 1B. In the first situation, only a radiometric calibration is executed, corresponding to a normalization of detector responses in each spectral band. On level 1B, besides the calibration, also radiometric deconvolutions along lines and columns and geometric corrections are applied.

The gray level interpolation associated to the geometric corrections may be performed in two different ways: nearest neighbour for lines and columns, or nearest neighbour for lines and cubic convolution for columns. In the former option, polynomials  $f$  and  $g$  are used to determine respectively the lines and columns to be suppressed or repeated. In the latter, polynomial  $f$  is used in the same way as in the former option, and polynomial  $g$  defines, within a given line, the four neighbours to be considered in the convolution. In both options, polynomial  $h$  is used to compute the number of black pixels corresponding to the corrected image left skew.

All operations executed by COR require the raw image to be read only once.

## 3. PREPROCESSING LEVELS 2A AND 2B

The HRV-SPOT imagery generation subsystem for levels 2A and 2 uses a geometric correction model which is applied in three steps.

In the first one, a direct mapping is determined through the photogrammetric model over the ellipsoid for a grid of  $61 \times 61$  breakpoints regularly distributed over the raw image. A set is obtained for each breakpoint, and the geodetic coordinates are transformed into projection coordinates (UTM, SGM, etc.), which are then converted into discrete image coordinates (I,J). As a consequence, a direct relation  $(L,C)-(I,J)$  is set up.

The second step begins with the direct mapping inversion, by using a grid of breakpoints regularly distributed over the corrected image. For this purpose, it is current to use from third up to fifth order

polynomials, which are defined by the resulting grid in the first step. This model has some disadvantages, as polynomials cannot represent high frequency distortions. Moreover, they are not reliable when applied to points located outside of the original grid. INPE is now searching into the determination of the inverse grid breakpoints from the four direct grid nearest ones.

The last step refers to the resampling process, where a gray level is determined for every point on the corrected image. The resampling includes a rotation over the images in order to orientate them northwards. Every line on the corrected image is related to 950 lines on the raw image in the P mode or 475 lines in the XS mode, so increasing the necessary computer memory, INPE intends to perform this resampling through the algorithms presented by Friedmann (1981) and by Craig and Green (1987).

The procedures above described are enough to produce a level 2A corrected image. In the case of level 2, ground control points are necessary to improve some geometric correction parameters, aiming at the use of the images as up-to-date planimetric maps. INPE has been concentrating its efforts in three possibilities: a polynomial model (Bahr, 1978), a Kalman filtering attitude correction model (Caron & Simon, 1975), and an orbit correction model, comprising an ephemeris data correction and some well-known numerical orbit integrators, with the purpose of producing a fully corrected image over a scene without ground control points (d'Alge et alii, 1988).

#### 4. LEVEL 3 PERSPECTIVES

The SPOT satellite has an off-nadir viewing capability and, as a consequence, a stereo viewing possibility. It is feasible to achieve a base-to-height ratio of around, being possible to use the images for topographic mapping. Moreover, the off-nadir viewing allows the same area to be observed on two or five successive days, depending on the required latitude. It also permits the bidirectional reflectance distribution function to be investigated, and covers an area which is larger than in the near vertical viewing case.

This preprocessing geometric level rectifies the off-nadir viewing images within a geodetic accuracy better than 50 m. The merging between an off-nadir viewing image and another image over the same scene shall occur within a half-pixel accuracy. The planimetric displacements due to the existing relief are corrected and the resulting images are northward oriented.

The relief displacement of a point on the Earth's surface depends on its height and on the HRV viewing angle. Therefore, for height of about 1.000m and a viewing angle of  $27^{\circ}$ , the planimetric displacement due to the relief reaches 500 m (Guichard, 1986).

The current methodology foresees the application of the same photogrammetric approach used for level 2. In the off-nadir viewing case, any of the sight directions intersects two ellipsoids, both related to the reference ellipsoid: one is defined by the maximum height, and the other by the minimum height over the scene to be corrected. As a consequence, a point on the corrected image is related to two different points on the raw image, and its true position is defined by some interpolation algorithm, considering the information of a digital terrain elevation model.

The researches about this geometric correction level are being carried at INPE's Geographic Information System, comprising four data sets: raw image, grid related to the maximum height ellipsoid, grid related to the minimum height ellipsoid, and digital terrain elevation model.

## 5. CONCLUSION

This year, BSDRS will receive and record 4,000 SPOT scenes. It is capable to process them only in levels 1A and 1B. For the next year BSDRS is expected to generate images also in levels 2A, 2 and 3. Nowadays, the software system of the SIPC is being adapted to process these levels. The first results of level 1B geometric evaluation were satisfactory, leading to an intrinsic error of about 30 meters and an extrinsic error of around 500 and 300 meters, in the across-track and along-track directions, respectively.

## REFERENCES

Bahr, H.P. Geometrical Analysis and Rectification of LANDSAT-MSS Imagery: Comparison of Different Methods--In: Symposium of Commission III--ISPRS, Moscow, USSR, 1978.

Caron, R.H.; Simon, K.W. Attitude Time-Series Estimator for Rectification of Spaceborne Imagery -- Journal of Spacecraft--Vol 12 nr. 1, pp 27-32. Jan 1975.

Craig, M.D.; Green, A.A. One-Dimensional Resampling of Digital Imagery to Sparse Output Grids. Photogrammetric Engineering and Remote Sensing, Vol. 53, nr. 5, May 1987.

Friendmann, D.E. Two-Dimensional Resampling of Line Scan Imagery by One-Dimensional Processing--Photogrammetric Engineering and Remote Sensing. Vol. 47 nr. 10, pp 1459-1467, Oct 1981.

Guichard, H. Utilization photogrammetrique et Cartographique de SPOT in: Semaines Internationales de Photogrammetrie, Stuttgart, RFA, 1983. Stuttgart, ISPRS, 1983.

d'Algs, J.C.L; Bezerra, P.C.R.; Medeiros, V.M. Geometric System Correction with Orbit Determination as an Option to Produce TM-LANDSAT Image-Maps without Ground Control Points. In: 16th Congress of International Society for Photogrammetry and Remote Sensing, Kyoto, Japan, 1988.

/08309

### Data Processing and Calibration of SAR Data in Japan

43070010a Kyoto Selections From INTERNATIONAL ARCHIVES OF PHOTOGRAHMTRY AND REMOTE SENSING in English Vol 27 1988 Part B11 pp 232-241

[Article by Korehiro Maeda and Hideo Sato; Earth Observation Center (EOC), National Space Development Agency of Japan (NASDA), 1401 Ohashi, Hatoyama-machi, Hiki-gun, Saitama-ken 350-03 Japan Commission I; presented at the 16th ISPRS held in Kyoto, Japan in July 1-10, 1988]

#### [Text] Abstract

Japanese Earth Resources Satellite-1(JERS-1) will be launched from Tanegashima Space Center, NASDA by H-I rocket in February 1992. The JERS-1 has two observation equipments: synthetic aperture radar (SAR) and optical sensor (OPS) which consists of visible, near-infrared and short-wave infrared radiometer. In order to evaluate parameters of SAR, to develop processing and calibration method and to evaluate the utility of SAR data in various fields of applications, NASDA conducted SAR-580 experiment by using variable parameter SAR mounted on Convair 580 owned by Canada Centre for Remote Sensing (CCRS) during October and November, 1983 in collaboration with many research organizations. As a part of this experiment, NASDA conducted calibration experiment in Tsukuba where several corner reflectors were set up. NASDA processed about 100 scenes of SAR-580 by newly developed autofocusing method and evaluated SAR data from various points of view. Moreover, Communications Research Laboratory (CRL) participated in SIN-B experiment planned and conducted by JPL in collaboration with several agencies including NASDA.

In this paper, outline of data processing and calibration for SAR data in Japan are presented.

#### 1. Introduction

Japanese Earth Resources Satellite-1 (JERS-1) is scheduled for launch in February 1992 and will be launched by H-I rocket from Tanegashima Space Center, NASDA. Space segment of the JERS-1 is jointly developed by NASDA and JAROS and ground segment is developed by Earth Observation

Center (EOC), NASDA. The JERS-1 has two observation equipments: synthetic aperture radar (SAR) and optical sensor (OPS). Main mission objectives of JERS-1 are to evaluate newly developed sensors and spacecraft and to collect data of the earth concerning resources exploration, geology, agriculture, forestry, land use, prevention of disaster, coastal monitoring, sea ice monitoring and others.

In order to evaluate parameters of SAR, to develop processing and calibration methods, to evaluate utility of SAR data in various application fields and to study future advanced SAR, NASDA conducted SAR-580 experiment by using variable parameter SAR mounted on Convair 580 owned by Canada Centre for Remote Sensing (CCRS) in October and November 1983 in collaboration with many research organizations. As a part of SAR-580 experiment NASDA conducted calibration experiment in Tsukuba Science City where several corner reflectors were set up. NASDA processed about 100 scenes of SAR-580 data and provided SAR-580 data to principal investigators who participated in SAR-580 data evaluation program in 1984-1986.

In this paper, data processing and calibration for SAR data in Japan are presented by focusing on SAR-580 data and JERS-1 data.

## 2. Outline of JERS-1 SAR data

### 2.1. Outline of JERS-1 SAR

Bread board model (BBM) of mission instruments of JERS-1 was developed by NASDA. Engineering model (EM) of mission instruments of JERS-1 is developed by Resources Remote Sensing System (RRSS) and Proto-flight model (PFM) will be developed by Japan Resources Observation System Organization (JAROS). On the other hand, Bus instruments of JERS-1 are developed by NASDA.

Table 1 shows the specifications of JERS-1 SAR. L band was selected by considering weight and power of payload and penetration through vegetation. It was confirmed in SAR-580 experiment and other experiments that L band penetrates vegetation such as trees deeper than C and X band. This is desirable for resources exploration.

### 2.2. JERS-1 data type and processing level

Ground segments of JERS-1 are developed by EOC, NASDA. Ground system for JERS-1 is under conceptual design in 1988. Basic design will begin in 1989. In order to develop processing system, it is necessary to define processing data volume, data type and processing level for JERS-1 data. In this case, both SAR data and OPS data should be considered. Table 2 shows tentative processing level of JERS-1 SAR data. Table 3 shows tentative data type of JERS-1 SAR data. Since the velocity of SAR is about 7km/sec and PRF is 1505.8-1606.0, sampling interval is about 4.5m. So, pixel size of 1 and 3 looks are defined as 3.125m and 12.5m, respectively. Spatial resolution of SAR is 18m (3 looks) and 6m (1 look). Though there are many window functions, typical window

functions (Square, Riesz and Hamming) can be selected. Concerning output data type, both amplitude and logarithmic expression can be selected by considering dynamic range. Since the logarithmic expression provides quasi-normal distribution, this is desirable in case of land use classification by combining with optical sensor data and using maximum likelihood method.

Table 1. Specifications of JERS-1 SAR

|                                            |                                                                          |
|--------------------------------------------|--------------------------------------------------------------------------|
| Altitude                                   | 568 km                                                                   |
| Transmit Frequency                         | L band (1.275 GHz)                                                       |
| Polarization                               | H-H                                                                      |
| Swath Width                                | 75 km                                                                    |
| Off-nadir Angle                            | 35 degree                                                                |
| Incident Angle                             | 38.7 degree (Center of Swath Width)                                      |
| Transmitted Pulse                          |                                                                          |
| Type                                       | linear down chirp                                                        |
| Bandwidth                                  | 15 MHz                                                                   |
| Initial Frequency                          | 1282.5 MHz                                                               |
| Pulse Length                               | 35 sec                                                                   |
| Sampling Rate                              | 17.1 MHz                                                                 |
| Pulse Repetition Frequency (PRF)           | 1505-1605 in 25Hz increments<br>(1505.8, 1530.1, 1555.2, 1581.1, 1606.0) |
| Noise Equivalent Signal to Ambiguity (S/A) | -20.5 dB<br>>14 dB                                                       |
| Raw Data Bit Precision                     | 31/30                                                                    |
| Raw Data Rate                              | 30x2 Mbps                                                                |

Table 2. Tentative processing level of JERS-1SAR data

- Level 0: Raw data
- Level 1: Basic image (Range and Azimuth Compression)
- Level 2: System corrected (Bulk) image  
Radiometrically and geometrically corrected image)
- Level 3: Precisely corrected image by using GCP.
- Level 4: Precisely corrected image by using Digital Terrain Model (DTM)

Remarks; Main product is level 2.

Table 3. Tentative JERS-1 SAR data processing types

|                        |                                                                                          |
|------------------------|------------------------------------------------------------------------------------------|
| Map projection method: | UTM (Universal Transverse Mercator)<br>SOM (Space Oblique Mercator)<br>PS (Polar Stereo) |
| Resampling method:     | Nearest Neighbor (NN)<br>Cubic Convolution (CC)                                          |
| Frame Size             | 75km x 75km (level 0: 75km x 90km)                                                       |
| Pixel Size             | 3.125m (1 look), 12.5m (3 looks)                                                         |
| Window Function        | Square, Reisz, Hamming                                                                   |
| Output Data Type       | Amplitude/Logarithmic expression                                                         |
| Recording Format (CCT) | Super structure<br>(Based upon CEOS WGD SAR format standardization)                      |
| Recording density(CCT) | 6250 BPI, 1600 BPI                                                                       |
| Number of Tracks (CCT) | 9                                                                                        |

### 3. Data processing flow of SAR data

#### 3.1. SAR-580 data

NASDA collected SAR data over 8 test sites (Tsukuba, Hiratsuka, Off-shore of Hiratsuka, Mt. Fuji, Oshima, Miyakejima, Akita (Futatsui) and Shizukuishi/Kosaka) in 28 October-4 November 1983 by using Convair 580 with variable parameter SAR which are chartered from CCRS based upon the arrangement between CCRS and NASDA which were concluded on 23 August 1983.

NASDA processed about 100 scenes of SAR data in 1984 by newly developed auto-focusing method. Figure 1 shows the data processing flow of SAR-580 data. There are two methods for auto-focusing: (1) to employ the relationship between target positional shift and processing parameter error, (2) to employ the relationship between image contrast in the processed image and processing parameter error. The first method was used for our program. Main feature of this program is to employ auto-focusing method both in range and in azimuth direction. The feed back loop of auto-focusing converges within 2-3 repetitions.

#### 3. 2. JERS-1 SAR data

Since JERS-1 has mission data recorder (MDR), it is possible to collect SAR data and OPS data all over the world excluding some of arctic and antarctic region (SAR:86.015 degrees N-90 degrees N, 78.661 degrees S-90 degrees south, OPS:82.338 degrees N-90 N, 82.338 degrees S-90 degrees S. If only land and coastal region is observed, about 30000 scenes are obtained. JERS-1 data will be received by Earth Observation Center (EOC) in Hatoyama, by Fairbanks ground station and Gatineau ground station in Canada. Data will be dumped at Fairbanks ground station. There may be other foreign ground stations to receive JERS-1 data within limited power and stored command number for spacecraft.

Minimum requirement of observation by JERS-1 is to observe land and coastal area in the world once during two years for SAR and twice during two years for OPS.

Figure 2 shows the data processing flow for JERS-1 data. In order to get high quality image, it is necessary to introduce auto-focusing method even to spaceborne SAR data processing. In case of JERS-1 SAR data processing, this auto-focusing method will be applied to azimuth direction by using relationship between target positional shift and processing parameter error. In principle, it is impossible to apply this method to very flat area such as calm ocean.

Processing level of JERS-1 SAR data will be explained as follows:

(a) Level 0: Raw data

Radar hologram data including data and parameters required for processing such as orbital data, attitude data, on-board calibration data, PRF, Sensitive Time Control (STC).

(b) Level 1: Basic image

Range and azimuth compressed image by using FFT accompanied by look processing (1 look and 3 looks) and auto-focusing. 1 look image is superior to 3 looks image in obtaining higher spatial resolution and detailed information.

(c) Level 2: System corrected image (Bulk image)

Geometrically and radiometrically corrected image. Geometric correction includes conversion from slant range coordinates to ground range coordinates, resampling. Radiometric correction includes STC compensation, antenna pattern compensation, incidence angle compensation, receiver gain compensation. (Position error: + over -1km)

(d) Level 3: Precisely corrected image

Precisely corrected by using GCP. By using GCP and map coordinates, antenna position is estimated and by using orbital data and attitude data precisely corrected image is obtained. (Position error: spatial resolution)

(e) Level 4: Geocoded image

Position error due to terrain relief is eliminated by using digital terrain model (DTM).

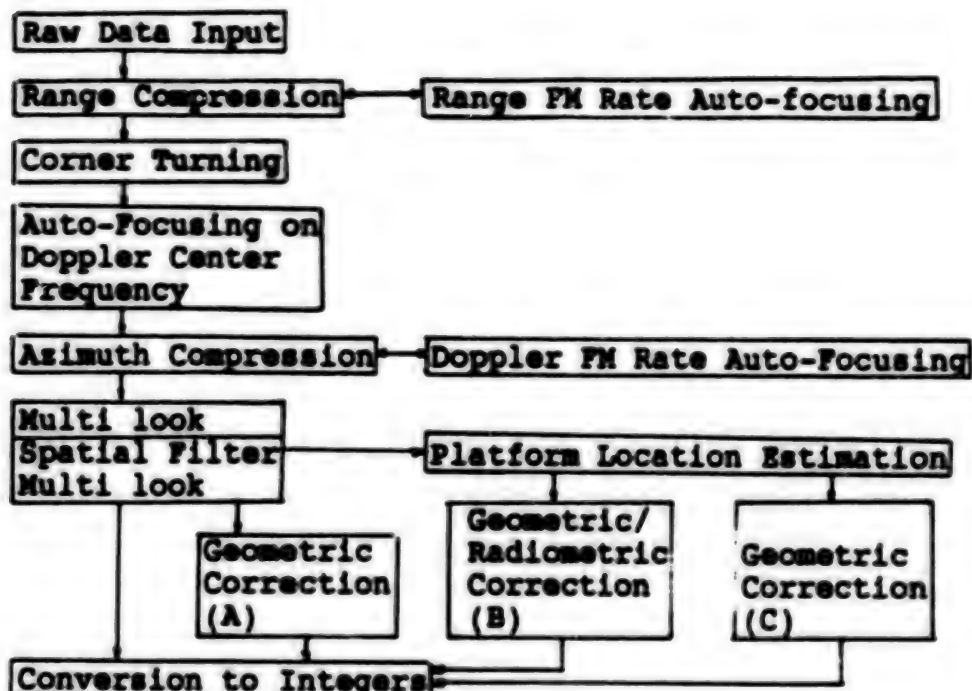


Fig 1. Data Processing Flow of SAR-580 Data

Note: 1. JERS-1 SAR simulation software is included.

2. Geometric correction (A): The multi-look image is converted from slant range coordinates to ground range coordinates and resampled to adjust image pixel spacing.

3. Platform location estimation: Using the GCP coordinates of the multi-look image and the map, platform position is estimated as an approximate function.

4. Geometric and radiometric correction (B): The results of the platform location estimation are used to correct for geometric distortion in the image data. The data is projected onto the map coordinates and radiometric distortion is corrected.

5. Geometric correction (C): Geometric distortion is corrected for terrain relief, using digital terrain model.

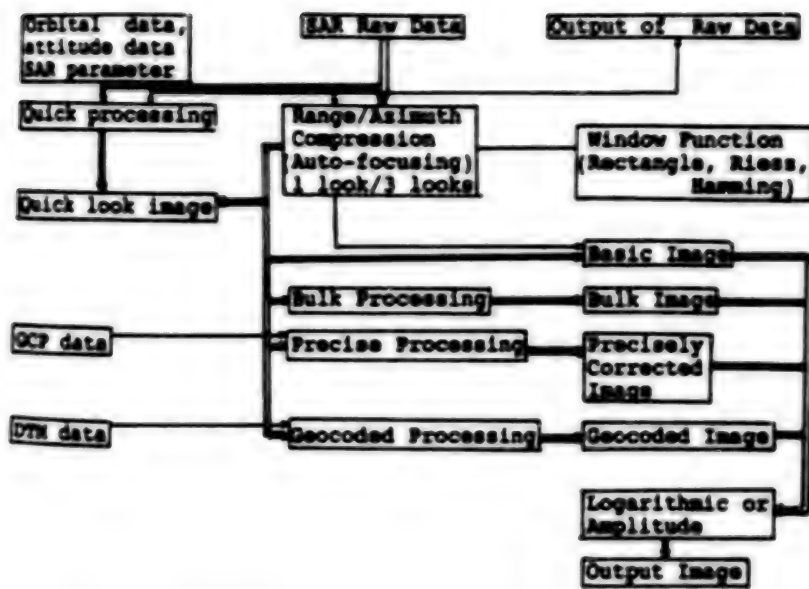


Fig. 2 Data Processing Flow of JERS-1 SAR data

#### 4. Calibration flow of SAR data

##### 4.1. SAR-580 data

Table 4. Type of Corner Reflection

| Type                                                 | Size /          | Number | Testsite             |
|------------------------------------------------------|-----------------|--------|----------------------|
| INTERA corner reflector                              | 1725mm          | 3      | Tsukuba Science City |
| NASDA corner reflector A                             | 1049mm          | 1      | ditto                |
| ditto                                                | B 822mm         | 4      | ditto                |
| ditto                                                | C 502mm         | 1      | ditto                |
| ditto                                                | D 376mm         | 1      | ditto                |
| ditto                                                | E 141mm         | 1      | only for test        |
| INTERA corner reflector                              | 287mm           | 3      | Tsukuba Science City |
| ERSDAC corner reflector                              | 714mm           | 5      | Oshima               |
| ISAS corner reflector<br>(Dihedral corner reflector) | 150mm/<br>177mm | 4      | Tsukuba Science City |

$$\delta_c = 4\pi a^4 / (3\lambda^2)$$



$$\delta_c = 8\pi a^2 b^2 / \lambda$$



As a part of SAR-580 experiment, NASDA conducted calibration experiment in Tsukuba Science City on 28 October and 4 November 1983. NASDA developed several corner reflectors. Size is selected depending upon wavelength for L band, C band and X band. Figure 3 shows one of corner reflectors. Figure 4 shows example of the dependency of back scattering coefficient on incidence angle by using calibrated SAR-580 data.



Fig. 3 Example of corner reflector

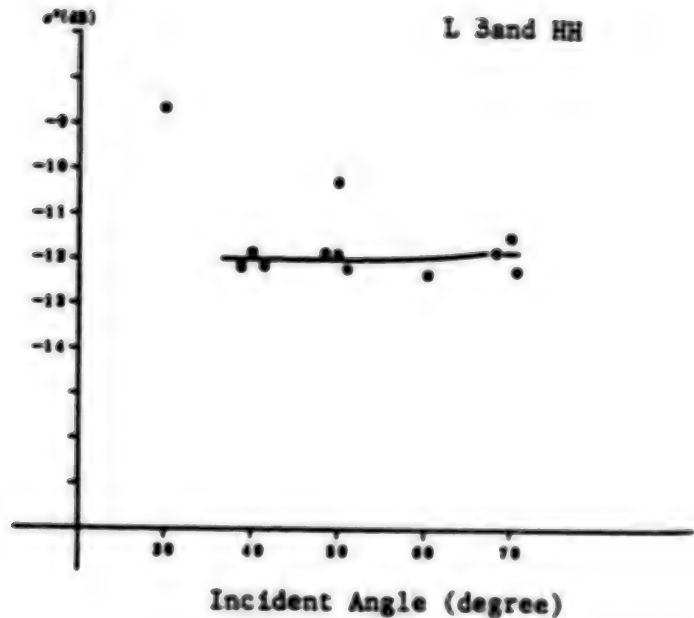


Fig. 4 Dependency of on incidence  
in case of field in  
Tsukuba

#### 4.2. JERS-1 SAR data

Calibration of JERS-1 SAR data is essential in various fields of application such as land use, monitoring of vegetation. Figure 5 shows calibration flow of JERS-1 SAR data.

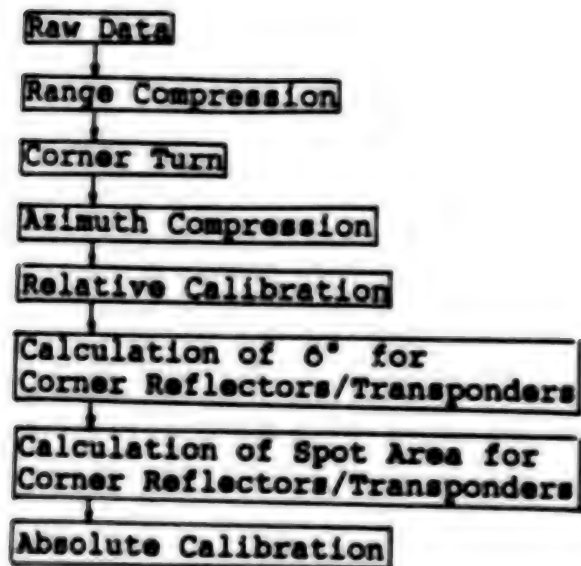


Fig. 5 Calibration Flow of JERS-1 SAR data

In Japan, there are very few testsites for space borne SAR calibration because very few flat and uniform areas exist. Therefore, it is necessary to develop special method for calibration which can be utilized in Japan.

If transponder set near lake or pond has delay time such as 5-6 sec between receiving and transmitting, point target appear in the lake or the pond. Since back scattering coefficient of the lake or pond is sufficiently small, it is easy to calibrate SAR data.

### 5. Evaluation program

Before SAR-580 experiment, committee was held 4 times and flight course and content of experiment were studied. As part of SAR-580 experiment, evaluation program was made and processed SAR-580 data were provided to principal investigators who participated in this program. All fruitful results were presented at SAR-580 experiment symposium in Tokyo on 25 September 1986.

The evaluation theme of SAR-580 data is as follows:

#### (a) Joint Research Organization

National Research Center for

On detection of ocean waves

## Disaster Prevention

National Institute for Environmental Studies  
Forestry & Forest Product

Tokai University Research  
and Information Center

Earth Resources Satellite Data  
Analysis Center (ERSDAC)

Analysis of urban land use  
utilizing SAR-580 image  
Possibility for interpretation  
on landslide landform  
Soil moisture measurement using  
SAR-580 data  
Evaluation of SAR-580 data on  
forest type classification  
An optical image display  
method and effectiveness for land  
cover classification using SAR  
data  
Geologic analysis of SAR-580  
data

## (b) Cooperative organization

Institute of Space and  
Astronautical Science (ISAS)  
Meteorological Research Institute

Studies on microwave signature  
Investigation on reflectivities  
of radar antenna reflection  
measured by SAR  
SAR imageries obtained in the  
sea areas around the Oshima and  
Miyake islands  
Inspection of ground surface  
state of Oshima and Miyakejima  
volcanoes with SAR-580 images  
Feasibility study of SAR image  
interpretation for planimetric  
objects  
Investigation of correspondence  
between Images in SAR-580 data  
and characteristics of land  
cover objects  
Image processing of synthetic  
aperture radar (SAR-580) data  
Evaluation of SAR-580 imagery

Geographical Survey Institute

Department of Computer  
Science, Iwate University

Science Information Processing  
Center, University of Tsukuba  
Remote Sensing & Image Research  
Center of Chiba University  
Kanazawa Institute of Technology

College of Engineering,  
Hosei University

Toba National College of  
Maritime Technology  
Remote Sensing Technology  
Center of Japan (RESTEC)

The classification of the ground  
cover types on the rugged  
terrain by the SAR-580 data  
Fundamental study for verifica-  
tion of classifying SAR images  
by checking the objects in field  
Sea surface phenomena investi-  
gation using the SAR data  
Detection of terrain height  
from stereo SAR image and  
optically processed images  
Accuracy of land cover classi-  
fication by SAR image

CRL participated in SIR-B experiments planned and conducted by JPL in collaboration with several agencies including NASDA in October 1984 and it was found that a simulated oil slick area over sea was clearly detected (Ref.8).

## 6. Conclusion

EOC, NASDA is developing JERS-1 ground system (Conceptual design). Processing level and format was studied in the committee on JERS-1 ground system. Considering user requirement and capability of spacecraft, basic and detailed design will begin from 1989.

## Acknowledgement

The authors would like to thank particularly Professor Hirozawa of ISAS, Mr. Nemoto of JAROS, Mr. Komai of ERSDAC, Dr. Kodaira of RESTEC and Dr. Fujita of CRL.

## References

1. K. Maeda et al., "Outline of SAR-580 experiment in Japan" Proceedings of 9th Canadian Symposium on Remote Sensing, St. Johns, Newfoundland, Canada pp 523-530 Aug.13-17 1984.
2. K. Maeda et al., "Results on Processing and Evaluation of SAR-580 data in Japan." Canadian Journal of Remote Sensing Vol 13, No 1, pp 11-18, July 1987.
3. K. Maeda et al., "Outline of SAR-580 Data Processing Method in Japan," Proceedings of IGARSS'86 Symposium, Zurich, Sep.8-11, pp 1413-1418, ESA SP-254 1986.
4. E.A. Herland "Some SAR-processing Results Using Auto-focusing." Proceedings of 3rd SEASAT SAR workshop on SAR image quality, 1980.
5. J.R. Bennet et al., "Features of Generalized Digital Synthetic Aperture Radar Processor," Proceedings of 15th International Symposium on Remote Sensing of Environment, 1981.
6. J.C. Curlander et al., "Automated Processing of Spaceborne SAR Data," Proceedings of International Geoscience and Remote Sensing Symposium pp 3.1-3.6, 1982.
7. Proceeding of Symposium on SAR-580 experiment in Japan, EOC NASDA, Sep. 25, 1986.
8. M. Fujita et al., "SIR-B Experiments in Japan: Sensor Calibration and Oil Pollution Detection Over Ocean," IEEE transactions on Geoscience and Remote Sensing Vol. GE-24, No 4, July 1986.

9. H. Hirosawa et al., "Calibration of Cross-polarized SAR Imagery Dihedral Corner Reflectors," Proceedings of International Geoscience and Remote Sensing Symposium pp 487-491 Ann Arbor, May 18-21 1987.

/08309

Studies on Object Reconstruction From Space Using Three Line Scanner Imagery

43070010b Kyoto Selections from INTERNATIONAL ARCHIVES OF PHOTOGRAHMTRY AND REMOTE SENSING in English Vol 27 1988 Part B11 pp 242-249

[Article by Heinrich Ebner and Franz Muller, Chair of Photogrammetry, Technical University of Munich, Arcisstr. 21, D-8000 Munich 2, Federal Republic of Germany; Senlin Zhang, Department of Photogrammetry and Remote Sensing, Wuhan Technical University of Surveying and Mapping, Luoyuroad 23, Wuhan, People's Republic of China; Commission I]

[Text] Abstract

The paper investigates the capability of object reconstruction from space for two specific projects. Both of them are based on the use of three line scanner systems allowing for simultaneous digital image recording from three different angles. An efficient model for combined point determination is proposed, considering the digital image data as well as orbit information, GPS and INS observations. The resulting accuracy is estimated from project oriented simulations.

Finally the possibilities for DTM generation, orthophoto production and stereo compilation from three line scanner imagery are discussed.

i. Introduction and Review

A line scanner or opto-electronic camera allows for digital image recording line by line according to the push-broom principle. A three line scanner records the object simultaneously in forward, downward and backward looking direction. The three-fold coverage makes a rigorous reconstruction of the object possible (Hofmann et al., 1982).

Three line scanner systems shall be used from space in conjunction with the MEOSST experiment (Lanzl, 1986) AND THE MOMS-02/D2 project (Ackermann et al., 1988).

The paper first describes the proposed mathematical model for combined point determination using three line scanner imagery and general control information.

Then accuracy estimations for the space projects MEOSS and MOMS-02/D2 are performed by means of computer simulations.

Finally the possibilities for DTM generation, orthophoto production and stereo compilation from three line scanner imagery are discussed.

## 2. Combined Point Determination Using Three Line Scanner Imagery

A three line scanner contains in the focal plane of the objective three linear CCD-sensors, which are oriented perpendicularly to the direction of flight. During the flight the shutter of the objective is open and the sensors are read out with constant frequency. Within each read cycle a digital image is recorded, consisting of only three lines. If read cycle frequency, speed of flight, image scale and size of sensor elements are in proper relation to each other the terrain is scanned with nearly square shaped object surface elements (Figure 1). Generally each object point is imaged three times, first by the forward looking sensor a, then by the downward looking sensor b and finally by the backward looking sensor c. So, classical frame photography with proper longitudinal overlap is replaced by a composition of a large number of successive three line images. Basically, each of them has its own exterior orientation.

Consequently the mathematical model for the reconstruction of the exterior orientation should use 6 unknown parameters for each three line image  $I_j$ . In practice, however, there is not enough information to determine such a large number of unknowns. A solution to this problem can be found by the introduction of a proper functional model for the variation of the exterior orientation parameters. In the simplest case piecewise linear functions can be used. Then so-called orientation images  $I_k$  are defined for which the parameters of the exterior orientation are unknown and the 6 parameters of an arbitrary image are represented by linear functions of the 12 unknown parameters of the two nearest orientation images  $I_k$  and  $I_{k+1}$ . For details see (Ebner and Muller, 1986).

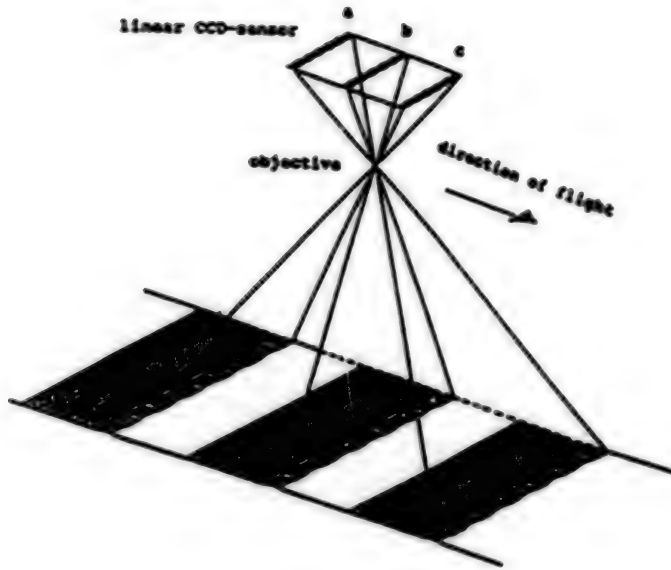


Fig. 1 Image Recording Using a Three Line Scanner

In that way point determination using three line scanner imagery can be performed similar to classical photogrammetric point determination. Based on the bundle method collinearity equations are formulated for the image coordinates  $x_{ij}$ ,  $y_{ij}$  of the object points  $P_i$  in the images  $I_j$ . The exterior orientation parameters  $\hat{x}_j$ ,  $\hat{y}_j$ ,  $\hat{z}_j$ ,  $\hat{\omega}_j$ ,  $\hat{\phi}_j$ ,  $\hat{\kappa}_j$ , however, are replaced by the unknown parameters  $\hat{x}_k$ ,  $\hat{y}_k$ ,  $\hat{z}_k$ ,  $\hat{\omega}_k$ ,  $\hat{\phi}_k$ ,  $\hat{\kappa}_k$ ,  $\hat{x}_{k+1}$ ,  $\hat{y}_{k+1}$ ,  $\hat{z}_{k+1}$ ,  $\hat{\omega}_{k+1}$ ,  $\hat{\phi}_{k+1}$ ,  $\hat{\kappa}_{k+1}$  of the neighbouring orientation images  $I_k$  and  $I_{k+1}$ .

All relevant image coordinates  $x_{ij}$ ,  $y_{ij}$  are considered as observations in a least squares adjustment. Further observation equations are formulated for the control point coordinates. Unknowns of the adjustment are the coordinates of the object points  $P_i$  and the parameters of the orientation images  $I_k$ . This concept can easily be generalized to combined point determination, if instead of or in addition to control points general control information is available, e.g., direct geodetic observations, measured orientation parameters or DTM data.

In conjunction with the planned space project M0MS-02/D2, GPS and INS observations are of particular interest. With the MEOSS experiment where such data are not available orbit information can be used.

### 3. Accuracy Estimations for the Space Projects MEOSS and M0MS-02/D2

#### 3.1. MEOSS Experiment

The Monocular Electro-Optical Stereo Scanner (MEOSS), which has been designed and manufactured by the Institute of Optoelectronics at the 'Deutsche Forschungs' und Versuchsanstalt fur Luft und Raumfahrt e.V.' (DFVLR) will be the first three line camera in space (Lanzl, 1986). The mission is planned for 1988 on the SROSS satellite provided by the Indian Space Research Organisation (ISRO).

Besides thematic applications relating to cartography, meteorology and geosciences, MEOSS offers the first possibility of three dimensional photogrammetric object reconstruction based on spaceborne three line imagery. Although the ground resolution is limited to 52 m by 79 m, the MEOSS image data may be used for basic investigations and tests of photogrammetric compilation methods for threefold stereo scanner data.

The intention of this paper is to give an a priori estimation of the accuracy of point determination using MEOSS imagery. By means of computer simulations with project oriented camera- and flight parameters, the theoretical standard deviations  $\sigma_{xi}$ ,  $\sigma_{yi}$ ,  $\sigma_{zi}$  of the unknown coordinates  $x_i$ ,  $y_i$ ,  $z_i$  of object points have been calculated. In (Hofmann and Muller, 1988) the principle of this method is described in detail.

The simulations point out:

--the advantages of a simultaneous adjustment of two overlapping strips versus single strip adjustment and

--the possibility of the integration of orbit models, which provide information about the satellite position with limited accuracy.

The first item has to be seen in conjunction with the important feature of the MEOSS mission, that areas of interest can be recorded twice from different orbits, providing sixfold overlap. The advantages of such a block adjustment of three line imagery have been demonstrated in (Ebner and Muller, 1987).

Figure 2 shows an example for 5 consecutive orbits in the course of the MEOSS experiment representing the coverage of one day.

The rastered areas have been arbitrarily selected to investigate the accuracy of the object reconstruction from MEOSS imagery:

--area A represents a single strip,

--area B represents a block, consisting of two strips, which intersect at an angle of approximately 22 grad.

--area C represents a block, consisting of two strips, which intersect at an angle of approximately 61 grad.

The characteristic data for the MEOSS simulations are listed in Table 1.

Concerning the chosen distance between orientation images, a remark is necessary: 16 km is probably a too pessimistic value, because the variations of the parameters of the exterior orientation might be described using longer intervals without increasing the interpolation errors.

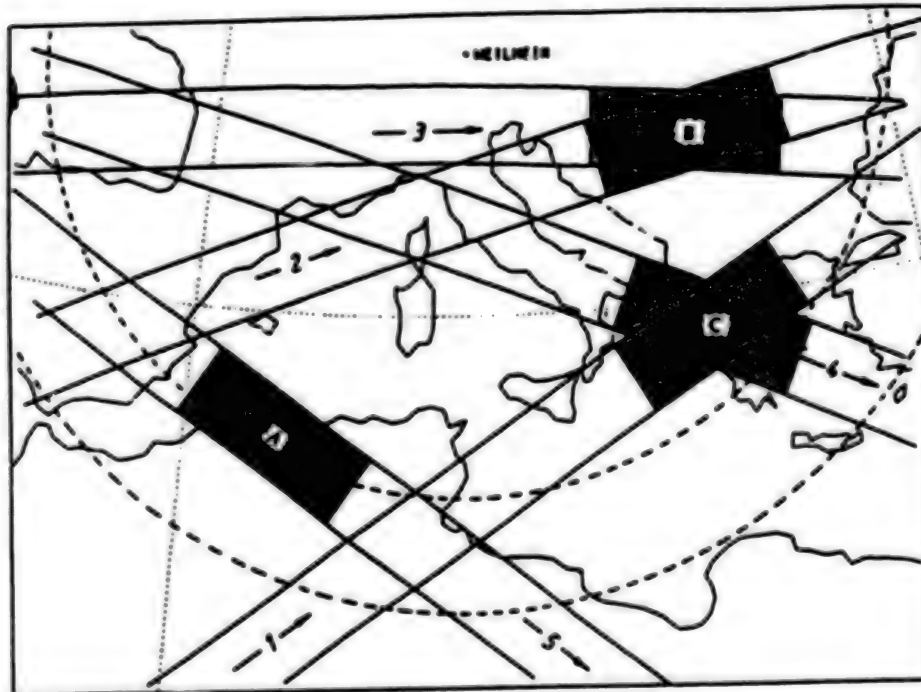


Fig. 2: Example for 5 consecutive orbits in the course of the MEOSS experiment (taken from Lanzl, 1986)

|                                                                                |                   |
|--------------------------------------------------------------------------------|-------------------|
| <u>camera parameters</u>                                                       |                   |
| calibrated focal length                                                        | 61.10 mm          |
| spacing forward/vertical sensor<br>and vertical/backward sensor                | 26.69 mm          |
| standard deviation of image coordinates $\sigma_0$                             | 5.0 $\mu\text{m}$ |
| <u>flight parameters</u>                                                       |                   |
| flying height                                                                  | 458 km            |
| baselength between forward/vertical look<br>and between vertical/backward look | 200 km            |
| strip length                                                                   | 600 km            |
| strip width                                                                    | 240 km            |
| distance between orientation images                                            | 16 km             |
| <u>object point distribution</u>                                               |                   |
| distance in flight direction                                                   | 5 km              |
| distance across flight direction                                               | 60 km             |
| height of all object points                                                    | 0 km              |

Table 1. Characteristic Data for the MEOSS Simulations

The following simulations have been performed:

--strip / block adjustment for A, B and C assuming error-free parameters of the exterior orientation (accuracy limits),

--strip / block adjustment for A, B and C using four error-free ground control points (GCP) for each strip,

--strip / block adjustment for A, B and C assuming given position parameters for the orientation images  $I_k$  with  $\sigma_{xk} = \sigma_{yk} = \sigma_{zk} = 100$  m (orbit information) in addition to the GCPs.

Table 2 shows the results of the simulations. Given are the rms values  $\mu_x^0, \mu_y^0, \mu_z^0$  of the theoretical standard deviations  $\sigma_{xi}, \sigma_{yi}, \sigma_{zi}$  for the adjusted object point coordinates  $x_i, y_i, z_i$ .

Table 2. Results of the MEOSS Simulations

|         | accuracy limits |             |             | 4 GCPs/strip |             |             | 4 GCPs/strip<br>given pos.param. |             |             |
|---------|-----------------|-------------|-------------|--------------|-------------|-------------|----------------------------------|-------------|-------------|
|         | $\mu_x$ [m]     | $\mu_y$ [m] | $\mu_z$ [m] | $\mu_x$ [m]  | $\mu_y$ [m] | $\mu_z$ [m] | $\mu_x$ [m]                      | $\mu_y$ [m] | $\mu_z$ [m] |
| Strip A | 33              | 32          | 106         | 1219         | 626         | 2780        | 152                              | 268         | 309         |
| Block B | 26              | 26          | 84          | 31           | 31          | 200         | 30                               | 30          | 91          |
| Block C | 30              | 30          | 98          | 37           | 37          | 176         | 35                               | 35          | 109         |

The following conclusions can be drawn from Table 2.

- The single strip shows poor geometry. The accuracy could be improved by using a greater distance between the orientation images, if the satellite dynamics allows for this.
- The use of two overlapping strips in a simultaneous block adjustment improves the accuracy of point determination drastically. Especially the achieved planimetric accuracy is close to the accuracy limit.
- The introduction of given position parameters (orbit information) further improves the accuracy, particularly in height.

### 3.2. MOMS-02/D2 Project

The MOMS-02/D2 project, which is also directed by the DFVLR, is based on a panchromatic three line scanner with high ground resolution in connection with multispectral channels (Ackermann et al., 1988). The use of the system is planned for 1991 during the German D2 mission on a NASA Space Shuttle flight.

One of the main tasks of the MOMS-02/D2 project is the rigorous and precise geometric evaluation of threefold stereo data. To secure that the high requirements of this mission concerning the geometry of object reconstruction are met, comprehensive studies have to be performed.

The simulation results given in this paper show a general trend, but should not be interpreted as final.

There is one characteristic feature of the project, which changes the geometry of photogrammetric point determination for the worse: the ratio of flying height and strip width is approximately 9:1.

Improvement of the geometry may be obtained by using information from navigation systems for the position and attitude parameters.

The following simulations have been performed:

--adjustment of a strip assuming error-free parameters of the exterior orientation (accuracy limits),

--adjustment of a strip using four error-free ground control points,

--adjustment of a strip assuming measured position and/or attitude parameters with different accuracies additionally to four error-free ground control points.

In practice attitude and position information can be derived from Inertial Navigation Systems (INS) and/or from the Global Positioning System (GPS).

Table 3 lists the characteristic data for the MOMS-02/D2 simulations.

In Table 4 the results of the investigations are summarized. Again, the rms values  $\mu_x^2$ ,  $\mu_y^2$ ,  $\mu_z^2$  of the theoretical standard deviations  $\sigma_{x_i}$ ,  $\sigma_{y_i}$ ,  $\sigma_{z_i}$  for the adjusted object point coordinates  $x_i$ ,  $y_i$ ,  $z_i$  are listed.

In this case, however, not all points have been used to calculate the rms values, but only the ones, which are located in the threefoldly covered area of the strip.

The obtained results may be analysed as follows:

--Compared to the accuracy limits (Sim. 11) the accuracy of the strip adjustment based on only 4 control points (Sim. 1) is poor.

--The use of measured attitude parameters (Sim. 2 to Sim. 4) improves the height accuracy to some extent. There is no difference, whether 1.0, 0.5 or 0.2 mgrad is assumed.

--Measured position parameters (Sim. 5 to Sim. 7) yield smaller values for  $\mu_x^A$  and  $\mu_z^A$ , but there are still significant differences to the accuracy limits.

--Really satisfactory results can only be obtained by the simultaneous use of accurate attitude and position data (Sim. 9 and Sim. 10).

Table 3. Characteristic Data for the MOMS-02/D2 Simulations

| <u>camera parameters</u>                                                       |                   |
|--------------------------------------------------------------------------------|-------------------|
| calibrated focal length                                                        | 660.00 mm         |
| effective spacing forward/vertical sensor<br>and vertical/backward sensor      | 300.42 mm         |
| standard deviation of image coordinates $\sigma_0$                             | 5.0 $\mu\text{m}$ |
| <u>flight parameters</u>                                                       |                   |
| flying height                                                                  | 334 km            |
| baselength between forward/vertical look<br>and between vertical/backward look | 152 km            |
| strip length                                                                   | 606 km            |
| strip width                                                                    | 36 km             |
| distance between orientation images                                            | 16 km             |
| <u>object point distribution</u>                                               |                   |
| distance in flight direction                                                   | 2 km              |
| distance across flight direction                                               | 9 km              |
| height of all object points                                                    | 0 km              |

The described studies will be continued. The final goal is a comprehensive analysis of the accuracy properties of combined point determination within the MOMS-02/D2 project.

Table 4. Results of the MOMS-02/D2 Simulations

|    | attitude data<br>$\sigma_u = \sigma_v = \sigma_w$<br>[mgrad] | position data<br>$\sigma_x = \sigma_y = \sigma_z$<br>[m] | estimated accuracy |             |             |
|----|--------------------------------------------------------------|----------------------------------------------------------|--------------------|-------------|-------------|
|    |                                                              |                                                          | $\mu_x$ [m]        | $\mu_y$ [m] | $\mu_z$ [m] |
| 1  | none                                                         | none                                                     | 21.8               | 8.0         | 64.1        |
| 2  | 1.0                                                          | none                                                     | 21.2               | 6.7         | 35.7        |
| 3  | 0.5                                                          | none                                                     | 21.2               | 6.6         | 35.7        |
| 4  | 0.2                                                          | none                                                     | 21.2               | 6.6         | 35.7        |
| 5  | none                                                         | 25.0                                                     | 11.1               | 7.4         | 24.3        |
| 6  | none                                                         | 5.0                                                      | 7.1                | 7.3         | 18.1        |
| 7  | none                                                         | 1.0                                                      | 6.7                | 7.3         | 16.6        |
| 8  | 1.0                                                          | 25.0                                                     | 6.7                | 4.4         | 14.1        |
| 9  | 0.5                                                          | 5.0                                                      | 2.6                | 2.1         | 6.2         |
| 10 | 0.2                                                          | 1.0                                                      | 1.6                | 1.6         | 4.2         |
| 11 | error-free orient. parameters                                |                                                          | 1.5                | 1.5         | 3.9         |

#### 4. Steps of Object Reconstruction and Conclusion

The process of object reconstruction based on digital imagery of three line scanners includes the following tasks.

- Image recording analogous to the push-broom principle (see Chapter 2).
- Determination of homologous points by a human operator or by methods of digital image matching.
- Preprocessing of additional control information, e.g., from INS or GPS.
- The main task consists in the reconstruction of the exterior orientation based on the mathematical model described in Chapter 2.
- After the reconstruction of the exterior orientation, DTM image points can be determined with methods of digital image matching, yielding DTM object points. Then the DTM surface can be mathematically described by proper models.

--Using the image data of line a, b or c orthophotos and central perspectives may be derived by means of digital image transformation methods.

--If an analogue film is produced from the original or transformed digital data, analytical plotters can be used for the evaluation of three line imagery.

--Finally digital mono plotting (compilation of the images generated by sensor a, b or c) and digital stereo plotting (stereoscopic evaluation of the imagery using lines a/v, a/c or b/c) is possible. These methods will play an important role in future photogrammetry.

#### References

Ackermann, F., Bodechtel, J., Meibner, D., Seige, P., Winkenbach, H. 1988, MOMS-02 - A Sensor for Combined Stereoscopic and Multispectral Earth Observation: Presented Paper, Commission I, ISPRS Congress, Kyoto

Ebner, H., Muller, F. 1986, Processing of Digital Three Line Imagery Using a Generalized Model for Combined Point Determination: Int. Arch. of Photogrammetry and Remote Sensing, Vol 26-3/1, pp 212-222, Rovaniemi.

Ebner, H., Muller, F. 1987, Combined Point Determination Using Digital Data of Three Line Opto-Electronic Cameras: 1987 ASPRS-ACSM Annual Convention, Technical Papers, Vol 2, pp 293-302, Baltimore.

Hofmann, O., Nave, P., Ebner, H. 1982, DPS - A Digital Photogrammetric System for Producing Digital Elevation Models and Orthophotos by Means of Linear Array Scanner Imagery: Int. Arch. of Photogrammetry, Vol 24-III, pp 216-227, Helsinki.

Hofmann, O., Muller, F. 1988, Combined Point Determination Using Digital Data of Three Line Scanner Systems: Invited Paper, Commission III, ISPRS Congress, Kyoto.

Lanzl, F. 1986, The Monocular Electro-Optical Stereo Scanner (MEOSS) Satellite Experiment: Int. Arch. of Photogrammetry and Remote Sensing, Vol 26-1, pp 617-620, Stuttgart.

/08309

### Earth Observation Programs in Japan

43070010c Kyoto Selections from INTERNATIONAL ARCHIVES OF PHOTOGRAHMETRY AND REMOTE SENSING in English Vol 27 1988 Part B11 pp 434-442

[Article by Tomifumi Godai, Director, Planning & Management Department, National Space Development Agency of Japan (NASDA), 2-4-1, Hamamatsu-cho, Minatoku, Tokyo 105, Japan, SS-1]

#### [Text] Introduction

In 1972 the first earth observation satellite ERTS (LANDSAT-1) was launched by NASA. A number of investigators from Japan participated in this ERTS program for the satellite data analysis. This was an initial step of space remote sensing activities of Japan. NASDA established the Earth Observation Center (EOC) at Hatoyama near Tokyo in 1978 and started direct reception of LANDSAT data in 1979. Since then, various organizations and universities in Japan have been involved in a wide range of remote sensing activities.

In 1976, NASDA, supported by various groups of Japanese experts, started the investigation study of the Japanese needs and eventual contributions in earth observation program. Following these activities, in 1978, the Space Activities Commission of Japan (SAC), which supervise all space activities in Japan, recommended in the "Outline of Japanese Space Policy" that "marine and land observation satellite series" should be developed in order to establish the earth observation technology and to step forward to operational satellites. This recommendation resulted in developing two remote sensing satellites, namely Marine Observation Satellite-1(MOS-1) and Japanese Earth Resources Satellite-1(ERS-1). NASDA started the development of MOS-1 in 1979 and was launched on 19 February 1987. NASDA also started the R&D of ERS-1 in 1980 and which is now in the critical design phase. Development task of ERS-1 is shared by MITI and NASDA. MITI is developing the mission equipment (sensors) while NASDA the satellite system. ERS-1 is currently planned to be launched in 1992.

Following the fulfillment of these programs, Japan is to pursue its next step earth observation programs. As a next generation earth observation satellite, NASDA plans to launch Advanced Earth Observing Satellite (ADEOS) in early 1994. Moreover, a new earth observation program with Polar Orbiting Platform(POP) is now planned and coordinated among the Space Station Partners, namely, NASA, NOAA, ESA, Canada and Japan. Currently, NASA, ESA and Japan have their own platform launch plans in late 1990's. The overall schedule of Japanese earth observation satellite programs is shown in Table 1.

## 2 MOS-1 Program

The Marine Observation Satellite-1(MOS-1), the Japanese first experimental earth observation satellite, was launched on 19 February 1987 successfully by NASDA. The aims of MOS-1 is to establish the basic technology for earth observation system, to carry out practical observation of the earth (primary the ocean) using on-board sensors and to verify the performance of the sensors.

### (1) Satellite System and Mission Instrument

The profile and description of MOS-1 are shown in Fig. 1 and Table 2. MOS-1 has three sensors and a Data Collection System Transponder (DCST). These sensors are the Multispectral Electronic Self Scanning Radiometer (MESSR), the Visible Thermal Infrared Radiometer (VTIR), and the Micro-wave Scanning Radiometer (MSR). The characteristics of the sensors are shown on Table 3.

### (2) MOS-1 Operation

After the launch of MOS-1 on 19 February 1987, with spacecraft check out for three months, images data from the three sensors were flawlessly acquired. NASDA is now performing six month experimental operation to check the compatibility between spacecraft and ground station for data reception and processing. After this test operation, MOS-1 shifts to routine operation status.

The ground support system for MOS-1 is shown in Figure 2. Earth Observation Center (EOC) is the main ground station responsible for mission management, scheduling, data acquisition and processing. In addition to EOC, MOS-1 data are also planned to be received at nine other receiving stations in the world. The world coverage of MOS-1 is shown in Figure 3.

### (3) MOS-1 Verification Program (MVP)

MOS-1 Satellite Program includes the MOS-1 Verification Program (MVP) in which the system parameters of mission instrument, function and characteristics of sensors and satellite systems, and its data

usefulness will be evaluated. In order to obtain fruitful result, NASDA publicly announced the opportunity to participate in the MVP. In response to this announcement, NASDA received a total of 114 proposals from 11 countries. After evaluation 93 proposals were selected. NASDA is now conducting the MVP by using MOS-1 data, airborne data, and ground/sea truth data in collaboration with the proposal selected organizations.

#### (4) MOS-1 Data Distribution

All the MOS-1 data acquired and archived by any ground station will be made available on public and non-discriminatory basis. On 10 August 1987, NASDA started to distribute MOS-1 data through Remote Sensing Technology Center of Japan (RESTEC). The concept of MOS-1 data distribution flow is shown in Figure 4.

### J. ERS-1 Program

Japanese Earth Resources Satellite-1 (ERS-1), with its launching scheduled in early 1992, is under development as a joint program of Ministry of International Trade and Industry (MITI) and NASDA. The main objectives of the ERS-1 are to establish the technology of the active microwave sensor, namely the Synthetic Aperture Radar (SAR), and the high resolution Optical Sensor (OPS), and to examine the terrestrial resources and environment, primarily focusing on the geological and topographical survey.

The profile and description of ERS-1 is shown in Figure 5 and Table 4. ERS-1 is planned to carry two sensors which are the SAR and OPS. The characteristics of these sensors are shown in Table 5. Their primary design was completed in 1987. The critical design has been started.

### 4. ADEOS Program

Following the fulfillment of MOS-1 and ERS-1 programs, NASDA plans to launch Advanced Earth Observing Satellite (ADEOS) in early 1994 as a next generation earth observation satellite.

The main objectives of ADEOS are as follows:

- (1) The development of advanced earth observation sensors.
- (2) The development of the modular satellite that is the prototype of the future platform.
- (3) The experiments on earth observation data relay using data relay satellites to form a global observation network.
- (4) The contribution to domestic and international cooperation by installing sensors developed by domestic and/or foreign organizations.

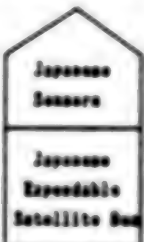
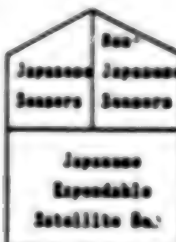
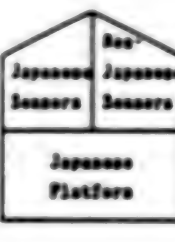
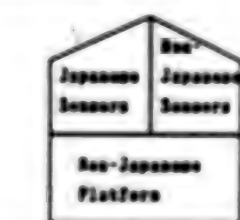
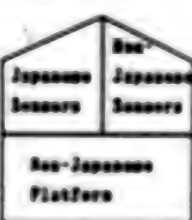
The profile and description of ADEOS are shown in Figure 6 and Table 6. ADEOS will carry two core sensors which are Ocean Color and Temperature Scanner (OCTS) and Advanced Visible and Near Infrared Radiometer (AVNIR). In addition to the core sensors, NASDA issued an Announcement of Opportunity (AO) to install the AO sensors as mentioned above. The characteristics of these sensors are shown in Table 7.

### S. Polar Orbiting Platform Program

Earth observation program by means of Polar Orbiting Platform (hereinafter referred to as POP Program) is being established among NASA, ESA, STA/NASDA and Canada who are the partners of the Space Station Program. The main objectives of POP Program are to guarantee the continuity of operational meteorological observation which is currently operated by NOAA satellite and to make effective observation of the area of earth science. According to the current schedule, NASA plans to launch one platform in 1995 and ESA plans to launch one in 1997. Japan also have a plan to launch its own platform in late 1990's. The countries who participate in POP Program within the frame work of the space Station Program will provide on-board sensor instruments. In Japan, NASDA's AMSR (Advanced Micro-wave Scanning Radiometer) and MITI's ITIR (Intermediate Thermal Infrared Radiometer) are planned to be provided to NASA POP as Core sensors. The characteristics of AMSR and ITIR are shown in Table 8.

To make this POP program more effective and fruitful, announcement of opportunity (AO) for the participation in this program was issued from NASA, ESA and STA respectively to the organizations and/or individual researchers concerned.

Table 1. Schedule of Japanese Earth Observation Satellite Programs

| Calendar Year                | 1987       | 1988                                                                              | 1989                                                                              | 1990                                                                               | 1991                                                                               | 1992                                                                               | 1993 | 1994 | 1995 | 1996        | 1997      | 1998        | 1999 | 2000+ |
|------------------------------|------------|-----------------------------------------------------------------------------------|-----------------------------------------------------------------------------------|------------------------------------------------------------------------------------|------------------------------------------------------------------------------------|------------------------------------------------------------------------------------|------|------|------|-------------|-----------|-------------|------|-------|
| Satellite Launch Schedule    | A<br>HOS-1 |                                                                                   | A<br>HOS-1b                                                                       | A<br>HOS-1c                                                                        |                                                                                    | A<br>HOS-2                                                                         |      |      |      | A<br>EPSP-1 | A<br>EPSP | A<br>EPSP-2 |      |       |
| Satellite Allocation Concept |            |  |  |  |  |  |      |      |      |             |           |             |      |       |

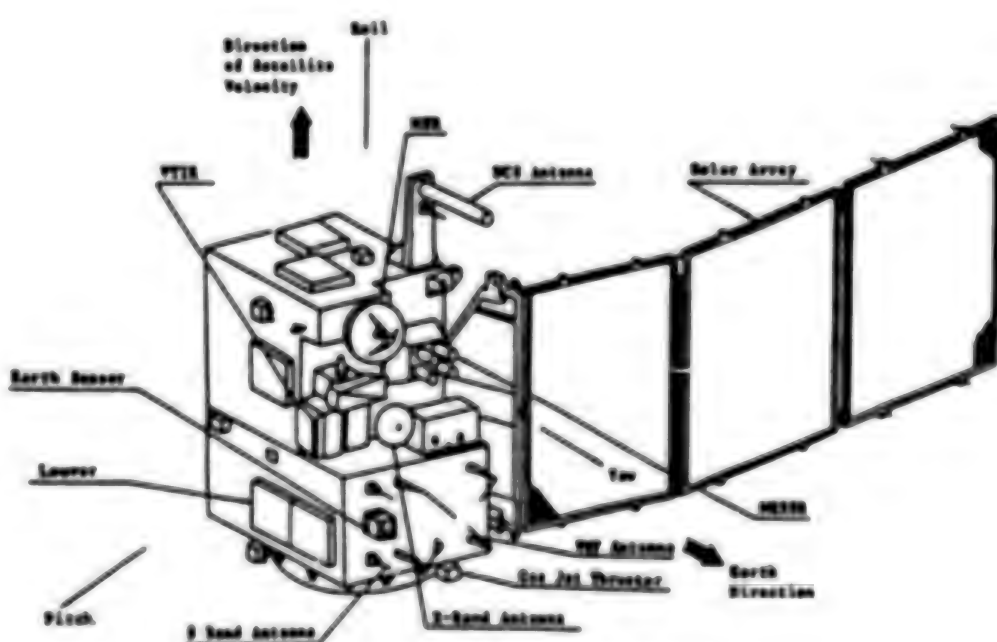


Fig. 1 Profile of MOS-1

Table 2. Description of MOS-1

| Item           | Parameter                                                                                                                                                                      |
|----------------|--------------------------------------------------------------------------------------------------------------------------------------------------------------------------------|
| Orbit          | Near-Polar (800km)<br>Sun-Synchronous<br>(Local Mean Time 10:00AM)<br>17 days Coverage Cycle Duration                                                                          |
| Weight         | 740kg                                                                                                                                                                          |
| Power          | Solar Array 640(WOL)                                                                                                                                                           |
| Stabilization  | 3-axis, Earth-Pointing                                                                                                                                                         |
| Launch Vehicle | S-3 from TNSC                                                                                                                                                                  |
| Design Life    | 2 Years                                                                                                                                                                        |
| Instruments    | MESSR (Multispectral Electronic Self Scanning Radiometer)<br>VTIR (Visible and Thermal Infrared Radiometer)<br>(Microwave Scanning Radiometer)<br>DCS (Data Collection System) |
| Launch date    | Feb. 18, 1987                                                                                                                                                                  |
| Status         | Flight segment PM Completed<br>PM Completed<br>and in flight                                                                                                                   |

Table 3. Characteristics of MOS-1 Sensors

| Sensor<br>Item                                                   | MESSR                                                   | VTIR       | MSR                                     |              |
|------------------------------------------------------------------|---------------------------------------------------------|------------|-----------------------------------------|--------------|
| Wavelength (μm)                                                  | 0.63 - 0.80<br>0.63 - 0.80<br>0.73 - 0.80<br>0.80 - 1.1 | 0.3 - 0.7  | 0.0 - 7.0<br>10.5 - 11.5<br>11.5 - 12.5 | —            |
| Frequency (GHz)                                                  | —                                                       | —          | —                                       | 23.0    31.4 |
| Geometric Resolution (1FOV in km)                                | 0.08                                                    | 0.8        | 1.7                                     | 32    33     |
| Radiometric Resolution                                           | (3dB)    (11.5dB)                                       | 0.08       | 0.08                                    | 18    18     |
| Beam width (km)                                                  | 100 (one optical element) × 2                           | 1000       | 330                                     |              |
| Scanning Method                                                  | electric                                                | mechanical | mechanical                              |              |
| Remarks    * Signal to noise ratio excluding quantitative noise. |                                                         |            |                                         |              |

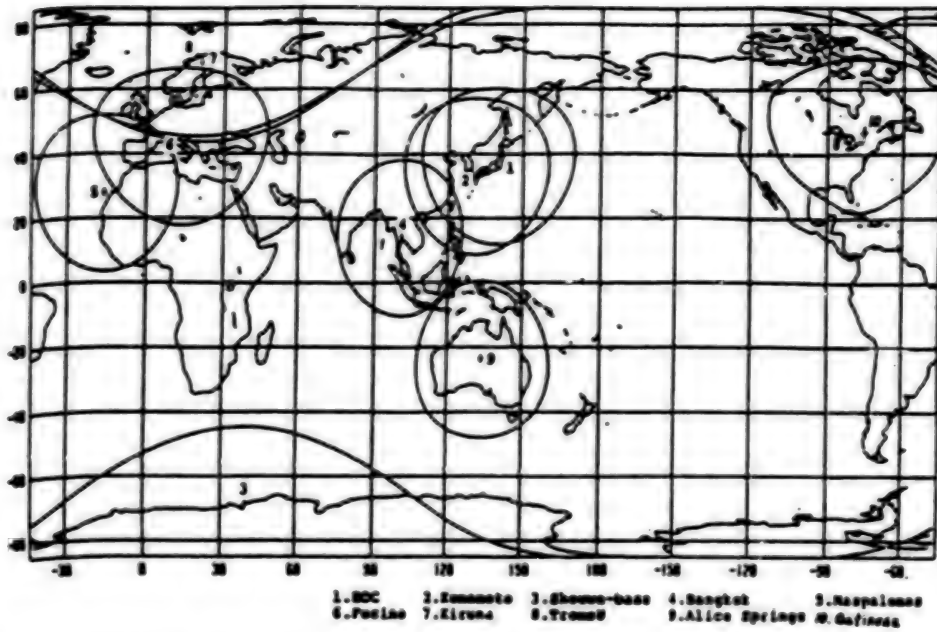


Fig. 4 World Coverage Map of MOS-1

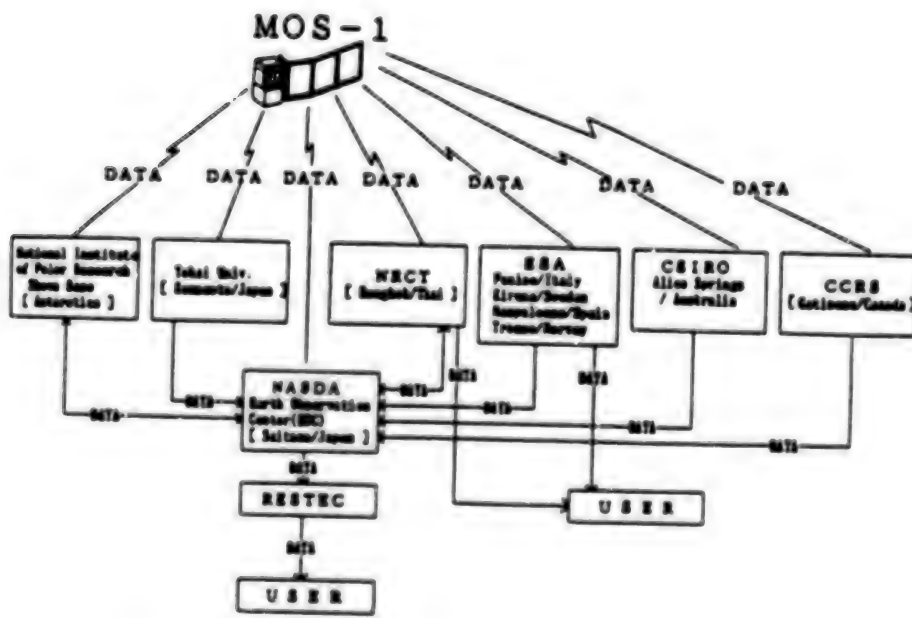


Fig. 5 MOS-1 Data Distribution Flow

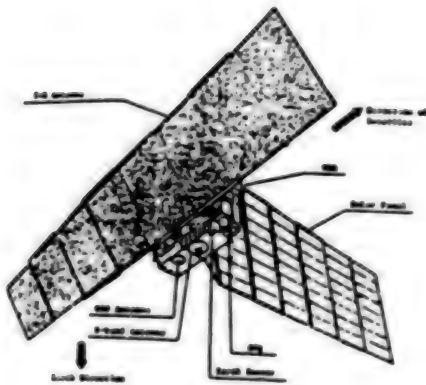


Fig. 6 Profile of ERS

Table 4. Description of ERS-1

| Item                           | Parameter         |
|--------------------------------|-------------------|
| Orbit                          | Semi-synchronous  |
| Altitude                       | Approx. 500 km    |
| Inclination                    | Approx. 87.7°     |
| Recurrent period               | 6 days (Westward) |
| Local max time<br>(descending) | 10:00-11:00 AM    |
| Number of orbit per day        | Approx. 18        |
| Weight                         | Approx. 1400 kg   |
| Launch Vehicle                 | SL-1 Rocket       |
| Design Life                    | 3 Years           |
| Launch Schedule                | Early 1992        |

Table 5. Specification of ERS-1 Sensors

| Sensor Item                        | SAR                            | OPS                     |                   |            |                                   |
|------------------------------------|--------------------------------|-------------------------|-------------------|------------|-----------------------------------|
|                                    |                                | Band                    | Center Wavelength | Band width | Rate                              |
| Wavelength ( $\mu\text{m}$ )       | L-band                         | 1                       | 0. 56             | 0. 08      |                                   |
|                                    |                                | 2                       | 0. 66             | 0. 06      |                                   |
|                                    |                                | 3                       | 0. 81             | 0. 10      |                                   |
|                                    |                                | 4                       | 0. 81             | 0. 10      |                                   |
|                                    |                                | 5                       | 1. 655            | 0. 11      | Band 1 is for off nadir viewing.  |
|                                    |                                | 6                       | 2. 055            | 0. 11      | Band 2 and 4 makes a stereo-pair. |
|                                    |                                | 7                       | 2. 19             | 0. 12      |                                   |
|                                    |                                | 8                       | 2. 335            | 0. 13      |                                   |
| Polarization                       | H-H                            | ———                     |                   |            |                                   |
| Band number                        | 1                              | 8 (approximately)       |                   |            |                                   |
| Spatial resolution (meter, square) | 18 (approximately)<br>(3 look) | 18 x 24 (approximately) |                   |            |                                   |
| Off Nadir Angle (degrees)          | 35                             | 15. 33 (Band 4 only)    |                   |            |                                   |
| Swath Width(Km)                    | 75 (approximately)             | 75 (approximately)      |                   |            |                                   |
| Stereoscopic Imaging Capability    | ———                            | Yes                     |                   |            |                                   |

Table 6. Description of ADEOS

| Item            | Parameter                           |
|-----------------|-------------------------------------|
| Orbit           | Geo-synchronous<br>(approx. 3000km) |
| Weight          | approx. 3000 kg                     |
| Power           | approx. 3.5 kw                      |
| Launch Vehicle  | D-2 Rocket<br>(Dual Launch)         |
| Design Life     | 3 Years                             |
| Launch Schedule | PT 1993                             |

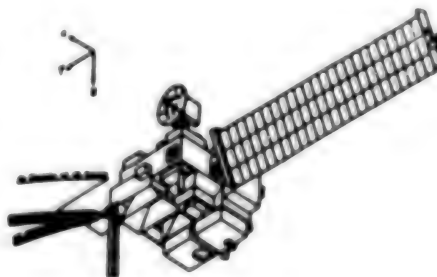


Fig. 7 Profile of ADEOS

**Table 7. Characteristics of ADEOS Sensors**

| BCTS(Basic Color and Temperature Scanner) |                                                                 |                                                    |
|-------------------------------------------|-----------------------------------------------------------------|----------------------------------------------------|
| Spectral Channels                         | Visible<br>Near-Infrared<br>Middle-Infrared<br>Thermal-Infrared | 3 Channels<br>1 Channel<br>1 Channel<br>3 Channels |
| PFO                                       | ±45 Degree(1400 nm at the altitude of 800 km)                   |                                                    |
| IFOV                                      | 0.05 mrad(0.7 nm at the altitude of 800 km)                     |                                                    |
| Data Rate                                 | 3.1 Mbps                                                        |                                                    |
| Height                                    | 100 km                                                          |                                                    |
| Power                                     | 200 W                                                           |                                                    |

| ATRS(Advanced Visible and Near-Infrared Radiometer) |                                                |                         |
|-----------------------------------------------------|------------------------------------------------|-------------------------|
| Spectral Channels                                   | Visible<br>Near-Infrared                       | 3 Channels<br>1 Channel |
| PFO                                                 | 4.5 Degree(80 nm at the altitude of 800 km)    |                         |
| IFOV                                                | 20 mrad(10 nm at the altitude of 800 km)       |                         |
| Polarizing Angle                                    | ±45 Degree(1500 nm at the altitude of 800 km). |                         |
| Data Rate                                           | 100 Mbps                                       |                         |
| Height                                              | 200 km                                         |                         |
| Power                                               | 250 W                                          |                         |

| AO Sensors (AO:Accessories of Opportunity) |                                     |                          |
|--------------------------------------------|-------------------------------------|--------------------------|
| Total Weight                               | Appears. 200 kg                     |                          |
| Total Power                                | Appears. 300 W                      |                          |
| Volume                                     | 700                                 |                          |
| Thermal                                    | Self Dissipation                    |                          |
| Data Rate                                  | < 100 Mbps                          |                          |
| PFO                                        | TBD                                 |                          |
| Schedule                                   | AO Release<br>Deadline for Delivery | Aug. 1997<br>End of 1997 |
|                                            |                                     | Bidelle of 1998          |

Table 8. Characteristics of AMSR and ITIR

| CANDIDATE SENSOR                                                   | AMSR<br>ADVANCED MICROWAVE SCANNING RADIOMETER                                                                                                                                                      | ITIR<br>INTERMEDIATE THERMAL INFRARED RADIOMETER                                                                                                                                                                                                                   |
|--------------------------------------------------------------------|-----------------------------------------------------------------------------------------------------------------------------------------------------------------------------------------------------|--------------------------------------------------------------------------------------------------------------------------------------------------------------------------------------------------------------------------------------------------------------------|
| BASIC SPECIFICATION<br>(TENTATIVE)                                 | <ul style="list-style-type: none"> <li>- FREQUENCY<br/>8.6, 10.65, 18.7, 23.8, 31.58 GHz</li> <li>- SPATIAL RESOLUTION<br/>8.2 - 24 km</li> <li>- SWATH WIDTH<br/>1,200 km</li> </ul>               | <ul style="list-style-type: none"> <li>- WAVELENGTHS<br/>0.85 - 13.7 <math>\mu</math>m (NUMBER OF BANDS:11)</li> <li>- SPATIAL RESOLUTION<br/>15m (ITIR)/30km<br/>60m (ITIR)</li> <li>- SWATH WIDTH<br/>30km</li> </ul>                                            |
| OBSERVATION FIELD AND<br>FEATURES OF UTILIZATION                   | <ul style="list-style-type: none"> <li>- OCEAN AND ATMOSPHERE OBSERVATION</li> <li>- DATA CONTINUITY OF NBS-1 ASA</li> </ul>                                                                        | <ul style="list-style-type: none"> <li>- GENERAL RESOURCES OBSERVATION</li> <li>- GEO-THERMAL OBSERVATION</li> </ul>                                                                                                                                               |
| TECHNOLOGICAL FEATURES<br>AND<br>EXPECTED<br>TECHNOLOGICAL RESULTS | <ul style="list-style-type: none"> <li>- MULTI-FREQUENCY</li> <li>- ESTABLISHMENT OF TECHNOLOGIES REQUIRED<br/>FOR LOW NOISE RECEIVER AND LARGE ANTENNA</li> <li>- ELECTRICALLY SCANNING</li> </ul> | <ul style="list-style-type: none"> <li>- PUSHPULL TYPE SENSOR SYSTEM</li> <li>- ESTABLISHMENT OF TECHNOLOGIES REQUIRED<br/>FOR HIGH RESOLUTION OBSERVATION</li> <li>- MULTI-BAND SENSOR COVERING NEAR INFRARED<br/>THROUGH THERMAL INFRARED WAVELENGTHS</li> </ul> |

/08309

### Estimation of the Simulated JERS-1 Data

43070010d Kyoto Selections from INTERNATIONAL ARCHIVES OF PHOTOGRAMMETRY AND REMOTE SENSING in English Vol 27 1988 Part B11 pp 770-777

[Article by T. Takemura, I. Kohno, I. Kakimoto (MSS), Mitsui Mining & Smelting Co., Ltd., System Development Office, 2-1-1, Nihonbashi-Muromachi, Chuo-ku, Tokyo, 103 Japan; K. Arai, K. Tonoike (ERSDAC), Earth Resources Satellite Data Analysis Center, No 39 Mori Bldg. 2-4-5, Azabudai, Minato-ku, Tokyo, 106 Japan]

#### [Text] 1. INTRODUCTION

OPS borne in JERS-1, which will be launched in 1992, is paid attention from the world, because it has four bands in short wave infrared region. The JERS-1 data were simulated by using the GER (GEOPHYSICAL ENVIRONMENTAL RESEARCH CORP.) 64 channels airborne imaging spectrometer (AIS) data and evaluated as mineral exploration tool. The area studied is Goldfield, Nevada of U.S.A.

#### 2. DESCRIPTION OF THE TEST SITE

Goldfield is located in south central Nevada (Fig. 1) and prospered in the gold rush the early years of this century. Gold deposits are centered at 3km NE of the town and are distributed in N-S direction. The ore bodies are irregular platy veins in the hydrothermally altered host rocks, which mainly consist of porphyritic rhyodacite. The altered zone is in a circular shape with a diameter of 4km (Fig. 1). Over 130 tons of gold were mined from this area and a small mining activity persists to now.

#### 3. THE AIRCRAFT DATA

GER AIS data consist of 63 channels data from visible through infrared region (Table 1). Scan parameters are in Table 2. The central wavelength of AIS channels and JRES-1 bands are in Table 3. Each pixel is rectangular, 20m in azimuth direction (NS), and 15m in range direction (EW). The imagery has been used without geometric correction.

The original data is provided in digital form and is converted to radiance by the conversion functions supplied by GER.

#### 4. JERS-1 DATA SIMULATION

Energy  $P_i$  of electromagnetic waves which streamed into the JERS-1 band  $i$  detector can be written as follows:

$$P_i = k \int Tr(\lambda) \cdot F_i(\lambda) \cdot H_o(\lambda) d\lambda$$

where  $k$  = constant value including f number of optical system

$Tr(\lambda)$  = transmission factor of the condenser system at wavelength  $\lambda$

$F_i(\lambda)$  = spectral transmission factor of the spectral system of band  $i$  at wavelength  $\lambda$

$H_o(\lambda)$  = radiance gotten by AIS at wavelength  $\lambda$

Gaussian noise is added to this energy  $P_i$  to correspond to S/N of band  $i$ , and  $P_i$  is digitized into 6 bits. The data thus digitized was used as the simulated JERS-1 band  $i$  data for study. Flow chart of JERS-1 data simulation is shown in Figure 2. Main properties of JERS-1 are shown in Table 4.

#### 5. EVALUATION OF THE IMAGES MADE FROM SIMULATED JERS-1 DATA

The images made from simulated JERS-1 data were evaluated as a mineral exploration tool. Simulated images were black-and-white images, falsecolor images, ratio images and log residual images. Black-and-white images of band 1, 3, 6 and 8 are shown in Photo 1 to 4. These images are excellent qualities, and their brightness differences due to spectral characteristics are recognized very well. Simulated images were evaluated from the standpoint of mapping altered zones. We tried to extract and classify the altered zone by studying spectral absorption features from simulated OPS data. Spectral reflectance of important altered minerals and JERS-1 bands in region of 2.0 $\mu$ m to 2.5 $\mu$ m are shown in Figure 3. (Photos 1 to 4 omitted)

From these simulated images and ground proof, several characteristics were recognized as follows:

##### (1) Falsecolor image (band 1,2,3=R,G,B)

The brightest zones correspond to mine dumps or dried waste pond. Goldfield town showed reddish color and it suggests the existence of vegetation.

##### (2) Falsecolor image (band 5,7,8=R,G,B)

Pinkish zones show the altered zone where alteration clay minerals are alunite, kaolinite, montmorillonite and sericite. These minerals have typical spectrum absorption near  $2.2\mu\text{m}$ , so the brightness of band 7 is relatively darkened and the altered zone became pink. However, the color difference among these minerals could not be recognized.

(3) Ratio image (band5/band7, band6/band7, band7/band8 = B,R,G)

Violet zones correspond to the altered zone as the pinkish colored zones of the preceding image.

(4) Log Residual image (band 1,2,3 = B,G,R)

The log residual technique is the method to remove effects of atmospheric scattering and absorption, and brightness difference due to slope orientation. This technique is effective to be applied in the area with many kinds of clay minerals and sparsely existing vegetation like Goldfield area because the minute change in reflectance is emphasized.

Image (4) has more variety of colors than image (1). Greenish zone corresponds to the iron oxide zone. This greenish zone coincides with the area extracted as the hematic zone by Chebyshev waveform analysis of GER that used 63 channels data. This fact shows the validity of JERS-1 data.

(5) Log Residual image (band 5,7,8 = R,G,B)

In image (5), the altered zone is in dark reddish, reddish and pinkish zones. The change in color suggests the difference of minerals.

## 6. CONCLUSION

The results of this JERS-1 data simulation over Goldfield area are as follows:

- (1) The area covered with vegetation can be extracted by using falsecolor images, ratio images and log residual images.
- (2) The altered zone where alteration clay minerals are montmorillonite, alunite, sericite, kaolinite, etc., can be extracted by using falsecolor images and ratio images.
- (3) The iron oxide zone can be extracted by using log residual images.
- (4) Clay minerals in the altered zone could be classified in log residual images.
- (5) We could not evaluate the possibility for extraction of carbonate rocks like limestone that have spectrum absorption in JERS-1 band 8 because of no carbonate rock in the study area.

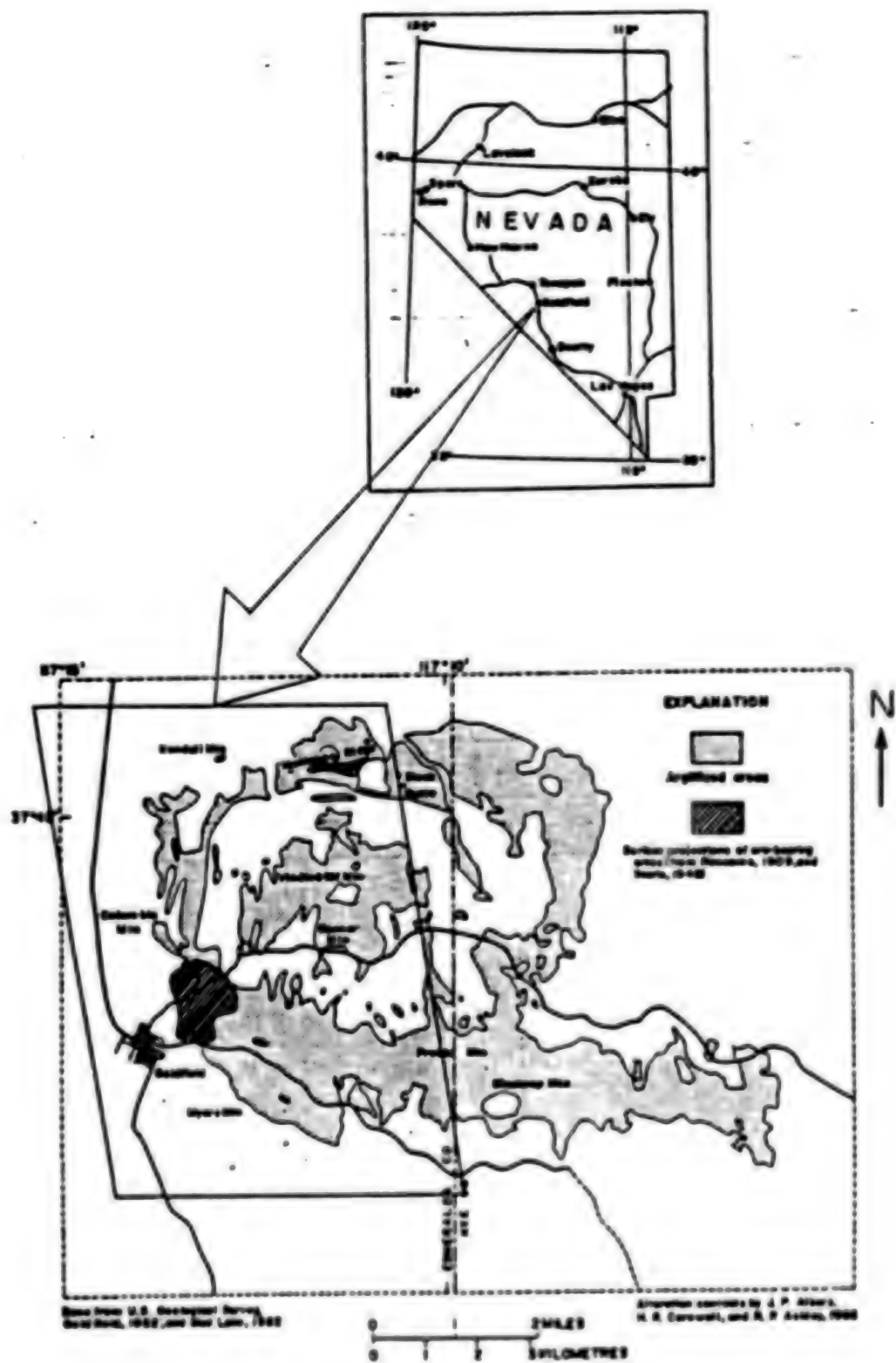


Fig. 1. Map of the Test Site

Table 1 FORMATION OF AIS DATA

|            | VISIBLE/NEAR INFRARED |               | INFRARED       |
|------------|-----------------------|---------------|----------------|
| CHANNEL    | 1 ~ 24                | 25 ~ 31       | 32 ~ 63        |
| BAND (nm)  | 420.9 ~ 984.5         | 1.020 ~ 1.880 | 1.978 ~ 2.5036 |
| BAND WIDTH | 25.4nm                | 120nm         | 18.5nm         |

Table 2 SCAN PARAMETERS

|                         |             |
|-------------------------|-------------|
| SWATH WIDTH             | 512 pixels  |
| SCANNING ANGLE          | 3 mrad.     |
| HEIGHT ABOVE THE GROUND | 20.000 feet |

Table 4 PARAMETERS OF OPS OF JERS-1

| RESOLUTION                                 | 18.3m × 24.2m |            |        |
|--------------------------------------------|---------------|------------|--------|
| SWATH WIDTH                                | 75km          |            |        |
| BAND                                       | WAVELENGTH    | BAND WIDTH | S/N    |
| BAND 1                                     | 0.58(μm)      | 80(nm)     | 46(db) |
| BAND 2                                     | 0.66(μm)      | 80(nm)     | 46(db) |
| BAND 3                                     | 0.81(μm)      | 100(nm)    | 46(db) |
| BAND 4(STEREOSCOPE)                        | 0.81(μm)      | 100(nm)    | 46(db) |
| BAND 5                                     | 1.65(μm)      | 110(nm)    | 42(db) |
| BAND 6                                     | 2.08(μm)      | 110(nm)    | 32(db) |
| BAND 7                                     | 2.19(μm)      | 120(nm)    | 33(db) |
| BAND 8                                     | 2.34(μm)      | 130(nm)    | 27(db) |
| BASE HEIGHT RATIO IN STEREOGRAPHIC IMAGING | 0.3           |            |        |
| QUANTIZATION                               | 8 BITS        |            |        |
| RECORDING DATA RATE                        | 30Mbps × 2CH. |            |        |

Table 3. The Central Wavelength of AIS Channels and JERS-1 Bands

| <u>CHANNEL</u> | <u>WAVELENGTH</u><br>( $\mu\text{m}$ ) | <u>CHANNEL</u> | <u>WAVELENGTH</u><br>( $\mu\text{m}$ ) | <u>CHANNEL</u> | <u>WAVELENGTH</u><br>( $\mu\text{m}$ ) |
|----------------|----------------------------------------|----------------|----------------------------------------|----------------|----------------------------------------|
| 1              | 0.4336                                 | 26             | 1.2000                                 | 51             | 2.2982                                 |
| 2              | 0.4570                                 | 27             | 1.3200                                 | 52             | 2.3146                                 |
| 3              | 0.4804                                 | 28             | 1.4400                                 | 53             | 2.3310                                 |
| 4              | 0.5038                                 | 29             | 1.5600                                 | 54             | 2.3475                                 |
| 5              | 0.5272                                 | 30             | 1.6800                                 | 55             | 2.3639                                 |
| 6              | 0.5506                                 | 31             | 1.8000                                 | 56             | 2.3803                                 |
| 7              | 0.5740                                 | 32             | 1.9880                                 | 57             | 2.3988                                 |
| 8              | 0.5974                                 | 33             | 2.0024                                 | 58             | 2.4132                                 |
| 9              | 0.6208                                 | 34             | 2.0189                                 | 59             | 2.4296                                 |
| 10             | 0.6442                                 | 35             | 2.0353                                 | 60             | 2.4460                                 |
| 11             | 0.6676                                 | 36             | 2.0517                                 | 61             | 2.4625                                 |
| 12             | 0.6910                                 | 37             | 2.0682                                 | 62             | 2.4789                                 |
| 13             | 0.7144                                 | 38             | 2.0846                                 | 63             | 2.4953                                 |
| 14             | 0.7378                                 | 39             | 2.1010                                 |                |                                        |
| 15             | 0.7612                                 | 40             | 2.1174                                 |                |                                        |
| 16             | 0.7846                                 | 41             | 2.1339                                 |                |                                        |
| 17             | 0.8080                                 | 42             | 2.1503                                 |                |                                        |
| 18             | 0.8314                                 | 43             | 2.1667                                 |                |                                        |
| 19             | 0.8548                                 | 44             | 2.1832                                 |                |                                        |
| 20             | 0.8782                                 | 45             | 2.1996                                 |                |                                        |
| 21             | 0.9016                                 | 46             | 2.2160                                 |                |                                        |
| 22             | 0.9250                                 | 47             | 2.2325                                 |                |                                        |
| 23             | 0.9484                                 | 48             | 2.2489                                 |                |                                        |
| 24             | 0.9718                                 | 49             | 2.2653                                 |                |                                        |
| 25             | 1.0800                                 | 50             | 2.2817                                 |                |                                        |

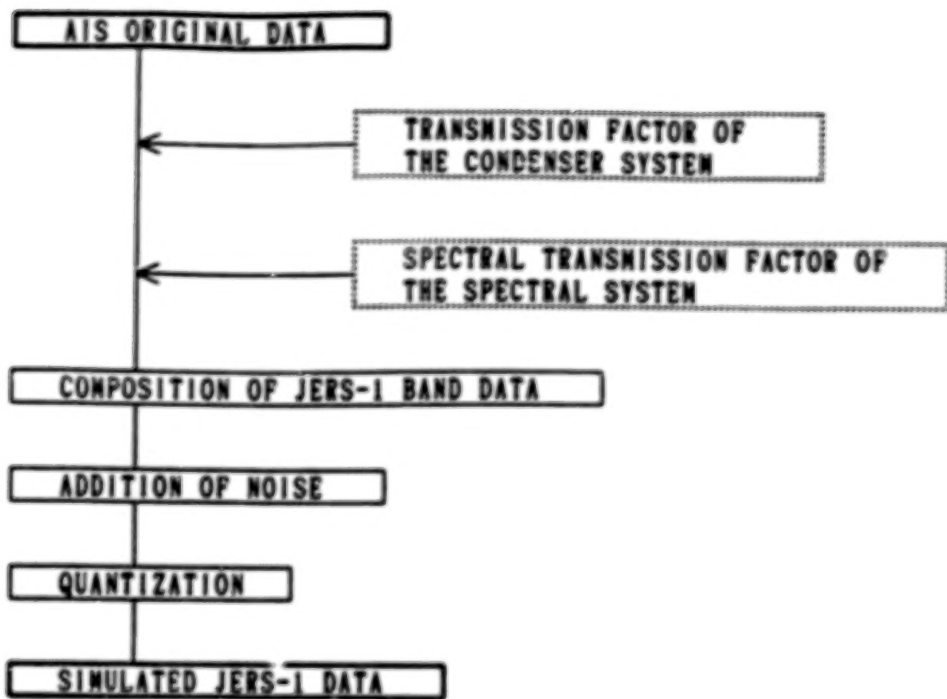


Fig. 2 Flow Chart of JERS-1 Data Simulation

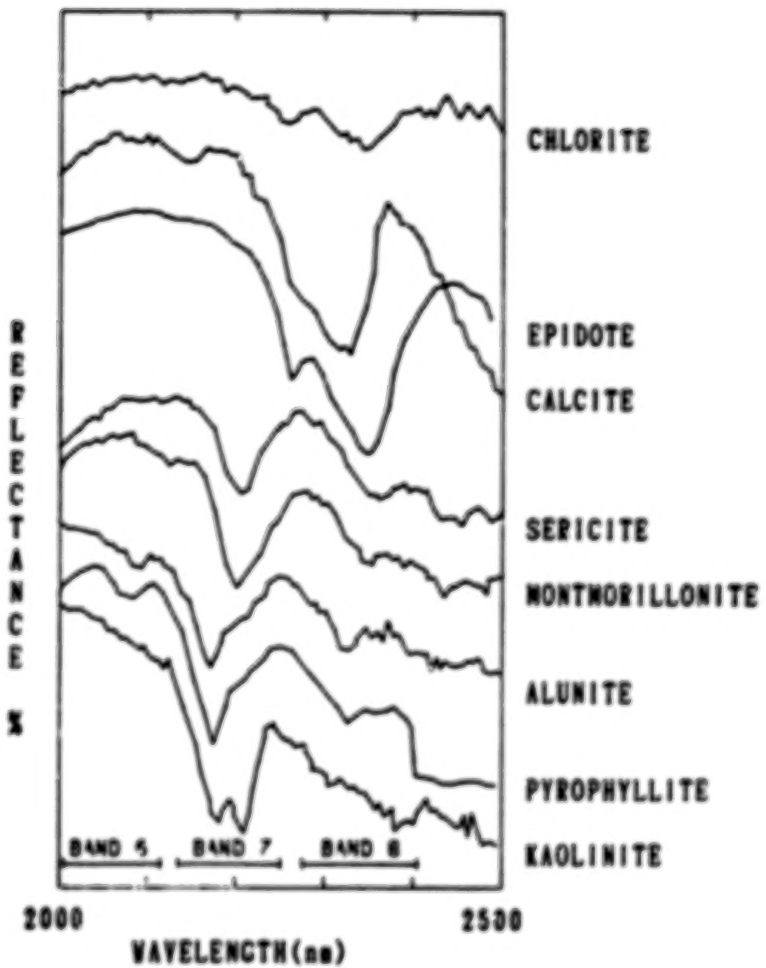


Fig. 3 Spectral Reflection Factor of Altered Minerals

/08309

END